The University of Southern Mississippi

The Aquila Digital Community

Summer 8-2015

Assessing Biogeochemical Impacts and Environmental Conditions Associated with Cross-Shelf High Chlorophyll Plumes in the Northern Gulf of Mexico

Erin Brooke Jones
University of Southern Mississippi

The University of Southern Mississippi

ASSESSING BIOGEOCHEMICAL IMPACTS AND ENVIRONMENTAL

CONDITIONS ASSOCIATED WITH CROSS-SHELF HIGH CHLOROPHYLL

PLUMES IN THE NORTHERN GULF OF MEXICO

by

Erin Brooke Jones

Abstract of a Dissertation
Submitted to the Graduate School
of The University of Southern Mississippi
in Partial Fulfillment of the Requirements
for the Degree of Doctor of Philosophy

August 2015

ABSTRACT

ASSESSING BIOGEOCHEMICAL IMPACTS AND ENVIRONMENTAL

CONDITIONS ASSOCIATED WITH CROSS-SHELF HIGH CHLOROPHYLL

PLUMES IN THE NORTHERN GULF OF MEXICO

by Erin Brooke Jones

August 2015

The northern Gulf of Mexico is a complex marine system subject to episodic physical phenomena such as loop current eddies. Flow fields generated by these eddies can result in cross-shelf exchanges between riverine influenced shelf waters and the offshore water column. This study considers the impacts of high chlorophyll plumes (HCPs) resulting from cross-shelf exchanges to the bio-optical properties of affected waters, and how these plumes are influenced by their environment. The seasonal, interannual and decadal chlorophyll cycles of the Gulf of Mexico and the northern Gulf of Mexico are described to provide context for evaluating the ecological effects of HCPs. To determine the ecological effects of such exchanges, a regional 2007 cross-shelf exchange event is investigated using remotely sensed observations. The offshore ratio of bio-optical signals observed during the exchange event implies a divergence in surface water composition from the typical composition. To explore the impact of this composition change on the regional carbon budget, net primary productivity (NPP) estimates during the exchange event are compared with the climatological estimates, revealing increases of up to 330% for the corresponding time period. Select HCP CHL fields are compared with physical parameters and environmental conditions to explore drivers of HCP formation and conditions affecting HCP characteristics. This work

supports suppositions that HCPs form as the result of a complex river-wind-circulation

system and adds to the current understanding of CHL dynamics in the northern

Gulf of Mexico by showing an association between HCP frequency and

environmental conditions.

The University of Southern Mississippi

ASSESSING BIOGEOCHEMICAL IMPACTS AND ENVIRONMENTAL

CONDITIONS ASSOCIATED WITH CROSS-SHELF HIGH CHLOROPHYLL

PLUMES IN THE NORTHERN GULF OF MEXICO

by

Erin Brooke Jones

A Dissertation
Submitted to the Graduate School
of The University of Southern Mississippi
in Partial Fulfillment of the Requirements
for the Degree of Doctor of Philosophy

Approved:

_____
Dr. Jerry D. Wiggert, Committee Chair
Assistant Professor, Marine Science

_____
Dr. Stephen D. Howden, Committee Member
Associate Professor, Marine Science

_____
Dr. Scott Milroy, Committee Member
Assistant Professor, Marine Science

_____
Dr. Steven E. Lohrenz, Committee Member
Dean, School for Marine Science and Technology,
University of Massachusetts, Dartmouth

_____
Dr. Richard W. Gould, Committee Member
Head, Bio-Optical/Physical Processes and Remote Sensing Section,
Naval Research Laboratory

_____
Dr. Karen S. Coats
Dean of the Graduate School

August 2015

DEDICATION

I dedicate this dissertation to James who has selflessly supported me throughout this pursuit, to Ella who inspired my return to academia, and to Andrew who challenged me to accomplish more than I believed possible.

ACKNOWLEDGMENTS

TABLE OF CONTENTS

LIST OF TABLES

LIST OF ILLUSTRATIONS

Figure

LIST OF ABBREVIATIONS

NGMx	Northern Gulf of Mexico
CHL	Satellite chlorophyll-a (standard algorithms)
CHL*	Normalized chlorophyll-a
CHL_Z	Z-normalized chlorophyll-a
CHL_A	Chlorophyll-a anomaly
SST	Sea surface temperature
SSH	Sea surface height
SSHA	Sea surface height anomaly
HCP	High chlorophyll plume
ENSO	El Niño-Southern oscillation
MEI	Multidecadal ENSO index
LC	Loop Current
LCE	Loop Current eddy
DOY	Day of year

CHAPTER I

INTRODUCTION

The Gulf of Mexico (Gulf) is a semi-enclosed basin uniquely subject to oceanic and land-ocean processes. The Gulf areally spans ~1.6 million km^2 (Muller-Karger et al., 2015) with a volume of ~2.4 million km^3 (http://www.epa.gov/gmpo/about/facts.html). The Mississippi River, the largest river in the United States (U.S.) flows into the Gulf at a rate of ~13,000 m^3 s^{-1} delivering sediment, nutrients and buoyant freshwater to Gulf shelf waters (Yuan et al., 2004).

The Gulf is economically and ecologically important to five bordering U.S. states and three countries (Adams et al., 2004; Muller-Karger et al., 2015). Economically, the U.S. provides the U.S. with tourism, fisheries and petroleum revenue (Adams et al., 2004).

Gulf circulation is driven by the Loop Current (LC) and its associated eddies (Morey et al., 2003a; Oey et al., 2005; Ohlmann et al., 2001; Schmitz et al., 2005). The LC is a rapid current bringing warm water into the Gulf in a 'loop' flow between the Yucatan and Florida currents (Hyun & Hogan, 2008; Oey et al., 2005; Schmitz et al., 2005; Sturges et al., 2009). The LC can transport between 24 and 32 Sverdrup (Sv) (Muller-Karger et al., 2015; Oey et al., 2005) and flows at rates between 1.5 and 1.8 m s^{-1}, thus it is an important link in the Atlantic Gulf Stream system (Oey et al., 2005 Schmitz et al. 2005). Intrusion of the LC into the Gulf varies from minimal current intrusion to intrusion across the continental shelf in the Northern Gulf (Oey et al., 2005; Sturges et al. 2005).

The LC sheds anticyclonic, warm-core eddies periodically throughout the year in a poorly understood fashion (Alvera-Azcarate et al., 2008; Hyun & Hogan, 2008; Sturges et al., 2005; Sturges et al. 2009). These eddies are typically large (~300 km) and westward propagating (Hyun & Hogan, 2008; Oey et al., 2005; Schmitz et al., 2005). Most anticyclonic LC eddies are formed as the distal end of the LC separates, forming an eddy (Oey et al., 2005; Schmitz, 2005; Sturges et al., 2009). Eddy formation is irregular, and many times eddy systems reattach to the main current before propagation occurs (Leben, 2005). Patterns of eddy formation have not been clearly shown (Alvera-Azcarate et al., 2008; Leben, 2005; Sturges et al., 2009), although Leben (2005) used satellite altimetry to show that eddy formation usually every 6-11 months (Leben 2005; Schmitz, 2005). Cold-core, cyclonic eddies also form near the edges of the LC and often interact with the current and with the LC eddies (Hyun & Hogan, 2008). In the northern Gulf of Mexico (NGMx), eddy circulation often reaches the continental shelf inducing sediment transport (Hyun & Hogan, 2008; Schmitz, 2005).

Due to the proximity of the shelf to the central basin, the interaction of these eddies with shelf waters has consequences across the Gulf. Adjacent counter-rotating eddies, or dipole eddies, induce currents capable of entraining shelf water and subsequently advecting shelf material to the oligotrophic deep water column of the central Gulf (Morey et al., 2003b, Teague et al., 2006; Schiller et al., 2011, Muller-Karger et al., 2015). Associated with these cross-shelf flows are high chlorophyll plumes (HCPs). HCPs frequently appear in the ocean color record for the NGMx, indicating a role in chlorophyll and bio-optical variability impacted offshore waters. Certain locations or "hotspots" within the NGMx are more likely to experience frequent HCPs (Morey et

al., 2003a). Hotspots in the eastern NGMx include the Mississippi River delta (Schiller et al., 2011; Morey et al., 2003a; Muller-Karger et al., 2015) and the West Florida shelf (Gilbes et al., 1996; Morey et al., 2003a). In the western NGMx, HCPs tend to form near the Texas-Mexican border (Biggs & Muller-Karger, 1994).

This study focuses on HCPs in the vicinity of the Mississippi River delta, defined here as filamentous tongues of CHL > 0.5 mg m^{-3} in the satellite observation record extending from coastal and shelf regions across the shelf break to south of 28˚N. Modeling studies of HCP development near the Mississippi River Delta in the NGMx have suggested that prominent HCPs in the region are linked to seasonal wind forcing of the Mississippi River plume (Morey et al., 2003a; Schiller et al., 2011). Winds in the NGMx set up seasonally oscillating (east in summer/west in winter) alongshore currents that constrain the Mississippi River plume to the continental shelf (Yuan et al., 2004). During summer months this leads to eastward spread of the Mississippi River plume near the vicinity of Desoto Canyon (Morey et al., 2003b; Schiller et al., 2011). Dipole eddy formation and LC impingement are frequent to the Desoto Canyon region. Models therefore suggest this region as a 'hotspot' of HCP generation due to the interaction of LC/eddy circulation and Mississippi River plume waters (Morey et al., 2003a.).

The components of the modeled HCP system, wind, offshore circulation, and river discharge, are each potentially subject to changing environmental of climatic conditions. The effects of the El Niño- Southern Oscillation (ENSO) on Gulf sea level was investigated by Kennedy et al. (2007), who show that winter low sea level in the Gulf is associated with warm phase or El Niño years in the ENSO cycle. Muller-Karger et al. (2015) did not find a similar link between ENSO and Gulf chlorophyll, but did find

a correlation between both sea surface temperature and wind speed with ENSO and the Atlantic Multidecadal Oscillation (AMO). The abundance of jellyfish in the Gulf was also shown to be positively correlated with ENSO, AMO and the Pacific Decadal Oscillation (PDO) (Robinson & Graham, 2013). These physical and biological links of the Gulf to global climate indices indicate that HCPs may be affected by climate change.

Satellite sensed chlorophyll concentration (CHL) serves as a proxy for phytoplankton biomass (Carder et al., 2003; Muller-Karger et al., 2015) and is suitable for use in detecting plumes resulting from offshore transport (Carder et al., 2003). However, in optically complex coastal or riverine waters, often denoted as Case II waters (Morel & Prieur, 1977), the satellite CHL signal is affected by materials such as detritus and chromophoric dissolved organic material (CDOM) (Carder et al., 2003). Therefore, a contrast in the relationship between CHL and satellite CDOM would indicate the intrusion of Case II waters to an oligotrophic Case I water environment, as expected during HCP intrusion to the offshore NGMx. CDOM is also known to have an inverse relationship with salinity and can be employed to estimate surface salinity from satellite measurements (Wang & Xu, 2008). The relationship between CDOM and salinity is strengthened in continental runoff and is therefore an effective measure of low salinity influx to the surface water column (Ferrari & Dowell, 1998). The presence of living and photosynthetically active phytoplankton within Case II waters can be verified by satellite measurements of fluorescence line height (FLH). Alterations in the FLH to CHL relationship could indicate physiological changes in phytoplankton or phytoplankton community composition change, indicative of advected shelf waters to the offshore NGMx.

Measurements of bio-optical properties observed by satellite sensors can also be useful in investigating the marine carbon cycle. As the primary producers of the marine environment, phytoplankton are important to the ocean carbon budget. Net primary productivity (NPP) is often used as a metric for photosynthesis, or carbon fixation by phytoplankton (Esaias, 1996; Muller-Karger et al., 2015). New production, dependent upon new nutrient input, and export production, carbon that is not recycled within the euphotic zone, contribute to the ocean carbon budget by increasing removal of carbon from the atmosphere. Advected shelf/riverine waters could be expected to increase NPP in impacted offshore waters by delivering nutrients to the mixed layer and through the introduction of shelf phytoplankton. In particular, the introduction of diatom-dominant shelf waters could increase export production greater than nutrient delivery alone (Buesseler, 1998) due to the sinking rate of diatoms relative to smaller offshore phytoplankton species.

<div align="center">Data and Methods</div>

Following is a data list and overview of satellite image processing methodology. A detailed list of chapter-specific data is included in each subsequent chapter. Also analytical method details are discussed in each chapter to clarify how results were reached.

Data

HCPs typically persist for only days, although some HCPs in the satellite record are observed to persist for weeks. Due to the capability of satellite sensors to observe short-temporal, large-spatial phenomenon, remote sensing data were used here to identify

HCPs and to detect and characterize both the mechanisms driving the HCPs and their biogeochemical impacts.

Satellite observations were retrieved from NASA and research repositories then processed and analyzed with in-house scripts. Bio-optical parameters (CHL, CDOM and FLH) from ocean color satellite sensors were evaluated to detect and characterize HCP impact to the water column. Ocean color parameters collected from NASA's Ocean Color Web (http://oceancolor.gsfc.nasa.gov/) include Level 3 (gridded spatially and temporally) and mapped image files from both MODIS-Aqua (CHL (OC3-algorithm), FLH and CDOM) and SeaWiFS (CHL (OC4-algorithm) only). CHL derived from these algorithms are evaluated and cross-sensor calibrated (prior to 2010) to reduce error to the range of error among *in situ* techniques for measuring chlorophyll. The observations were collected for the range of 1998-2002 (SeaWiFS) and 2003-2011 (MODIS-Aqua). To determine the impact of HCPs on productivity and carbon budget, level 4 (modeled estimates of parameters derived from Level 1-3 data) net primary productivity (NPP) estimates were downloaded from Oregon State University's Ocean Productivity website (http://www.science.oregonstate.edu/ocean.productivity). The Carbon-based Productivity Model (CbPM) was selected over the standardly used Vertically Generalized Productivity Model due to decreased dependency on CHL, a complication due to the expected Case II characteristics of HCPs. The CbPM algorithm estimates NPP as a function of surface carbon (determined from particulate backscattering coefficients observed via ocean color satellite), phytoplankton growth rate (derived from the CHL to carbon ratio and depth dependent irradiance). As a means of identifying offshore circulation features conducive to HCP formation (eddies and LC), merged multi-platform sea surface height (SSH)

fields generated by the Colorado Center for Astrodynamics Research Group (CCAR) were retrieved from the oceanic data products available on the GOMEX-PPP website (http://abcmgr.tamu.edu/gomexppp/). To detect upwelling near HCPs, a potential source of nutrient input, and to verify the presence of eddies, sea surface temperature (SST) fields from MODIS-Terra data files were obtained. The SST data consist of 8-day averaged Level 3 mapped grids from NASA's Ocean Color Web. QuikSCAT weekly mean wind fields (½° x ½° resolution) produced by CERSAT were obtained (http://cersat.ifremer.fr/) to assess whether wind conditions favor eastward Mississippi River plume spread at the time of HCP formation.

To complement satellite surface observations, available *in situ* data and model output, were collected from data repositories. To better interpret the HCP impact across varying water column depths and to distinguish shelf and offshore waters, bathymetry for the NGMx was accessed from the National Geophysical Data Center's (NGDC) (http://www.ngdc.noaa.gov/mgg/coastal/crm.html) Coastal Relief Model (CRM). Daily Mississippi River discharge values from U.S. Army Corps of Engineers site 01100mis located at 31˚ N and 91.6˚ W (Tarbert Landing, MS) were obtained for the period 1998-2010 to evaluate the effect of riverine input to both HCP formation and NGMx CHL variability. Salinity and currents, used to explore the dependency of HCP-associated advection of riverine waters to offshore circulation features over varying depths, were obtained from the Naval Oceanographic Office's American Seas Prediction system (AMSEAS) (http://www.northerngulfinstitute.org/edac/oceanNomads/AmSeas.php). The AMSEAS model output was selected due to its NGMx focus providing fine spatial resolution (1/36th degree) of regional oceanographic features. Depth levels of 0, 3, 4, 5, 8,

12, 15, 20, 30, 50, 100, and 200 m were examined to detect HCP depth penetration. To

provide insight to the effects of global climate change to HCPs and NGMx CHL

variability, ENSO variations were obtained via the Multivariate ENSO Index (MEI)

website supported through NOAA (http://www.esrl.noaa.gov/psd/enso/mei/).

Methods

Perl and MATLAB scripts were written to automate the processing of

observations. Ocean color parameters (CHL, FLH and CDOM), productivity estimates

(NPP), physical fields (SST, winds, surface currents and SSHa), and bathymetrical output

were processed with in-house scripts that access procedures included in SeaWiFS Data

Analysis System (SeaDAS) in order to extract and plot the data for the NGMx (defined as

Gulf waters north of 24˚N). MATLAB programs were also developed for regional

extraction of data. The extractions were then geographically plotted using scripts created

to utilize the tools found in the University of Hawaii's Generic Mapping Tools (GMT,

Wessel & Smith, 1998). Each plot is constrained by the bounds 98°W 82°W and 24°N

31°N. The processed grids were then plotted using GMT software. Parameter-specific

plotting details are described below. Analytical techniques for each parameter are

described in respective data chapters.

Ocean Color

To facilitate visualization of bio-optical parameter dynamics, missing data points

(pixels) were smoothed through a minimum curvature interpolation program in GMT.

This smoothing or surfacing procedure can produce mathematical noise as false minima

and maxima and was therefore constrained by setting the tension factor in the

interpolation program to 0.25 (scale of 0-1 where 0 is no smoothing and 1 is complete

smoothing). The resultant plots were compiled into an animated time series for each parameter using Adobe Creative Suite software. These animations were used to identify features of interest and preliminarily assess bio-physical interactions, particularly those associated with the transport of shelf waters and materials to the offshore environment. While CHL values seen in nearshore areas are typically visualized using a logarithmic scale, here a split color scale was used. This color scale consisted of distinct color palettes that were designed to simultaneously discern regions of high CHL (>5 mg m^{-3}), mid CHL (> 0.5 mg m^{-3}) and low CHL (> 0.5 mg m^{-3}) concentrations. This distinction allows the dynamics of CHL in all observed areas to be simultaneously discerned.

Physical Fields

Physical satellite measurements of SST, SSH, and wind fields were treated similarly to ocean color (i.e. GMT minimum curvature plotting, as described in the previous section). Additionally, SSH fields were plotted as contours to highlight SSH fronts and wind field vectors were drawn to detect wind direction. These fields were compared with ocean color fields to explore physical forcing of CHL enhancement.

Hypotheses

Initial observations of CHL variability within the NGMx system revealed that an overall seasonal CHL pattern for the NGMx east of the Mississippi River is not readily discernible. However, a peak in CHL observed in summer months for most years (~80%), seasonally similar to expected HCP development, suggested that HCPs are responsible for short-term, high-magnitude increases in summer CHL.

H1. It is hypothesized that the midyear (summer) peaks observed in the eastern NGMx CHL patterns are induced by HCP impingement.

As individual HCPs gradually lengthen southward over several days, thereby impacting surface waters along their paths at different times, the contribution to the CHL cycle was expected to be temporally offset with respect to latitude.

H2. It is hypothesized that the division of the eastern NGMx into 3 latitudinally distinct sub-regions will show that midyear (summer) peaks in CHL affect the sub-regions at a temporal offset due to the gradual extension of individual HCPs.

The modeled marine system described above, dipole eddy and/or LC and cyclonic eddy circulation features entraining the wind-driven eastward spread of the Mississippi River plume, points to advection as the primary process responsible for HCP formation.

H3. It is hypothesized that HCPs forming near and east of the Mississippi River delta in the NGMx concurrent with dipole eddies are the result of advection of shelf waters.

The advection of nutrients, shelf plankton species, and low salinity waters inherent to Case II riverine/shelf waters to the oligotrophic central Gulf was expected to impact phytoplankton biomass, primary productivity and bio-optical relationships.

H4. It is hypothesized that HCPs resulting from advection of Mississippi River influenced waters are significant contributors to offshore biogeochemical processes.

These hypotheses are addressed in the subsequent chapters of this thesis. In Chapter II a complete record of Gulf and NGMx bio-optical properties are evaluated to determine the role of HCPs within the seasonal and interannual ocean color cycles. Trends in Gulf bio-optical properties are considered across seasonal, annual and decadal time scales. In Chapter III a single well-defined HCP is examined to describe biogeochemical characteristics associated with HCPs and to determine physical

conditions supporting HCP formation. Chapter III has been published in the journal

Remote Sensing of Environment (Jones & Wiggert, 2015). Chapter IV assesses the

proposed river-wind-circulation marine system described in computer models of cross-

shelf transport in the NGMx via satellite observations of actual HCP events. Finally, in

Chapter V, a review of the major findings of the thesis is presented.

CHAPTER II

A SATELLITE STUDY OF BIO-OPTICS IN THE NORTHERN GULF OF MEXICO:

DECADAL, INTERANNUAL, SEASONAL AND EPISODIC SIGNALS

Introduction

The Gulf of Mexico (Gulf) is a semi-enclosed basin with both oceanic deep water processes and significant land-ocean interaction. The biogeochemical cycles of the Gulf determining ecosystem and biota health are subject to massive storms, river input, mesoscale eddies, and shifting seasonal wind patterns (Biggs & Muller-Karger 1994; Walker & Rabalais, 2006). These environmental conditions set up responses in phytoplankton distribution across the Gulf that drive satellite viewed chlorophyll-a signals (CHL) and bio-optical signals, both seasonally and long term.

By developing a climatology for CHL (1997 – 2007), Martinez-Lopez and Zavala-Hidalgo (2009) were able to show that shelf and shelf-break CHL in the Gulf are highly variable with little to no seasonal pattern. This is in direct contrast to the seasonal cycle dominance of off-shelf CHL (Muller-Karger, 1991). The seasonality of off-shelf waters is linked to the seasonal sea surface temperature (SST) patterns in the Gulf of high April-August SST and lower September-March SST (Chang & Oey, 2010; Muller-Karger et al., 2015). CHL cycles of high CHL in winter months, due to temperature dependent deepening of the mixed layer, and low CHL in summer months, due to shoaling of mixed layer, show little interannual variability in the satellite record (Muller-Karger et al., 2015). A secondary peak in CHL is noted in most years in the northeastern Gulf (Morey et al., 2005; Muller-Karger et al., 1991;). The peak is suggested to be due to Mississippi River plume intrusion to the eastern Gulf. When compared with both El Niño-Southern

Oscillation (ENSO) and Atlantic Multidecadal Oscillation (AMO), long term trends in CHL have not shown a notable change in central Gulf CHL values over decadal timescales, despite an increase of 0.17° C to 0.3° C per decade (1981-2011) in SST (Muller-Karger et al., 2015).

Determining the cycles and episodic contributions to alterations in phytoplankton distribution is necessary for understanding ecosystems in the northern Gulf of Mexico (NGMx). The validity of CHL for describing NGMx phytoplankton biomass distributions was set by Walker and Rabalais (2006), where they found that satellite observed CHL was quantifiable on the NGMx shelf from annual to weekly temporal resolutions. This study attempts to derive the seasonal, interannual, and decadal cycles of CHL as a baseline for the detection and interpretation of plumes of elevated CHL as high chlorophyll plumes (HCPs) entering the central Gulf from the NGMx shelf.

Additionally, the seasonal cycles of bio-optical properties (normalized fluorescence line height (FLH) and chromophoric dissolved organic material (CDOM)) are included to determine the relative seasonality of these properties to CHL and the impact of HCPs on bio-optical relationships in the NGMx. This analysis is supplemented with modeled primary productivity (NPP) estimates to evaluate any contribution of HCPs to the NGMx carbon budget.

Data and Methods

Data

Remotely sensed Level 3 mapped data ocean color parameters from NASA's Ocean Color Web (http://oceancolor.gsfc.nasa.gov/) were obtained to evaluate bio-optical conditions in the Gulf. The data include 4 and 9 km MODIS-Aqua (chlorophyll

concentration (CHL), normalized fluorescence line height (FLH) and colored dissolved organic matter (CDOM)) from 2003 – 2011 and SeaWiFS (9 km CHL) from 1998 – 2002. Measurements of CDOM are reported as unitless indices based on the description from NASA's Ocean Color Web (oceancolor.gsfc.nasa.gov/DOCS/Ocean_Level-3_SMI_Products.pdf). The global data sets were processed with MATLAB to extract NGMx values bounded by coordinates 98° W, 82° W, 24° N and 31° N. Gulf extracted values were mapped for visualization and feature detection using the University of Hawaii's Generic Mapping Tools (GMT) software (Wessel & Smith, 1998). Distortion artifacts were reduced in the data by anti-aliasing before the data was gridded using a surface gridding algorithm. Detailed documentation of the anti-aliasing and surface gridding routines can be accessed through the GMT website (http://gmt.soest.hawaii.edu/). Following extraction and plotting, time series fields of each parameter were animated so as to highlight the temporal evolution. These animations allowed for visual detection of temporal patterns and anomalous features, such as filamentous HCPs resulting from the advection of shelf waters due to cross-shelf transport. While the broad range of CHL values seen in nearshore areas are typically visualized using a logarithmic scale, here a split color scale was used allowing the dynamics of CHL in all observed areas to be simultaneously visualized.

Modeled net primary productivity (NPP) estimates were obtained from Oregon State University's Ocean Productivity website (http://www.science.oregonstate.edu/ocean.productivity). The full temporal range of Vertically Generalized Productivity Model (VGPM) described in Behrenfeld and Falkowski (1997) and the Carbon based Productivity Model (CbPM) described in

Behrenfeld et al. (2005) and Westberry et al. (2008) were retrieved. Estimates for NPP based on 8-day SeaWiFS and MODIS-Aqua CHL values were obtained. The CbPM, which differs from other satellite-NPP models in its determination of light attenuation in the water column and use of backscatter and absorption to determine NPP, was used in the analyses presented below. CbPM estimates of NPP can greatly improve accuracy by accounting for changes in the physiology of phytoplankton species, with changes in biogeochemical factors, an important consideration for HCP impingement to the oligotrophic Gulf and resultant influx of optically complex and species differentiated waters. The validity of CbPM for estimating NPP in oligotrophic Gulf waters and near the Mississippi River outflow is shown in Jones and Wiggert (2015), where they establish that CbPM estimates are in the range of previously reported *in situ* productivity values.

Bathymetry for the NGMx was obtained from the National Geophysical Data Center (NGDC) (http://www.ngdc.noaa.gov/mgg/coastal/crm.html) Coastal Relief Model (CRM). The modeled fields were downloaded from a compiled ASCII file with a resolution of 15 arc-seconds.

Methods

Three selected regions of interest (NGMx, Open Water and Study Area) were chosen with the aim of understanding how CHL variability in the NGMx is linked to environmental factors (Figure 2.1). For the purposes of this study, NGMx refers to waters bounded by the coordinates 98° W, 82° W, 31° N and 24° N (Figure 2.1). The NGMx region includes coastal, shelf and deep waters with distinct environmental conditions and seasonal influences. The NGMx region provides insight to how the northeastern Gulf fits into the overall trend in CHL variability within the NGMx. The Open Water region is

selected to minimize shelf and coastal influences on the CHL cycle, thus providing a baseline for analysis influenced primarily by deep ocean and atmospheric conditions. The Study Area is selected within the NGMx highlighting the region with high HCP impingement. The Open Water denotes the region bounded by the coordinates 93° W, 85° W, 27° N and 24° N (Figure 2.1). This region was selected to include surface waters above the deep basin and thus minimize shelf and coastal water influence to the CHL cycle. Doing so provides insight to the Gulf CHL cycle due solely to oceanic and atmospheric conditions (e.g. eddy-pumping, ambient temperature). This isolation provides a baseline for interpreting Study Area dynamics and attributing observations to specific events. Within the NGMx several locations were observed to be prone to HCP formation (e.g. northeastern Gulf, Louisiana-Texas shelf, western Gulf). To isolate Mississippi River plume induced HCPs suggested by the previously mentioned model studies, the northeastern Gulf was chosen as the region of interest. The denoted Study Area is inclusive of the area within the northeastern Gulf where HCPs are expected following the modeling studies of Morey et al. (2003) and Schiller et al. (2011). The bounds of this region (88° W, 86° W, 30° N and 25° N (Figure 2.1) were determined through examination of a number of HCP incidents affecting the northeastern Gulf. This region was selected to include waters above a gradient of depths in the area where HCPs tend to develop as a result of the dipole eddy entrainment of the Mississippi River eastern spread.
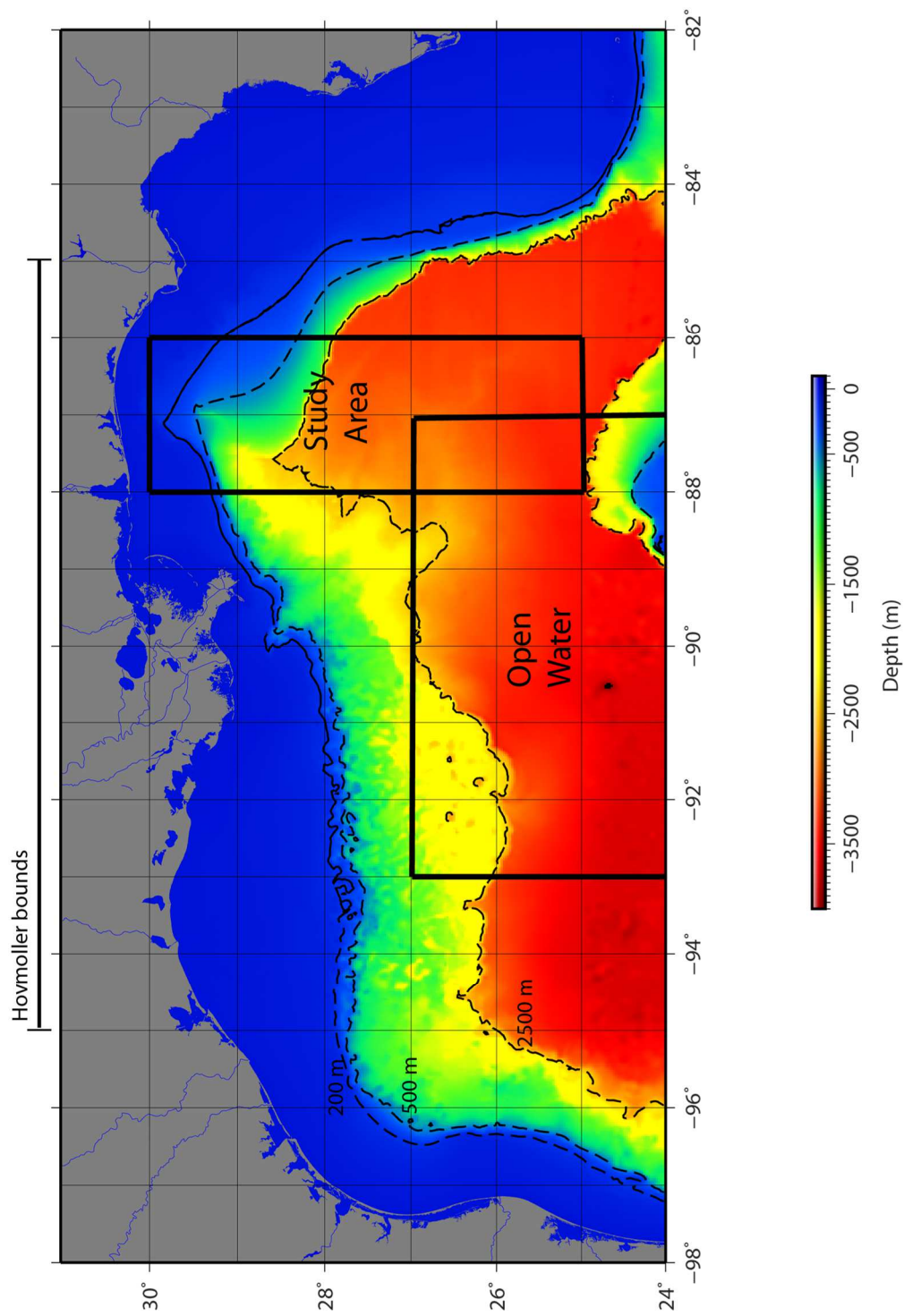
Figure 2.1. Bathymetry (m) for the Gulf with analysis regions outlined. The NGMx region consists of all valid (marine) points in the Figure, the Open Water region is selected to minimize shelf water inclusion for central Gulf comparison and the Study Area encompasses the region frequented by substantial eastward HCP.

To determine the role of HCPs in the NGMx, and in particular the relationship between HCPs and CHL variability, the observed seasonal cycle and interannual variability of CHL is described. The combined 14-year SeaWiFS (1998-2002) and MODIS-Aqua (2003-2011) 8-day CHL dataset is spatially-averaged for regions of interest (NGMx, Open Water and Study Area (Figure 2.1) to explore how CHL varies temporally within each defined region. The spatially-averaged values are then temporally-averaged to simulate a mean year for each region, allowing description of the seasonal cycle. An apparent increase in CHL amplitude, as well as increasing enhancement-peak frequency over time, motivated the exploration of decadal trends in CHL. To explore this, a mean value of CHL was found for each year within the dataset of spatially-averaged CHL value. The mean annual CHL values were plotted with the corresponding annual minima and maxima. A simple linear regression analysis was performed for the decadal mean, maxima and minima, respective to time, to determine long term (14 year) change.

Monthly composites of CHL for the 2002 – 2011 ocean color MODIS-Aqua satellite record are used in an empirical orthogonal function analysis (EOF) to determine the contributing modes to CHL variability in the NGMx. For a single variable (e.g. CHL), EOF analysis decomposes a data set to compute spatial variability and time series values for each mode contributing to the overall variability of the variable. EOF also calculates the percent contribution of each mode to the overall variability. In a sense, EOF expresses the original time series of data as a sum of individual modes. Here, latitude and longitude boundaries were reset in the EOF computation to minimize extraneous spatial contributions to the CHL variance in the Study Area. To perform the EOF, satellite CHL

pixel values were first normalized by the temporal mean at each pixel location. An

autocovariance matrix, or matrix of covariance among the normalized CHL pixel values,

was then calculated and used to find eigenvalues and eigenvectors. From these, EOF

amplitudes and mode variance percentages were computed. Eigenvalues were then

plotted to show spatial variability of CHL modes.

<div align="center">Results</div>

Throughout the following analyses, each year is described in 8-day periods (46

per year), rather than 7-day weeks to remain consistent with the 8-day composite ocean

color measurements. Reference to each period is made by the date for the first day of

each period (e.g. Jan-01-2009 refers to the 8-day period beginning on the first day of

2009 or period-1 of 2009).

Trends in CHL Variability

NGMx seasonal. Overall, the NGMx spatially-averaged CHL observations show

high variability throughout the year as smaller sections of the Gulf contribute to the CHL

signal at different times, although a seasonal cycle supersedes local maxima. A

comparison of spatially-averaged NGMx CHL fields for the 14-year ocean color dataset

reveals a clear seasonal CHL pattern of elevated CHL in fall and winter months, with

decreased CHL in spring and summer months (Figure 2.2a). Differing seasonal

variability linked to specific regions, primarily shelf regions, lead to a variable mean

CHL pattern; however, regional perturbations do not supersede the overall seasonal

pattern. CHL variability across the NGMx is somewhat lower during late spring and mid-

summer months (Figure 2.2b). The minimum NGMx value of CHL for the spatially- and

temporally-averaged year (Figure 2.2b) occurs during the 8-day period beginning

August-5, with a mean value of 0.47 mg m^{-3}. The maximum NGMx CHL value for the

spatially- and temporally-averaged year (0.88 mg m^{-3}) occurs during the period beginning

December-27. The minimum and maximum are both approximately 2 standard deviations

(st. dev. = 0.12 mg m^{-3}) from the annual mean value of 0.67 mg m^{-3}.
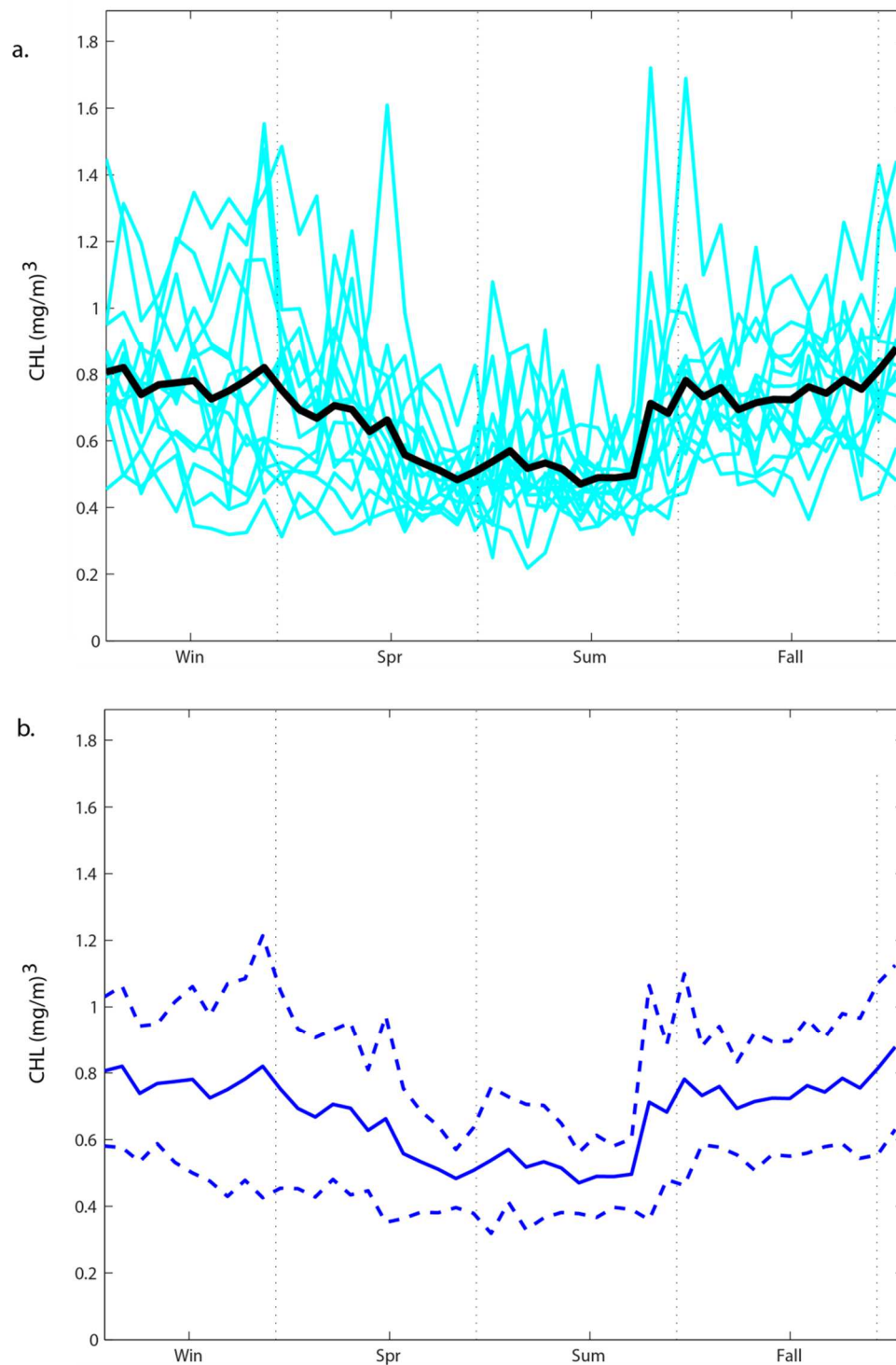
Figure 2.2. Spatially-averaged NGMx CHL. (a) CHL values from SeaWiFS and MODIS-Aqua are plotted for years 1998-2011 in blue. The spatially- and temporally-averaged 14-year mean CHL for the NGMx region is plotted in black. (b) Spatially- and temporally-averaged 14-year mean CHL and standard deviation. The CHL mean is plotted (solid line) with corresponding +/- standard deviation (dashed lines).

NGMx interannual. A 14-year time series of spatially-averaged NGMx CHL is shown in Figure 2.3a. The mean CHL value is the same as the spatially- and temporally-averaged mean (0.67 mg m^{-3}), but without temporally-averaging the individual years, the standard deviation among the measurements increases to 0.24 mg m^{-3}. Peaks indicative of CHL enhancement (defined here as CHL > 2 standard deviations above the mean or 0.48 mg m^{-3}) occur 15 times in the 14-year data set, or with an approximate frequency of 1.1 enhancement-peaks/yr (Table 2.1). The actual range of enhancement-peaks/yr is 0-4, with six of the 14 years experiencing no peaks of CHL greater than 2 standard deviations above the mean and two years experiencing more than 2 enhancement-peaks. The CHL enhancement-peaks occur in all seasons, yet with a higher frequency in winter months (5 of 15). The maximum NGMx CHL is seen during the period beginning September-6-2005 with a value of 1.72 mg m^{-3} (more than 4 standard deviations above the mean). This differs from the seasonal maximum reported above, which occurs in winter. The minimum NGMx CHL of the 14-year time series was recorded at the period beginning on July-12-2000 with a value of 0.22 mg m^{-3}, revealing that the spatially-averaged CHL does not fall to < 2 standard deviations below the mean at any point.

Table 2.1

Gulf of Mexico CHL enhancement-peaks

	NGMx Enhancement-Peaks	Open Water Enhancement-Peaks	Study Area Enhancement-Peaks
1998	177	1 41 73	1 65 177 201
1999			225
2000			
2001		9 33	153 193
2002		1 57	
2003	73	17	169
2004	353	361	209
2005			
2006		41	
2007	57	33	49
2008	129 185	17	177
2009	305 329 361	33	177
2010	1 41 81 233	17 41 57 81	41 81 233
2011	113 177	33	33 177

Note. The day of year (DOY) for each observed enhancement-peak across the regional 14-year spatially averaged time series. For reference winter months are DOY 355-80, spring months are 81-170, summer months are 171-263 and fall months are 264-354.

Although the year-to-year CHL means oscillate between increasing and decreasing years (Figure 2.3b), linear regression analysis shows that the mean annual NGMx CHL is increasing by 0.012 mg m^{-3} yr, less than the standard deviation of 0.12 mg m^{-3} yr. The linear 14-year maxima trend is also increasing (0.034 mg m^{-3} yr), and the

minima is relatively constant over time (-0.00086 mg m^{-3} yr). The differentiation between the minima and maxima trends reflects the increasing distance between the minima and maxima amplitudes over the 14-year record, indicating more anomalous CHL concentrations and perhaps greater extreme forcings. In concurrence with Siegel et al. (2013), this result is hampered by the limited temporal availability of satellite data. In truth, 14 years of data does not allow a comparison of multiple decades, therefore it is not known whether the decadal trends seen over the full dataset are cyclical, or represent a long term shift in CHL concentration. As found here, Siegel et al. (2013) similarly find more interannual than long-term variability in the global SeaWiFS CHL record.

Figure 2.3. 14-year time series of NGMx CHL. (a) The 14-year spatially averaged 8-day CHL composites are plotted to highlight interannual variability. Horizontal lines are drawn at the mean (0.67 mg m^{-3}) and enhancement-peak threshold (1.15 mg m^{-3}). (b) The NGMx annually averaged mean CHL (blue), annual CHL maxima (black and red) and annual CHL minima (black and green).

Open Water seasonal. A comparison of spatially-averaged CHL fields over the 14-year ocean color dataset is again performed for the Open Water region. Within the Open Water region, variability is low relative to the strong seasonal cycle (Figure 2.4a.) The spatially- and temporally-averaged mean CHL year is unimodal with high CHL during winter months and low CHL during summer months (Figure 2.4b). Variability is also greater during winter months, suggesting that deep water mixing during colder months drives the seasonal cycle. The spatially- and temporally-averaged CHL mean for the Open Water region is 0.13 mg m^{-3}, with a standard deviation of 0.04 mg m^{-3}. The minimum CHL value for the spatially- and temporally-averaged year (0.08 mg m^{-3}) is less than one standard deviation from the mean and occurs during the period beginning June-17. The maximum is observed for the period beginning February-2 with a spatially- and temporally-averaged CHL value of 0.21 mg m^{-3}, approximately 2 standard deviations above the mean.
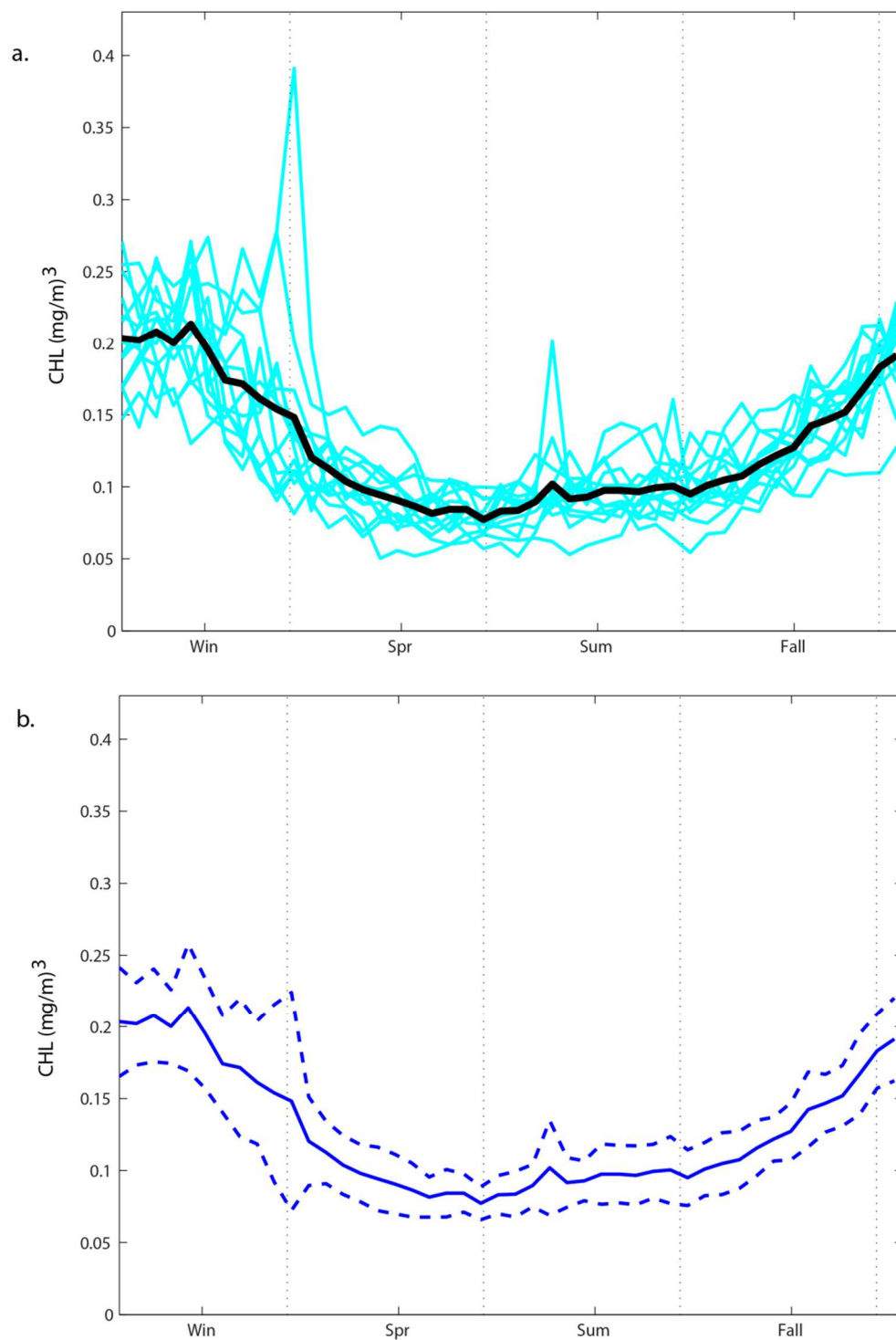
Figure 2.4. Spatially-averaged Open Water CHL. (a) CHL values from SeaWiFS and MODIS-Aqua are plotted for years 1998-2011 in blue. The spatially- and temporally-averaged 14-year mean CHL for the Open Water region is plotted in black. (b) Spatially- and temporally-averaged 14-year mean CHL and standard deviation. The CHL mean is plotted (solid line) with corresponding +/- standard deviation (dashed lines).

Open Water interannual. The full 14-year time series of CHL averaged across the Open Water region is shown in Figure 2.5a. Here the spatially-averaged mean value is again 0.13 mg m^{-3}, and the standard deviation is slightly higher than the temporally-averaged value at 0.05 mg m^{-3}. Keeping the same definition of enhancement-peaks (CHL > 2 standard deviations above the mean), the frequency of 1.3 enhancement-peaks/yr (a total of 18) is similar to the NGMx region. In the Open Water region, the enhancement-peaks are evenly distributed across the 1998-2011 observational period and tend to occur in clusters during winter months (Table 2.1), reflective of the strong seasonal cycle. The only enhancement-peak to occur outside of the winter season is observed during the first week of spring in 2010. This peak is the regional maximum of spatially-averaged CHL over the 14-year dataset at 0.39 mg m^{-3}. The minimum CHL value observed is 0.05 mg m^{-3} and occurs in the period beginning on April-30-2009, which is six weeks earlier than the temporally-minimum noted above (June-17). Interestingly, the maximum CHL value is more than 5 standard deviations above the mean and the minimum is less than 2 standard deviations below the mean. This range is nearly identical to that of the NGMx region despite the difference in variability and the difference in timing of the minima and maxima.

The Open Water regional annual CHL means, minima, and maxima were derived to explore decadal trends (Figure 2.5b). Over the 14-year time series, the annual mean CHL remained generally stable at -0.002 mg m^{-3} yr^{-1}. This contrast to the NGMx region suggests that shelf and/or coastal drivers are the source of the observed increase in CHL across the Gulf. Maxima did increase over time (0.005 mg m^{-3} yr^{-1}). The annual minima decreased over time (0.002 mg m^{-3} yr^{-1}. The divergence of amplitudes points to

decreasing stability in the marine environment and suggests that the annual CHL

maxima, in the Open Water region, are more sensitive to episodic influences than the
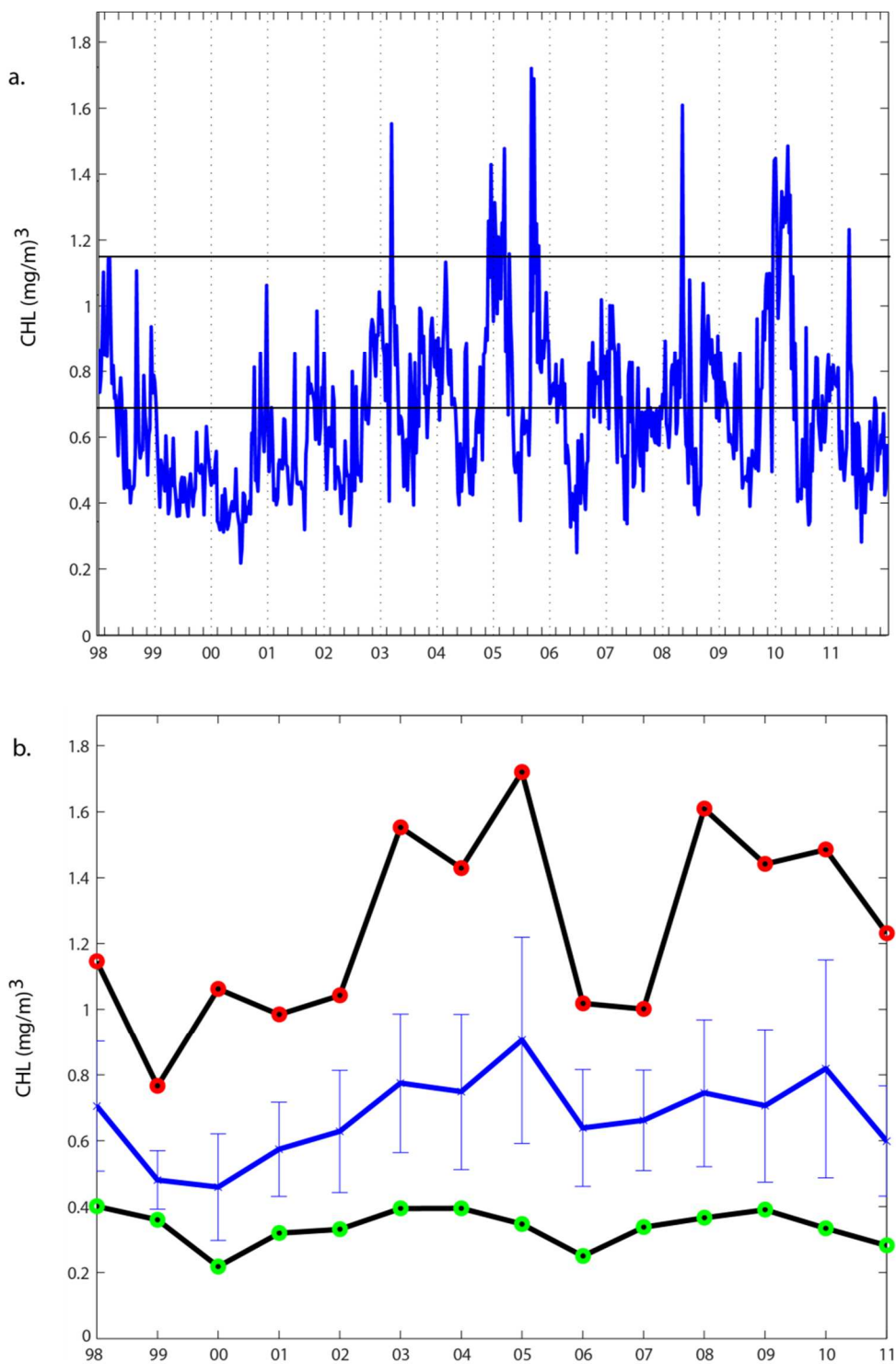
mean concentrations.
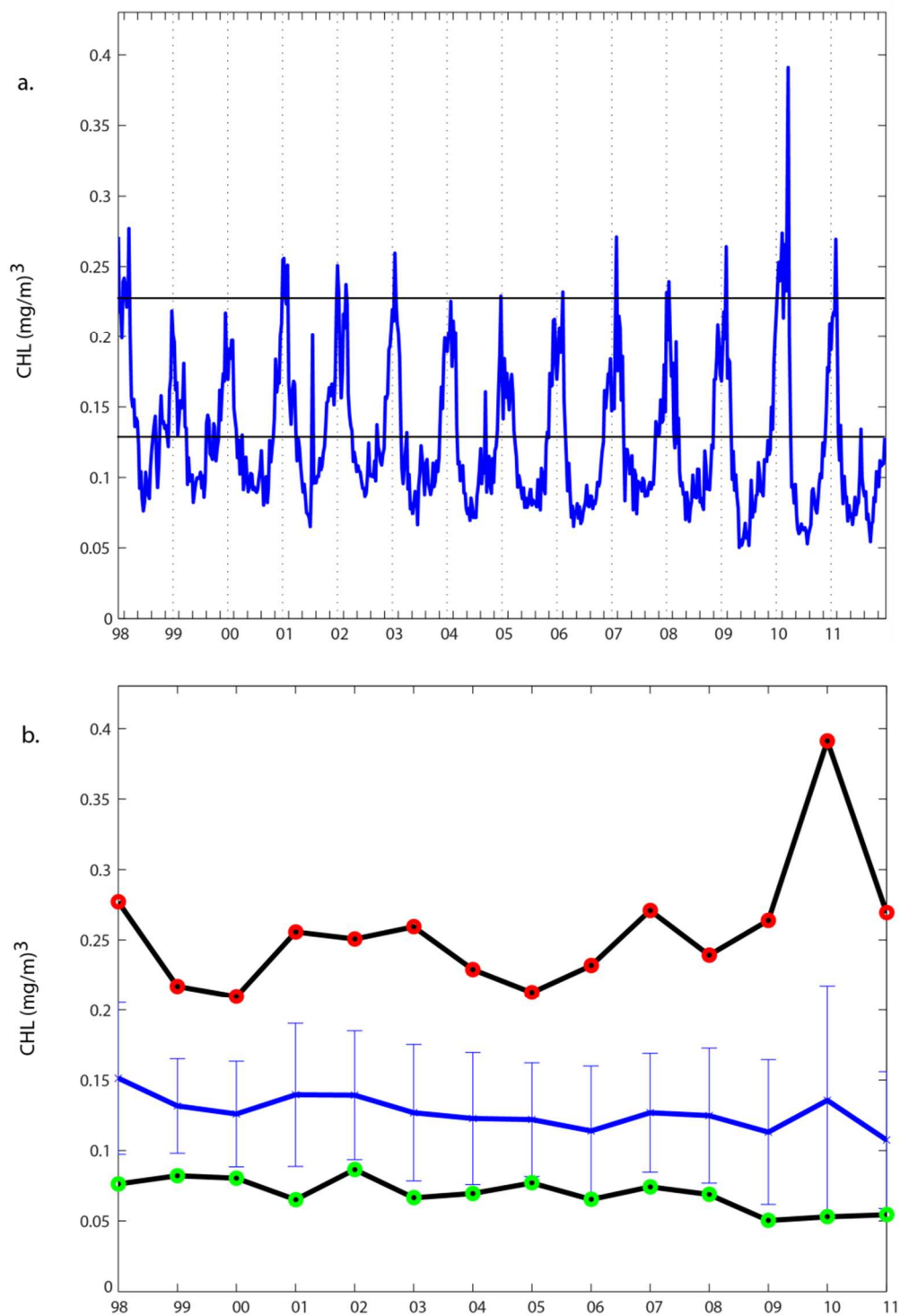
Figure 2.5. 14-year time series of Open Water CHL. (a) The 14-year spatially averaged 8-day CHL composites are plotted to highlight interannual variability. Horizontal lines are drawn at the mean (0.13 mg m^{-3}) and enhancement-peak threshold (0.23 mg m^{-3}). (b) The Open Water annually averaged mean CHL (blue), annual CHL maxima (black and red) and annual CHL minima (black and green).

Study Area seasonal. Variability in the Study Area, as depicted by the spatially-averaged CHL fields in Figure 2.6a, is concentrated in the spring and summer months. Fall is relatively stable and similar in pattern to the Open Water region. The spatially- and temporally- averaged seasonal CHL cycle in the Study Area is generally bimodal with a main peak in the spring/summer and elevated values in winter (Figure 2.6b). This seasonal bimodality is likely due to contrasting influences of offshore seasonal variability and shelf/coastal processes (e.g. riverine input). The greatest CHL peaks are seen during summer, with values high enough to overcome the expected seasonal cycle described in the Open Water region (Figure 2.6a). The timing and magnitude of the midyear peaks suggest that CHL enhancement processes originating in shelf waters, possibly due to coastal processes, are responsible for the elevated summer CHL measured in the Gulf. The spatially- and temporally-averaged mean is 0.24 mg m^{-3} with a standard deviation of 0.06 mg m^{-3}. The minimum CHL value for the spatially- and temporally-averaged year (0.15 mg m^{-3}) is less than two standard deviations from the mean. The maximum spatially- and temporally-averaged CHL value of 0.42 mg m^{-3} is nearly 3 standard deviations above the mean.
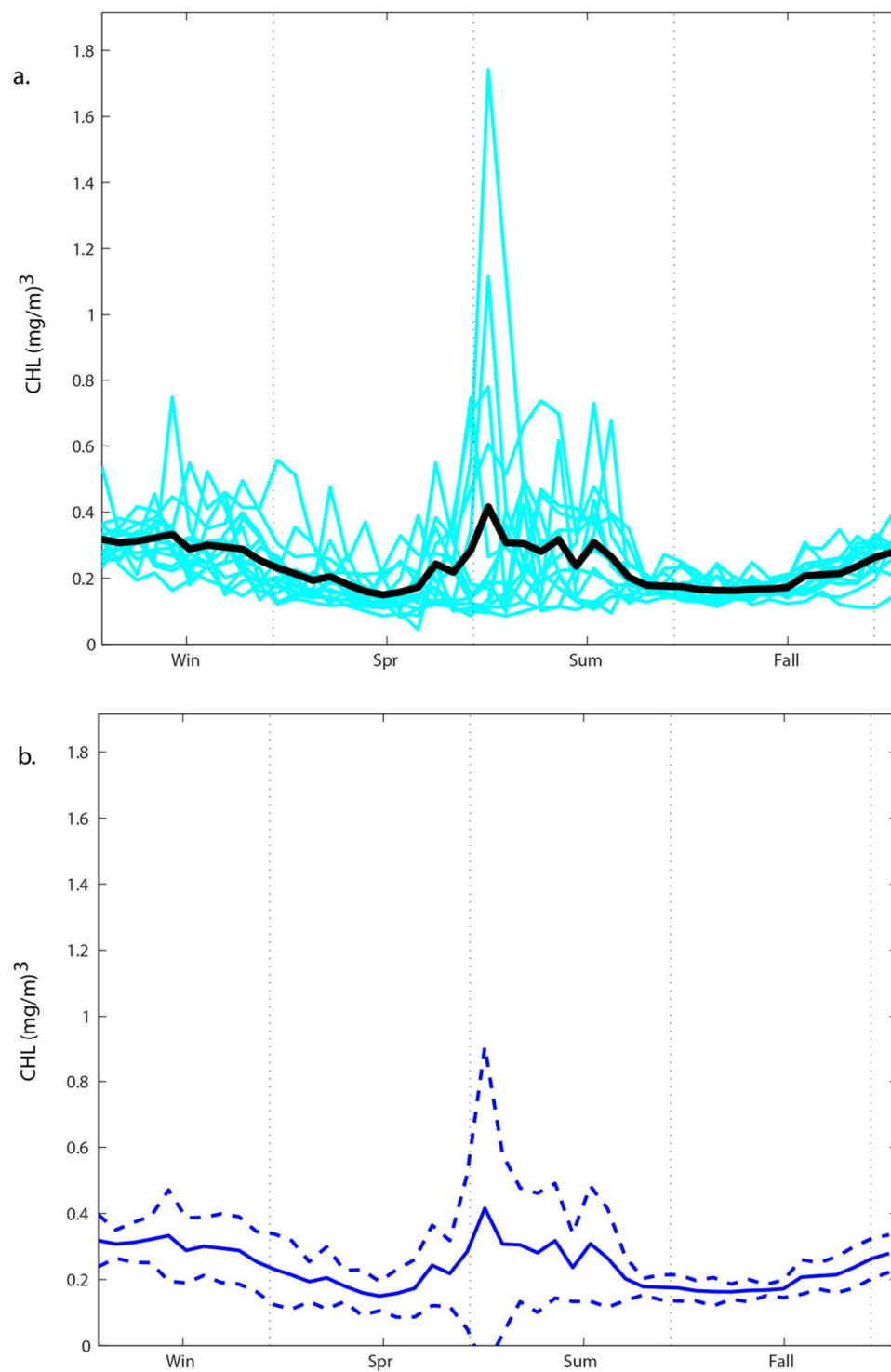
Figure 2.6. Spatially-averaged Study Area CHL. (a) CHL values from SeaWiFS and MODIS-Aqua are plotted for years 1998-2011 in blue. The spatially- and temporally-averaged 14-year mean CHL for the Study Area is plotted in black. (b) Spatially- and temporally-averaged 14-year mean CHL and standard deviation. The CHL mean is plotted (solid line) with corresponding +/- standard deviation (dashed lines).

Study Area interannual. In Figure 2.7a the Study Area 14-year time series of spatially-averaged CHL is plotted. A mean of 0.24 mg m^{-3} is found for the region with a standard deviation of 0.14 mg m^{-3}. The threshold for enhancement-peak designation is 0.51 mg m^{-3} (equivalent to 2 standard deviations > mean). In all, 17 enhancement-peaks are recorded for the Study Area or an average frequency of 1.2 enhancement-peaks/yr (Table 2.1). Years 1998 and 2010 have the highest enhancement-peak frequencies of 4 and 3 per year respectively. Ten of the fourteen years observed experiences at least one enhancement-peak, typically during the seasonal midyear peak timeframe noted above. Nine of the 17 enhancement-peaks fall within this summer midyear peak range, three occur in winter and two in spring. No enhancement-peaks are observed during the stable fall months. The enhancement-peak measured during the period beginning June-26-2008 is the 14-year maximum CHL concentration of 1.74 mg m^{-3}. The maximum is more than 11 standard deviations above the mean and is observed the same year as the NGMx 14-year maximum CHL value, albeit approximately 3 months later. The year 2008 is not anomalous for the Open Water region, indicating that the unusually high enhancement-peaks for the Study Area and NGMx regions are due to shelf/coastal processes not affecting the deep ocean surface waters. The minimum CHL concentration recorded for the Study Area was 0.045 mg m^{-3} during the period beginning May-25-2007.

A plot of the annual CHL means, minima and maxima (Figure 2.7b) shows the trend in these data over the full range of CHL measurements. Here the mean CHL does not show a significant change over time. The increase of 0.0002 mg m^{-3} yr^{-1} over the 14-year data series is the most constant of all three evaluated regions. The regional annual CHL minima also change little over time (-0.0031 mg m^{-3} yr^{-1}). The maxima, however,

does show an increasing trend in CHL (0.032 mg m^{-3} yr^{-1}) as well as stronger oscillations that the other measurements for this region. The rate of change in maxima over time is less striking than that of the NGMx region, but is similar in oscillation. As with previous comparisons, this likely points to the strong influence of coastal/shelf processes such as continental runoff and coastal upwelling on the two regions.
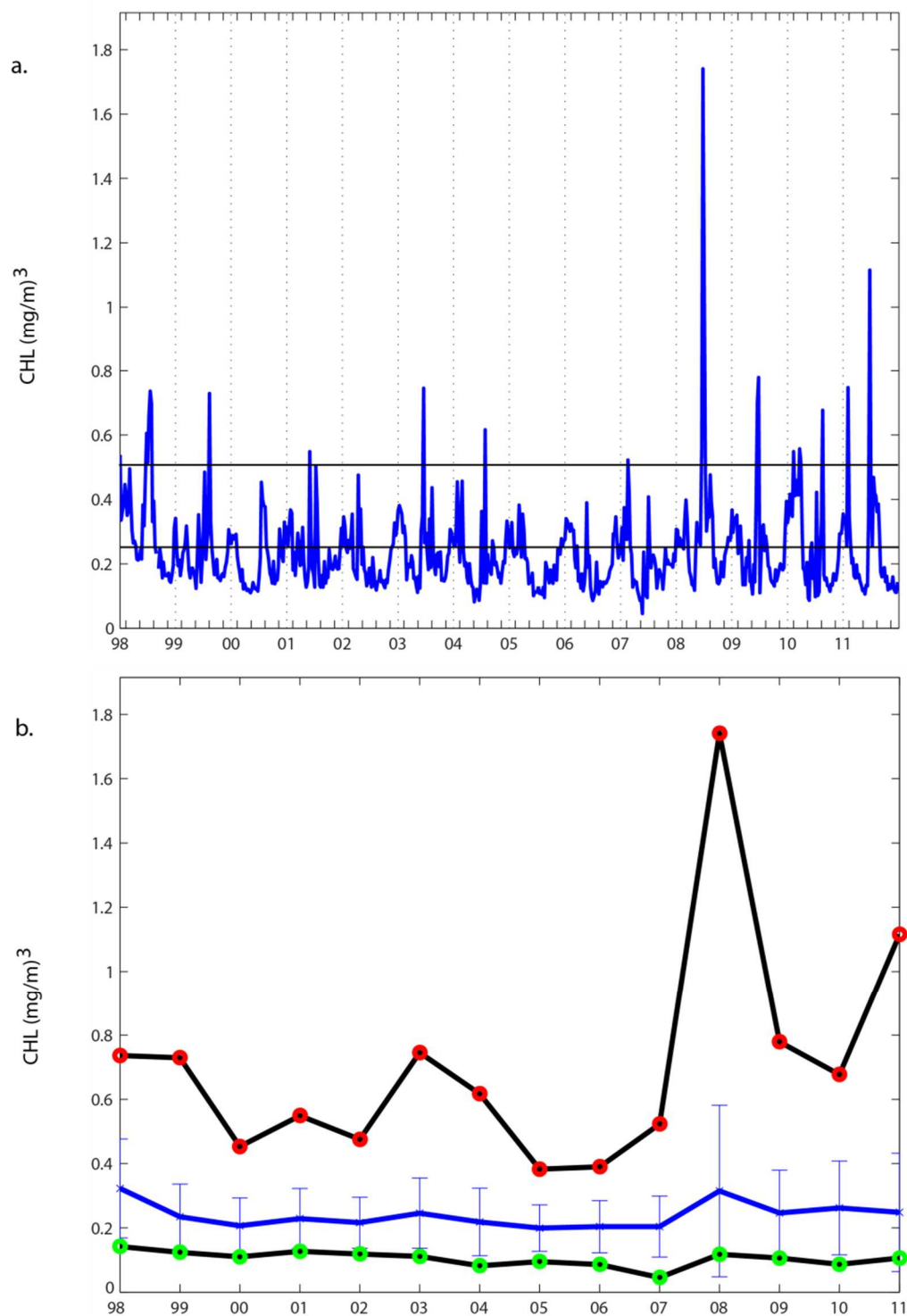
Figure 2.7. 14-year time series of Study Area CHL. (a) The 14-year spatially averaged 8-day CHL composites are plotted to highlight interannual variability. Horizontal lines are drawn at the mean (0.24 mg m^{-3}) and enhancement-peak threshold (0.51 mg m^{-3}). (b) The Study Area annually averaged mean CHL (blue), annual CHL maxima (black and red) and annual CHL minima (black and green).

HCPs and Bio-Optical Analysis

To determine the role of HCPs in the seasonal and interannual bio-optical cycles of the Gulf, the 8-day composites of CHL, FLH, CDOM, and CbPM are analyzed. Where possible, the full 14-year series of SeaWiFS/MODIS-Aqua data are utilized, but for comparison among parameters only MODIS-aqua observations are shown. The results show that the temporal patterns of HCPs do not align with the temporal patterns of Study Area midyear peaks, as hypothesized in preliminary observations, but do share some similarities. Further, the results show that the characteristics of bio-optical parameters diverge significantly from typical conditions when associated with HCPs.

HCPs and CHL Cycles

HCPs (> 0.5 mg m^{-3})extending from the Mississippi River delta to the Study Area and reaching southward to at least 28° N are listed in Table 2.2. An average of 2.7 HCPs/yr or 37 total HCPs manifest within the Study Area over the 14-year satellite record. The actual count of HCP/yr ranges from 0 in 2010 to 5 in years 2005 and 2011. The HCPs vary in persistence and spatial coverage as discussed in the following chapters. HCPs are more likely to occur in spring and summer with 16 and 15 incidents, respectively, but are observed in every season. A catalog of the CHL composite images associated with the HCPs shows that HCP length is associated with timing (Figure 2.8), summer HCPs tend to extend south of 27° N and spring HCPs typically remain more northward. As in the CHL cycle analyses above, the years 1998, 1999, 2009 and 2010 are anomalous for HCPs in that no recorded HCPs extend beyond to 27° N within the Study Area. Note that the Study Area is chosen to specifically explore HCPs extending

southeastward of the Mississippi River delta, therefore the lack of HCPs in the anomalous

years could indicate that either no extensive HCPs formed or that extensive HCPs during

these years were formed west of the Study Area.

Table 2.2

HCP occurrences in the NGMx

	DOY
1998	265
1999	65,113,137
2000	201
2001	81,153,193,279
2002	89
2003	105,121,161,264
2004	121,209,249,265
2005	65,89,137,193,217
2006	145,201,209
2007	153,185,217,241
2008	185
2009	113
2010	-
2011	73,105,169,177,217

Note. The day of year (DOY) for each observed HCP within the 14-year spatially averaged time series extending to or beyond 28^0 N.

For reference winter months are DOY 355-80, spring months are 81-170, summer months are 171-263 and fall months are 264-354.

Figure 2.8. Catalog of HCP events in the NGMx. The 8-day CHL composites of periods corresponding to the start date of HCPs are shown for years 1998-2011.

In Figure 2.9, time series of individual years for the Study Area full satellite record are plotted in conjunction with HCP occurrence to investigate links between HCPs and seasonal CHL. In particular, the hypothesized link to midyear peaks is investigated. The CHL data are spatially-averaged for the entire Study Area region, and the HCPs are marked as the first 8-day period on which they meet the criteria for inclusion. For most HCPs, this is the only time period involved; however, some HCPs do span multiple 8-day periods and/or appear in the satellite record before meeting inclusion criteria. The plots show that midyear peaks and HCPs are not necessarily coincident. Although HCPs are observed during midyear peak timing, they span a much larger temporal range and are not always indicated during midyear peaks. This suggests that HCPs are episodic in nature, despite their relative seasonal prevalence.
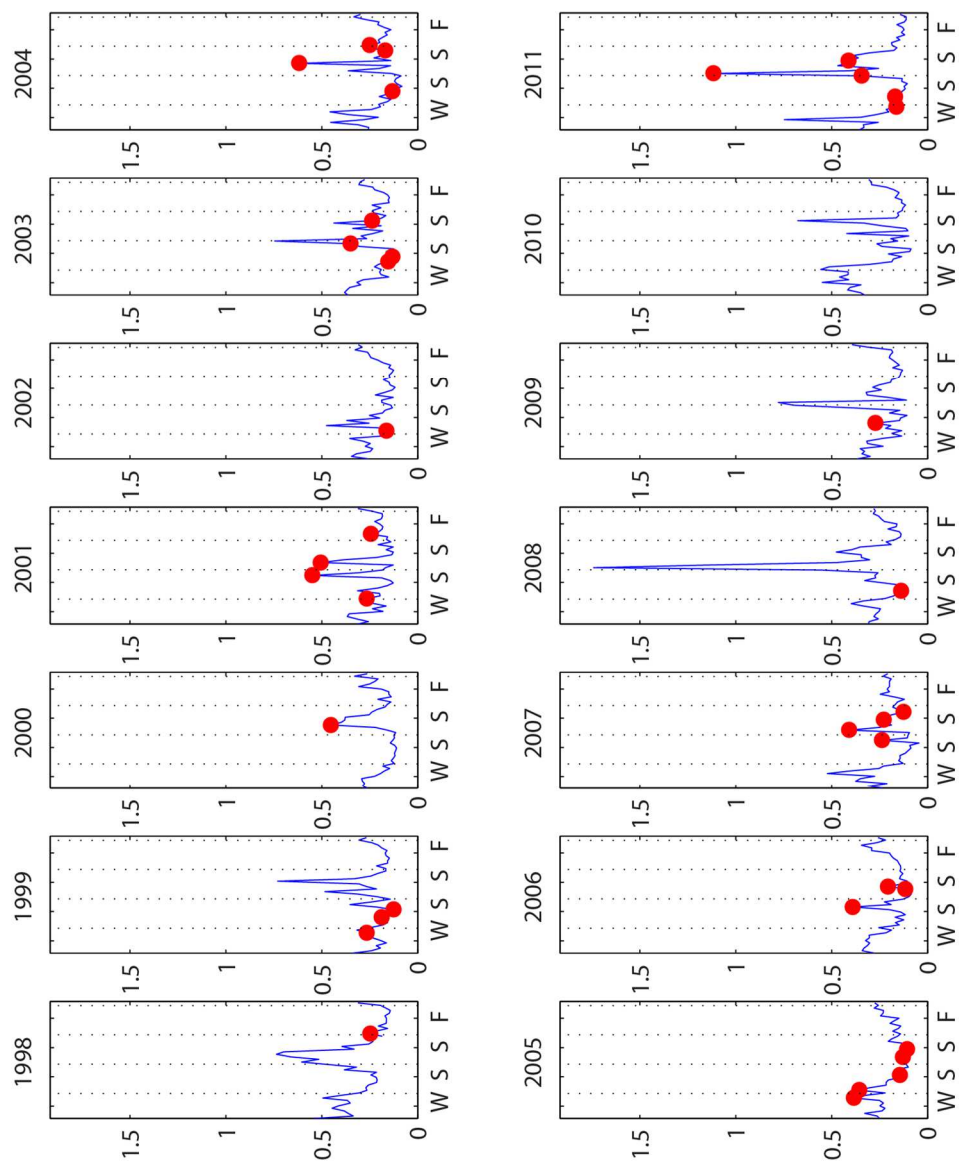
Figure 2.9. Study area midyear peaks and HCPs. The time series of spatially-averaged CHL for each year 1998-2011 is plotted in blue. The HCPs from Table 2.2 are marked in red to show the relationship between CHL magnitude and HCP occurrence as well as interannual HCP frequency.

Although episodic and infrequent, implication to the importance of HCPs to the NGMx CHL dynamic is shown through empirical orthogonal function analysis (EOF), as seen in Figure 2.10. Modes 1-4 contributed to 90.29% of the CHL variance, therefore, to eliminate mathematical noise, only these modes were considered (Figure 2.10). The time series of Mode 1 follows a seasonal pattern with relatively low interannual variability. Mode 1 accounts for 62.71% of regional variance and suggests that the region is primarily sensitive to seasonal cycles of CHL concentration. Mode 2 is also seasonal, although with increased interannual variability. The distribution map associated with mode 2 suggests that mode 2 variance is due to seasonal river discharge. Mode 3 distribution indicates that CHL concentration oscillates from nearshore to off-shore in the vicinity of the Mississippi River delta. This is consistent with HCP conditions as typically constrained high CHL waters are able to spread east of the Mississippi River delta due to seasonal winds. Further, the Mode 3 time series shows a similar pattern to that suggested in Table 2.2 for HCP occurrence. Differences between the table and Mode 3 may be contributable to differences in spatial domain. Mode 4 does not immediately demonstrate a link to known phenomena in the region; however, the distribution map does suggest an oscillation between CHL magnitude east and west of the Mississippi River delta.
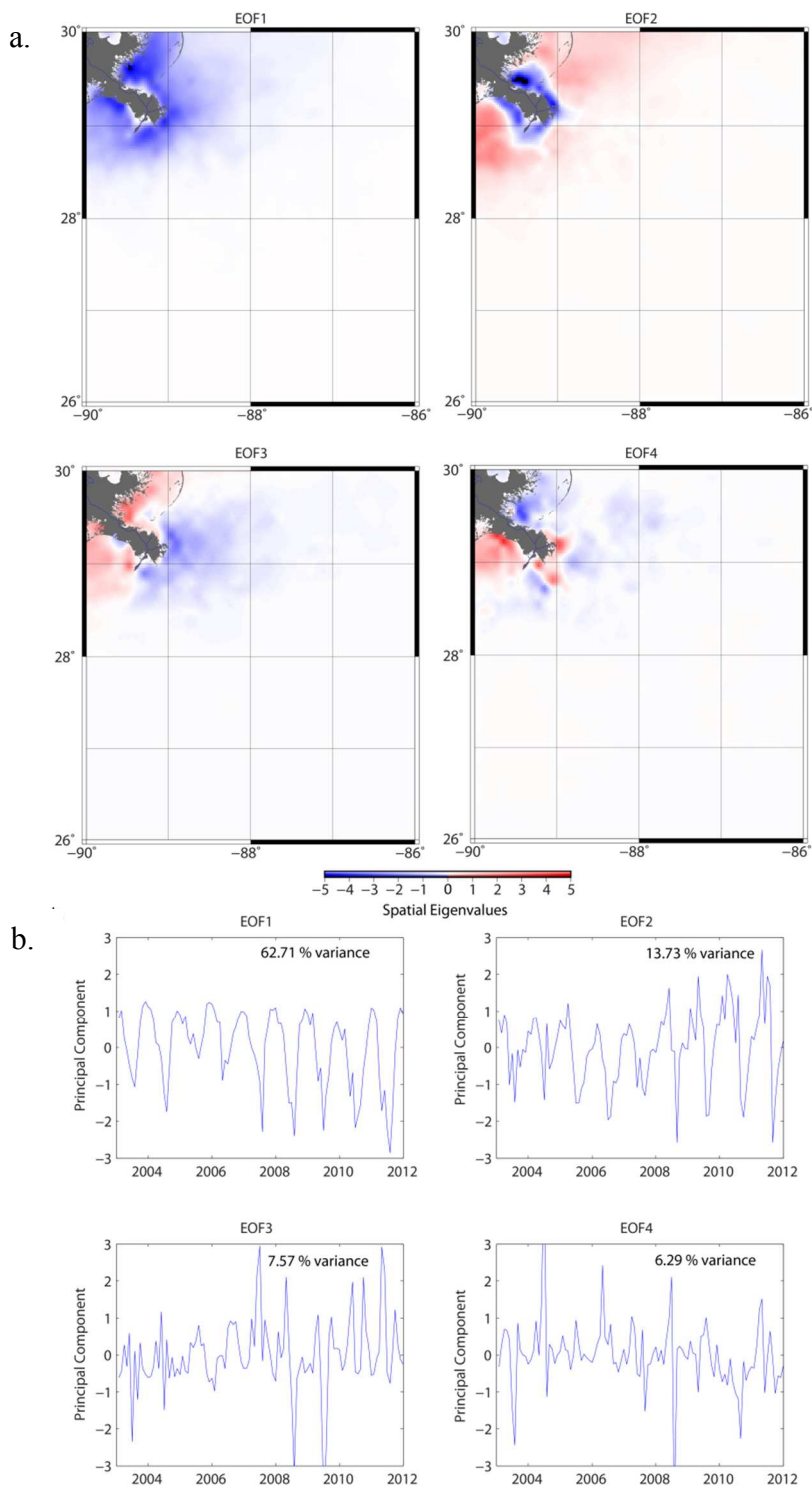
Figure 2.10. EOF reconstruction of CHL in the NGMx. Monthly composites of CHL for the 2002 – 2011 ocean color satellite record are used in the EOF analysis to determine the contributing modes to CHL variability in the NGMx. (a). Reconstructed time series of the first 4 EOF modes. (b). Distribution of CHL for each of the first 4 EOF modes.

HCP Influence on Bio-Optical Ratios

The MODIS-Aqua ocean color data set (2002-2011) was evaluated to provide

insight to the effect of HCPs on bio-optical properties within the Study Area. Parameters

chosen were CHL, CDOM and FLH with the intent to determine the extent of the HCP

impact on the regional processes and distinguish shelf/riverine waters (CDOM heavy)

from nutrient stimulated offshore waters (CDOM deplete). With that aim the 10-year

MODIS-Aqua parameters were spatially- and temporally- averaged (Figure 2.11a-c) to

reflect the typical conditions at selected latitude bands within the Study Area. Added to

these were corresponding data plots from the CbPM estimates of NPP (Figure 2.11d).

Both the CHL and FLH fields follow a bimodal pattern of high winter—low spring—

high summer—low fall values. CHL summer highs vary in relative amplitude to winter

highs with distance to the shelf (i.e. nearest the shelf the summer high is dominant and

farther offshore the winter high is dominant). FLH summer highs (maximum of 0.007 W

m^{-2} μm^{-1} sr^{-1}) are minor compared to winter highs (maximum of 0.011 W m^{-2} μm^{-1} sr^{-1})

across all bands. CDOM is bimodal as well, but tends to achieve maximum values in late

winter and early spring (maxima range of 2.9-4.5) with a secondary and less persistent

peak following in summer (maxima range of 2.3-4.1). The CbPM NPP seasonal cycle

differs considerably from the ocean color observations. Distance to the shelf affects not

only the magnitude of NPP, but also the seasonality. Nearest the shelf at the 29° - 28° N

band, winter lows are rapidly followed by elevated NPP in early spring. Late spring again

drops to low productivity and is then followed by summer highs. NPP levels off through

fall months before dropping again in winter. The seasonal pattern is similar at the 28° -

27° N band with the exception that NPP remains low throughout the spring before rising

in mid-summer months. The 27° - 26° N band is bimodal with productivity highs in late winter/early spring and again in fall months. The dominant summer NPP elevations seen in the two nearer shelf bands are absent from the most distant band.
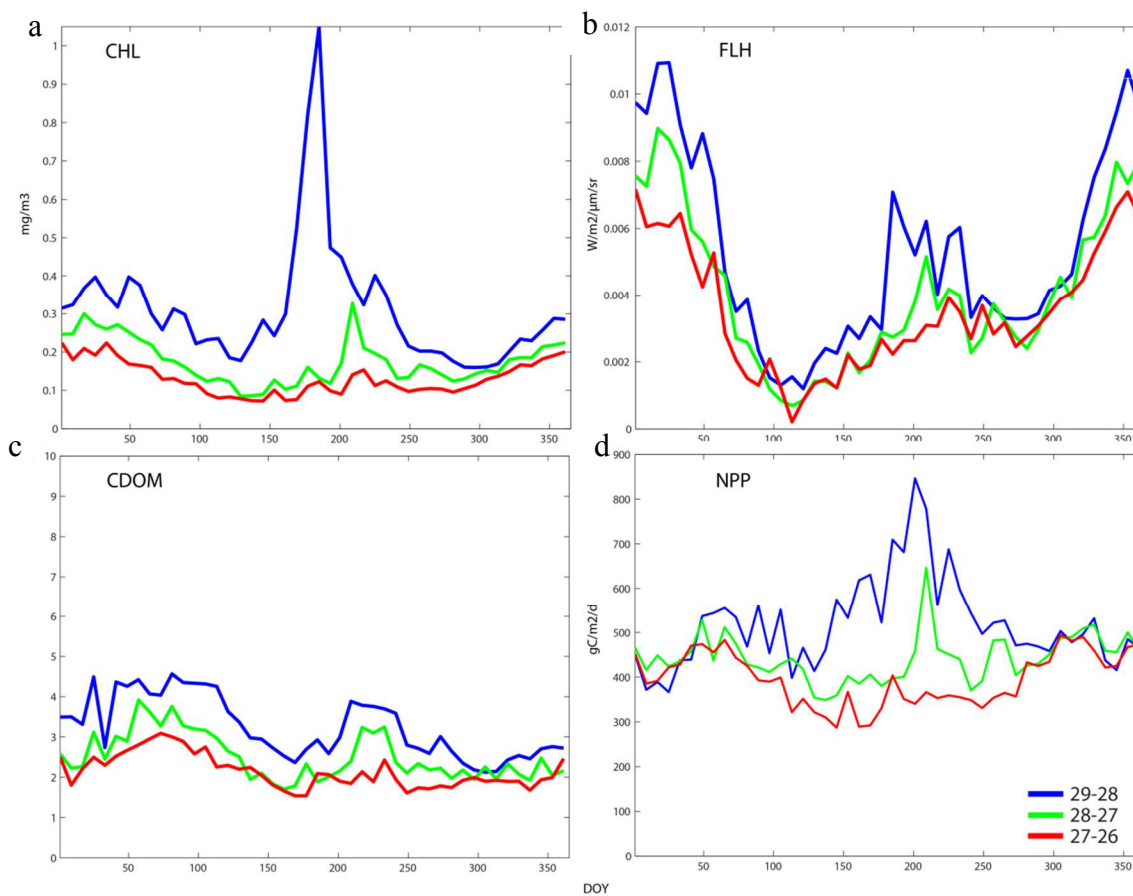
Figure 2.11. Study Area bio-optical parameters. The MODIS-Aqua (a) CHL, (b) FLH, (c) CDOM spatially- and temporally-averaged 10-year means are plotted to show variation with respect to distance to shore. Also shown are MODIS-Aqua derived NPP estimates (d). For each plot the 29^0-28^0 latitude band is blue, the 28^0-27^0 band is green and the 27^0-26^0 band is red.

The relationship of the MODIS-Aqua ocean color parameters across all latitude bands within the Study Area is given is Figure 2.12a. Scatterplots of the parameter-parameter fields are generated with latitude bands differentiated by color to highlight the parameter relationships across the gradient of distance to shore. The plot shows that the

relationships between and among parameters is well defined with distance to shore as a controlling factor in the ratios. CHL to FLH decreases rapidly moving away from shore despite a minimal change in FLH magnitude. CHL to CDOM also generally decreases with increasing distance to shore. The CHL to CDOM ratio undergoes a shift in slope at the shelf break. On the shelf CDOM is relatively constant while CHL rapidly decreases from ~ 1.5 – 0.5 mg m^{-3}. South of the shelf break the rate of change in CHL slows, while CDOM decreases from an index value of 5 to less than 2. The short range in FLH values allows the CHL to CDOM ratio to drive the relationship among the three parameters as seen in the 3-way parameter scatterplot. The same latitude bands are plotted again in Figure 2.12b coincident with the 2007 HCP discussed in subsequent chapters. This HCP is shown here as an example of the potential effect on typical ocean color properties. The figure displays the disruption in the defined parameter relationships and in the expected delineation between bands of latitude. CDOM and FLH maximum values are elevated during the HCP event (from 5-10 and from 0.005-0.02 W m^{-2} μm^{-1} sr^{-1}, respectively). The nearer shore bands experience lower than normal CHL concentrations, while the offshore bands are elevated in CHL. The removal of CHL from nearshore to offshore points to the mixing of water types consistent with the offshore advection of surface shelf waters. This is result is considered in more detail in following chapters.
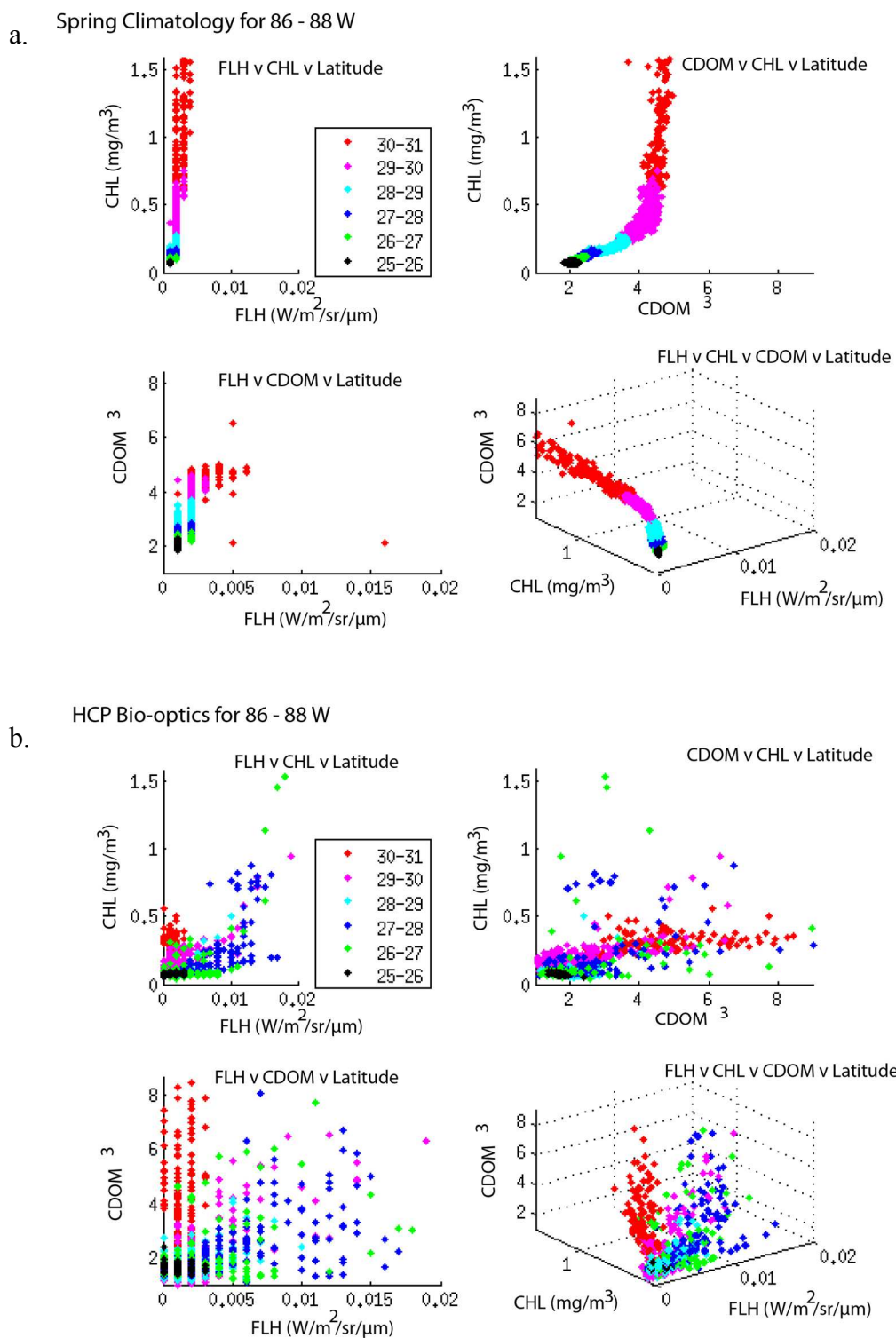
Figure 2.12. Bio-optical parameter ratios. Scatterplots of the interrelationships among CHL, CDOM and FLH are shown for (a) climatological conditions and (b) during an HCP event. Bands of latitude are highlighted by color to distinguish geographical influence to bio-optical ratios.

Discussion

Although the depth and areal size of the Gulf of Mexico set up a somewhat oceanic environment, within the semi-enclosed Gulf the proximity of coastlines and deep ocean waters creates the potential for frequent cross-shelf transport. Plumes of elevated chlorophyll (HCPs), as observed by satellite ocean color sensors, can manifest in the northern Gulf when southward cross-shelf transports develop near the Mississippi River delta and continental shelf (Morey et al., 2003b; Schiller et al., 2011). These HCPs are the biogeochemical response to nutrient and particle rich riverine and shelf waters flowing into the oligotrophic waters of the central Gulf (Jones & Wiggert, 2015; Muller-Karger et al., 2015). The results presented above reveal the complexity of the bio-optical cycles in which HCPs play a role.

Included in the Gulf CHL evaluations are coastal, shelf, and open waters, each prone to localized processes that may themselves vary temporally. When viewed as a single body of water, the seasonal cycle of CHL in the Gulf is subject to erratic variability induced by averaging across differing environments. The opposite is found for the oligotrophic central Gulf where the seasonal cycle sufficiently describes the observed pattern in CHL concentrations. This central region of the Gulf is relatively free from direct land runoff and nearshore processes, allowing for a baseline estimation of Gulf CHL variability and comparison with global changes (explored in later chapters of this thesis). The section of the northeastern Gulf, chosen to describe the seasonal cycle of CHL for waters directly impacted by HCPs, shares similarities with both the seasonal central gulf and the erratic NGMx measurements.

Contributing to the seasonal cycle within each region of the Gulf studied in this work are enhancement-peaks of CHL (i.e. peaks in CHL > 2 standard deviations above the 14-year regional mean). Timing of these peaks varies by region. The inclusive NGMx region experiences enhancement-peaks throughout the year, likely due to localized processes elevating shelf CHL at different times. Winter is invariably the season of enhancement-peak detection for the oligotrophic central Gulf. However, if this influences the NGMx enhancement-peak timing, the effect is not direct as the two regions share only two enhancement-peak periods (Table 2.1). The northeastern Gulf experiences enhancement-peaks of CHL from winter through spring, similar to the NGMx region. Unique to itself, the northeastern Gulf is most likely to experience enhancement-peaks in spring and summer months (midyear peaks). The midyear peak aggregation (13 of 17 enhancement-peaks) points to seasonally changing conditions in the northeastern Gulf. The timing suggests that this may be due to the eastward spreading Mississippi River plume under the influence of southerly shifting seasonal winds. This recurs annually and is a contributing factor to the development of detectable HCPs (Jones & Wiggert, 2015; Schiller et al., 2011). The resultant seasonal influx of riverine waters and nutrients could drive CHL elevation across the region, regardless of HCP development. Complicating interpretation of this area is the fact that 7 of the 17 enhancement peaks in the northeastern Gulf in the satellite record are coincident with enhancement-peaks in the other two regions. Whether this is due to the northeastern Gulf influencing other waters, or being influenced by other Gulf regions is unclear. Intuitively it would seem that the central waters, which never experience summer enhancement-peaks, would be more likely to impart a seasonal influence on the northeastern Gulf region and that the

northeastern Gulf region is contributing to the high CHL signal of the NGMx system during coincident enhancement-peaks. These suppositions have not been explored here, but understanding these links would further understanding of the regional CHL cycle. The timing of HCPs was expected to follow the cyclical midyear peak observations of CHL in the northeastern Gulf. However, the work presented here shows that although more frequent in spring and summer months, HCPs have a wide seasonal range. In fact, given the dependence of the HCPs on both wind patterns and offshore circulation (Jones & Wiggert, 2015), the only link between HCPs and midyear peaks may be wind patterns forcing CHL elevation in the HCP headwaters via Mississippi River plume spread or wind-driven upwelling. The mechanisms responsible for HCP development are investigated in more detail in subsequent chapters of this thesis.

In addition to influence by seasonal/interannual CHL cycles, HCP frequency of development and magnitude are potentially under the influence of long term changes in Gulf CHL. The satellite record shows that mean CHL across the Gulf is slightly rising at a rate of 0.028 mg m^{-3} yr^{-1}. This minimal rise agrees with previous global CHL studies showing that global CHL has not significantly increased during the SeaWiFS era (Siegel et al., 2013; Gregg & Rousseaux, 2014). While mean interannual CHL in the northeastern Gulf is somewhat constant, the long term trends in annual maximum CHL are rising at a similar rate for both the NGMx and Study Area regions. The rate of the rise is an order of magnitude higher for these regions than for the central Gulf waters. This discrepancy suggests that the increasingly high CHL values observed may have both oceanic/atmospheric drivers (e.g. changes in circulation or SST) and coastal/shelf drivers (e.g. increased river input). Due to the short data record available and the apparent shifts

in values seen in CHL maxima over time, this analysis would benefit from further study including shorter term trend evaluation.

HCP frequency varies interannually, yet a connection between changes in mean or maximum CHL was not found in this study. The lack of HCP influence upon regional interannual dynamics is likely due to spatial averaging. In Jones and Wiggert (2015), the authors found that the spatial impact of HCPs to the surface CHL signal was constrained to the bounds of the HCP. Thus the spatial averaging used here to determine the CHL patterns in the HCP region of impact would effectively mute individual HCP signals from the CHL cycle. This points to the episodic quality of HCPs within the CHL cycle. The disruption of the typical ocean color parameter ratios associated with the representative HCP presented in the results, supports the idea that HCPs are episodic and fall outside of the standard conditions. Interestingly, the bio-optical properties of waters within the HCP were affected inversely to the properties north of the HCP, suggesting the transport of shelf waters to the central Gulf.

This study provides a comprehensive survey of CHL dynamics related to the northeastern Gulf of Mexico, thereby providing a background for the interpretation of bio-optical measurements associated with regional HCPs. Insight into the unique midyear CHL peaks of the northeastern Gulf and the apparent links of the bio-optical system to outside forcing suggest a complicated marine system controlling both regular regional CHL patterns and the development of HCPs. To sufficiently determine the effect of HCPs on the regional bio-optical environment would necessitate an evaluation of individual HCPs. Such a study is presented in this thesis and would be complemented by additional HCP investigation.

CHAPTER III

CHARACTERIZATION OF A HIGH CHLOROPHYLL PLUME IN THE

NORTHEASTERN GULF OF MEXICO

Introduction

This chapter has been previously published in Remote Sensing of Environment

(Jones & Wiggert, 2015). Circulation in the northern Gulf of Mexico (NGMx) is largely

influenced by the Gulf of Mexico Loop Current (LC) and its associated eddy field

(Morey et al., 2003a; Ohlmann et al., 2001; Schmitz et al., 2005). The LC is a rapid

current bringing warm water into the Gulf of Mexico (Gulf) via the Yucatan current and

exiting the Gulf as the Florida Current, thereby forming an important link in the Atlantic

Gulf Stream system (Schmitz et al., 2005). Extension of the current into the Gulf

fluctuates aperiodically (Alvera-Azcárate et al., 2009; Hyun & Hogan, 2008; Sturges et

al. 2005). The extension of the LC is responsible for the highly energetic eddy field

associated with the LC and the variable nature of the LC extension results in a complex

circulation-biota relationship for the Gulf.

Directly linked to the LC extension is the shedding of Loop Current eddies (LC

eddies), formed as the distal end of the current intrusion pinches off forming an

anticyclonic eddy (Oey et al., 2005; Schmitz et al., 2005; Sturges et al., 2009). The

shedding of eddies by the LC varies temporally (Alvera-Azcárate et al., 2009; Hyun &

Hogan, 2008; Sturges et al., 2005, 2009) along with the variable extension of the main

body of the LC with LC eddy formation intervals reported as ranging from 3 – 17 months

(Morey et al., 2003a). Cyclonic eddies tend to form near the edges of the LC or LC

eddies and often continue to interact with these features (Hyun & Hogan, 2008), at times

leading to the formation of counter-rotating cyclone-anticyclone systems or pairs. Such eddy pairs (sometimes referred to as dipole eddies) have been observed and investigated both throughout the Gulf (Hamilton et al., 2002; Salas-de-León et al., 2004) and in energetic ocean systems worldwide (Pegau et al., 2002; de Ruijter et al., 2004; Feng et al., 2007).

In addition to the biogeochemical impact of each eddy (Falkowski et al., 1991; McGillicuddy et al., 1998; Siegel et al., 2011), interaction between the members of the eddy pair can potentially alter biogeochemical conditions of the water column. Cyclone-anticyclone pairs can cause environmental and ecosystem impacts due to interactions with the water column, bottom topography, and other circulatory features including other eddies (Biggs & Muller-Karger, 1994; Toner et al., 2003). The confluence of the counter-rotating pairs can result in an offshore current of up to 80 cm s^{-1} (Schiller et al., 2011). A typical volume transport of ~30 Sv (Biggs & Muller-Karger, 1994; Brooks & Legeckis, 1982) observed between these pairs is of similar magnitude to that of the nearby Florida Current. Flow associated with these currents or jets can persist for days (Teague et al., 2006), moving water masses seaward across the shelf break and into deep waters (Jochens & DiMarco, 2008; Ohlmann et al., 2001; Teague et al., 2006). Morey et al. (2003a) showed that specific areas of the NGMx are frequent pathways for these cross-shelf flows, including the western side of the DeSoto Canyon. This is likely due to the fact that cyclonic eddies are often near the canyon (Wang et al., 2003), thus available to pair with LC eddies. Cross-shelf flows induced by eddy pairs have been shown to contribute to the advection of shelf material into the central Gulf (Chassignet et al., 2005; Hamilton & Lee, 2005; Hamilton et al., 2002). Fresh water, sediments, and coastal

suspended particulates can be transported across the shelf to the slope and central basin

when the causative eddy pairs are sustained for sufficient time and positioned over the

continental slope (Chassignet et al., 2005; Hamilton & Lee, 2005; Morey et al., 2003a;

Toner et al., 2003). The transport of slope water and materials is observable via satellite

ocean color as plumes or tongues of elevated chlorophyll-a composition (Brooks &

Legeckis, 1982; Schiller et al., 2011), features herein referred to as high-chlorophyll

plumes (HCP)s. Although dependent on the aperiodic presence of eddy pairs, HCPs

exhibit a seasonal pattern, present primarily in late spring and summer months (Morey et

al., 2003b; Teague et al., 2006). This is due to the influence of the Mississippi River

plume on the regional shelf waters. Understanding the relationship between the

Mississippi River plume and NGMx wind stress provides insight into this

seasonal dependence.

The Mississippi River contributes ~13,000 m^3 s^{-1} of freshwater to the NGMx

(Morey et al. 2003a.), which is more than half of the total freshwater input to the Gulf

(Hitchcock et al., 1997; Jochens & DiMarco 2008). The waters near the source spread out

as a low-salinity (~26.25) surface layer plume on the surrounding shelf (Hitchcock et al.,

1997, Salisbury et al., 2004). Unlike open ocean surface waters, the buoyant riverine

plume is enriched in dissolved organic matter, particulates and nutrients (Yuan et al.,

2004). The potential for the Mississippi River plume to influence community structure

and primary productivity far from the shelf was demonstrated by Wawrik et al. (2003).

Dispersal of these riverine waters is dependent on wind stress, which tends to direct the

plume to the northwest during fall and winter and to the east during spring and summer

(Hitchcock et al., 1997; Morey et al., 2003a, 2003b; Salisbury et al., 2004; Teague et al.,

2006). When the plume's propagation is eastward, these lower salinity waters are prone

to entrainment by the eddy field in the vicinity of DeSoto Canyon (Jochens & DiMarco,

2008; Morey et al., 2003a,b). An excellent description of a similar marine system in the

South China Sea is given by Tang et al. (2004) who used SeaWiFS ocean color

measurements to characterize an HCP generated by wind-mediated cross-shelf upwelling.

Similarly, to corresponding features in the NGMx, this HCP appeared to be a jet or

filament of riverine-enriched coastal waters extending offshore due to both seasonal wind

forcing and offshore circulatory features.

The purpose of this work was to consider the biological impact from the flow of

water and materials across the shelf break due to a counter-rotating eddy pairs. Only with

the advent of the synoptic, upper ocean bio-optical observations provided by the Coastal

Zone Color Scanner (CZCS), did it become possible to obtain holistic views of the

impact of mesoscale features on biological patterns (e.g., Biggs & Muller-Karger, 1994;

Denman & Abbott, 1994). Even today, full understanding of the physical-biogeochemical

interactions associated with eddy pairs remains incomplete due to the complexity of the

associated three-dimensional mixing patterns. Despite the constraints imposed by the

imaging limitations of CZCS technology, Biggs and Muller-Karger (1994) demonstrated

that eddy pairs were responsible for increased offshore productivity and for the transport

of shelf waters and particulates to the central Gulf.

The present study builds upon these previous efforts to further an understanding

of how cross-shelf HCPs affect phytoplankton biomass and primary productivity both

near and offshore. To achieve this, observations from satellite ocean sensors are used to

measure bio-physical parameters, giving the advantage of large-spatial, short-temporal

scale analysis. A combined time series of SeaWiFS and MODIS-Aqua CHL data, as well as the addition of CDOM and FLH from MODIS-Aqua observations, provides a long-term dataset to evaluate bio-optical properties associated with NGMx HCPs. The relationships among CHL, FLH, and CDOM were expected to vary greatly between shelf and offshore waters and to be significantly altered by the HCP. A consistent CHL:FLH:CDOM signature along the HCP would suggest surface shelf water advection and the transport of shelf/riverine phytoplankton to the offshore environment. To further consider the biogeochemical impact of these events, the contribution of an observed HCP to a net primary productivity (NPP) budget was determined.

This paper is comprised of four sections. Following the background presented in the Introduction, the Data section describes the types of data analyzed in the present study and denotes how each dataset was employed. The Results section presents a detailed HCP feature study, including HCP detection, bio-physical interactions concurrent with HCP formation, HCP-associated bio-optical observations, and finally, HCP-associated enhanced NPP estimates. The final Discussion section provides a summary of the findings and their implications.

<div align="center">Data and Methods</div>

Animated time series of 8-day composite ocean color fields from NASA's Ocean Color Web (http://oceancolor.gsfc.nasa.gov/) were created to detect temporal patterns and anomalous features, such as filamentous HCPs associated with cross-shelf transport. The animated data included MODIS-Aqua 2003-2011 4 and 9 km resolution chlorophyll concentration (CHL), normalized fluorescence line height (FLH) and chromophoric dissolved organic matter (CDOM), and SeaWiFS (1998-2002) CHL only. Standard

algorithms were used for CHL to minimize bias between platforms. Hu et al. (2003) report a percent error of less than 50% for spring-summer NGMx satellite to *in situ* measurements. Utilization of 8-day composite data allows for the elimination of most cloud interference; however, error could potentially be introduced due to uneven averaging across the spatial domain. CDOM is reported as a unitless index value based on the algorithm given by Morel and Gentili (2009).

Sea surface temperature (SST) fields processed from MODIS-Terra data files were used in seasonal evaluation, to verify eddy presence and to detect upwelling. These data consisted of 8-day averaged L3 mapped grids from 2001-2009, with 4 km spatial resolution.

Sea surface height (SSH) fields generated by the Colorado Center for Astrodynamics Research Group (CCAR) were accessed from the GOMEX-PPP data products site (http://abcmgr.tamu.edu/gomexppp/) to identify eddies and advective paths associated with cross-shelf flow. The data consist of ¼° merged multi-platform SSH fields from 2004–2010 described in Leben et al. (2002).

SeaWiFS and MODIS-Aqua based 8-day Carbon based Productivity Model (CbPM) net primary productivity (NPP) estimates, described in Behrenfeld et al. (2005) and Westberry et al. (2008), were accessed through Oregon State University's Ocean Productivity website (http://www.science.oregonstate.edu/ocean.productivity). CbPM estimates were found to be more consistent with reported *in situ* NPP estimates for the NGMx.

Bathymetry (15 arc-second resolution) examined for the NGMx were generated by the National Geophysical Data Center (NGDC)

(http://www.ngdc.noaa.gov/mgg/coastal/crm.html) Coastal Relief Model (CRM). The bathymetry was overlain with CHL concentrations to aid in delineating an off-shelf domain inclusive of the studied HCP.

To examine the possibility of wind-driven Mississippi River plume dispersal and wind-mediated upwelling on CHL enhancement, QuikSCAT weekly mean wind fields (½° x ½° resolution) produced by CERSAT were analyzed (http://cersat.ifremer.fr/). These were plotted with colored maps of wind magnitude overlain with the wind vector fields. Monthly climatologies of QuikSCAT wind measurements were similarly plotted with data accessed through the Scatterometer Climatology of Ocean Winds (SCOW) located at (http://numbat.coas.oregonstate.edu/scow/index.html), and were provided courtesy of Oregon State University's Cooperative Institute for Oceanographic Satellite Studies (CIOSS). A full description of the processing of the wind climatology datasets is found in Riesien and Chelton (2006, 2008).

Results

In this analysis, each year is described in 8-day periods, rather than 7-day weeks to remain consistent with the 8-day composite ocean color measurements. Reference to each period is made by the date for the first day of each period (e.g. Jan-01-2009 refers to the 8-day period beginning on the first day of 2009 or period-1 of 2009). For most of the results presented here, reference is made to period-20, the 8-day period beginning June 2 of all 365-day years.

Cross-Shelf HCP Detection

The animation of mapped CHL showed that cross-shelf HCPs of productive shelf waters enter the central basin an average of 2.7 times per year when considering the

northern Gulf coastline from the Mississippi River Delta (Birdfoot Delta) to the eastern

boundary of DeSoto Canyon. The extension of the HCPs into the basin varied as did HCP

duration and the extent and direction of the lateral drift of the HCPs. While most HCPs

were seen to move westward, presumably linked with eddy migration, some moved

eastward or dissipated before any notable propagation. To differentiate HCPs associated

with the aforementioned wind-eddy-Mississippi River system, only HCPs forming on the

shelf or shelf, in the vicinity of DeSoto Canyon and with an overall CHL concentration of

> 0.5 mg/m^3 are considered. A total of 37 HCPs appear in the NGMx east of the Birdfoot

Delta with a continuous ocean color signal extending from the Mississippi River plume

southward to at least 28° N (Table 3.1). Of the recorded HCPs, 17 are referred to as

extensive HCPs (distal end beyond 27° N), and 20 are referred to as limited HCPs (distal

end between 28° N and 27° N). Spring HCPs are more likely to be limited HCPs (14 of

20) while less than half (7 of 17) of extensive HCPs occur during spring. The table also

denotes which HCPs are concurrent with eddy pairs, per SSH comparison. With 13 of the

17 extensive HCPs associated with an eddy pair, versus only 4 of 20 for those HCPs

constrained to 28° N, there is an evident link between extensive HCPs and

eddy pair involvement.

Table 3.1

Northeastern Gulf of Mexico HCP record

	28 °		27 °
1998	-		-
1999	3/6/1999		-
	4/22/1999		
2000	3/21/2000		-
2001	3/22/2001		7/12/2001
	6/2/2001		
2002	7/12/2002	*	3/22/2002
2003	4/15/2003	*	5/1/2003
	6/26/2003	*	8/21/2003
2004	4/22/2004		7/27/2004
	5/6/2004	*	
2005	3/6/2005		3/30/2005
	5/17/2005		7/12/2005
	8/5/2005		
2006	7/20/2006		5/25/2006
			7/28/2006
2007	9/14/2007		6/2/2007
			7/4/2007
2008	4/18/2008		-
2009	-		-
2010	-		-
2011	4/15/2011		3/14/2011
	6/18/2011		6/26/2011
			8/5/2011

Note. Start dates within the SeaWiFS-MODIS CHL record of NE GMx HCP extensions to 28 °and 27 °. Asterisks mark HCPs with clear eddy pair involvement as indicated by the SSH fields.

Visual observation of the mapped CHL animations revealed the presence of two HCPs that suggested cross-shelf transport events for the period beginning June-02-2007 (period-20 of 2007, Figure 3.1). One HCP was observed extending southward from the Birdfoot Delta in Louisiana to the central Gulf basin and another extending from the

Texas-Mexico Coast eastward across the shelf break. Of the two, the HCP extending from the tip of the Birdfoot Delta was chosen for further analysis due to its spatial extension and because its bounds were clearly discernible. Distinguishing the bounds of an HCP, while typically problematic, is necessary in order to facilitate the accurate attribution of its CHL enhancement relative to other environmental factors (e.g., seasonal mixing, eddy pumping, etc…). The continental shelf southeast of the Birdfoot Delta, beneath the surface HCP, is narrower than that to the west. This narrow shelf allows more direct interaction between offshore features and surface riverine waters across varying water column depths. The potential for dynamic bio-physical relationships across the gradient was considered throughout the study, leading to the division of the HCP-affected region into bathymetrically distinct sub-regions.
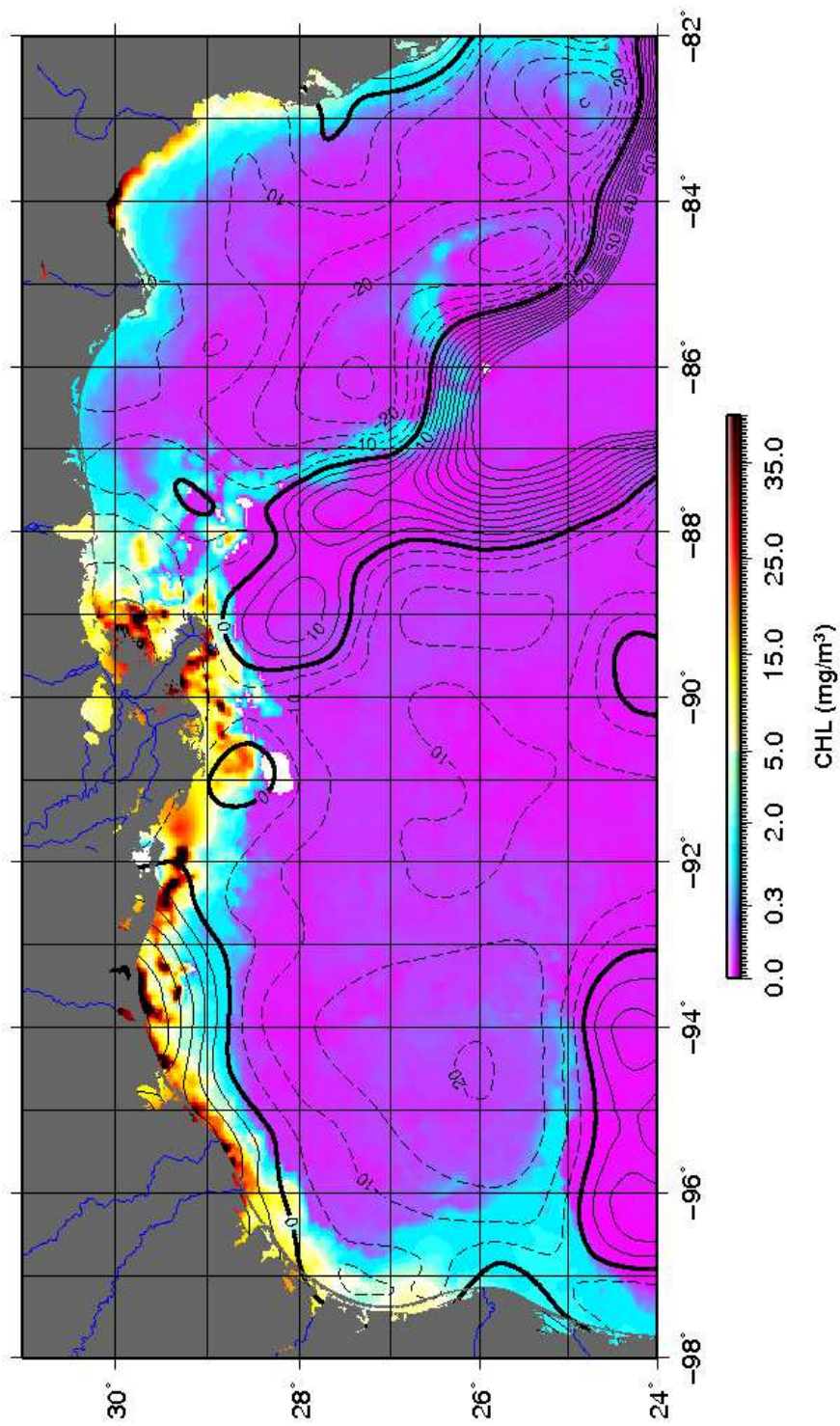
Fiure.3.1. SSH contours (cm) for June-6-2007 superimposed on the 8-day composite MODIS-Aqua CHL (mg/m³) field for June-2-2007. The thick solid line represents the 0-isobar or +/- SSH front. The thin solid lines are positive SSH and the dashed lines are negative SSH. The image shows a cyclone-anticyclone pair in the NGMx coincident with the chlorophyll field superimposed to illustrate the spatial relation of the eddy pair and the offshore propagating HCP.

Biophysical Interaction

Of interest to this study were HCPs associated with a cross-shelf flow field driven by counter-rotating eddy circulation. To detect such a cyclone-anticyclone system, temporally corresponding SST and SSHa fields were compared. Isolated areas of positive SSHa with high SST were defined as anticyclonic eddies, while a negative SSHa with low SST indicated the presence of a cyclonic eddy. Such cyclone-anticyclone systems were seen to be regular features in the NGMx, particularly when considering semi-detached LC eddies. However, these systems were typically found without a coincident HCP. The SSHa fields revealed the presence of a local cyclone-anticyclone pair associated with the HCP. Superposition of the CHL and SSHa fields revealed that the HCP lay along the expected pathway of entrained waters advected between the cyclone-anticyclone pair (Figure 3.1), thus indicating cross-shelf transport.

Motivated by past analyses that identified mean seasonal wind stress as a driver of Mississippi River plume dispersal (Hitchcock et al., 1997; Morey et al., 2003a, 2003b; Teague et al., 2006), wind field vectors from QuikSCAT were superimposed on the CHL field concurrent with the HCP (Figure 3.2b). When compared with monthly and CHL climatology plots (Figure 3.2a), the scatterometer data showed that prevailing winds were southerly and south-westerly in the study region, not the typically south-easterly winds expected during this time. The anomalous wind field was more similar to the typical July wind field, consistent with the eastward propagation and subsequent cross-shelf transport of the Mississippi River plume seen frequently in late summer months (Morey et al., 2003a).
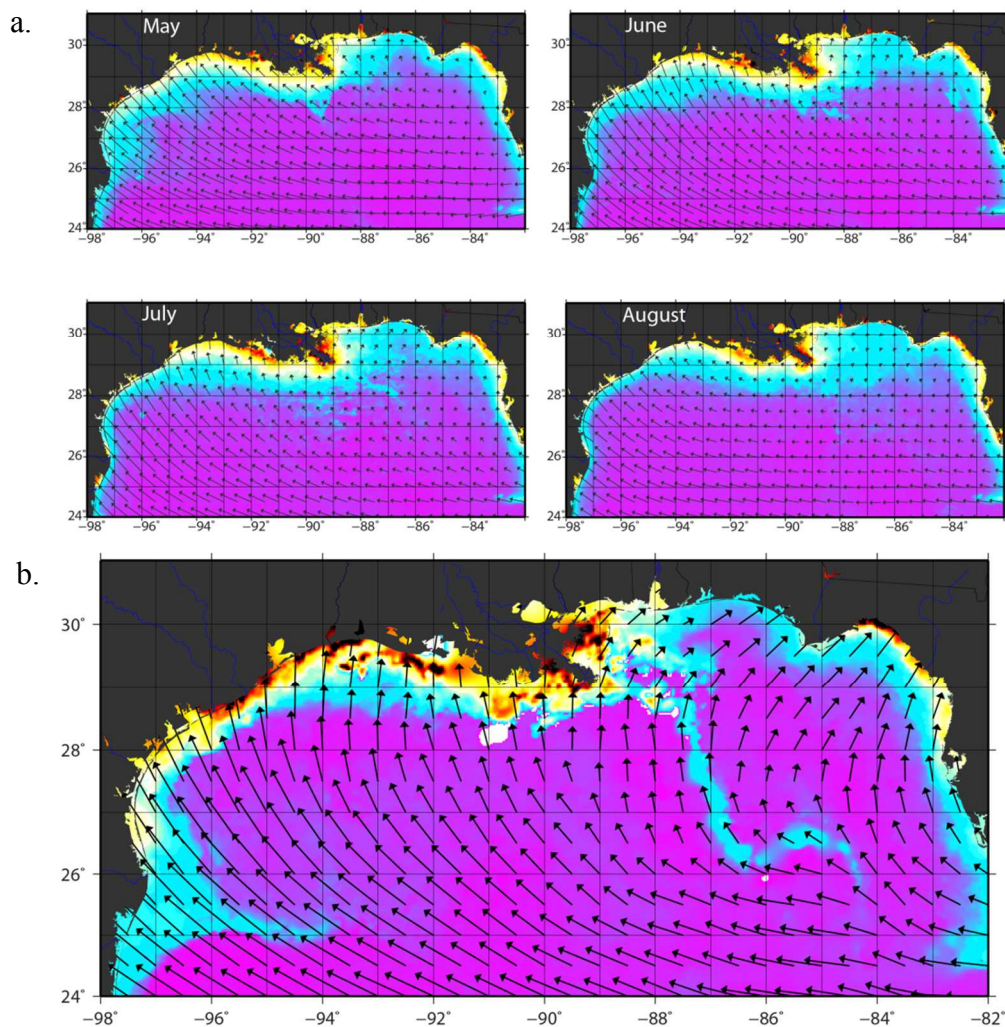
Figure 3.2 NGMx wind patterns. (a) Monthly mean wind patterns from SCOW, shown with corresponding monthly climatologies of CHL (mg m^{-3}) from MODIS-Aqua. (b) QuikSCAT 7-day composite wind vectors for June-2-2007 superimposed on the 8-day composite MODIS-Aqua CHL (mg m^{-3}) field for June-2-2007.

To rule-out wind or circulation-driven upwelling as the primary contributor of CHL to the HCP, the wind field was also examined in concert with SST. Wind vectors along the length of the HCP did not suggest upwelling conditions, thus direct wind-mediated upwelling was not considered to be the main driver of the CHL enhancement (Figure 3.2b). A high contrast map of SST plotted with an overlay of CHL contours (0.5

mg m^{-3} concentration) for the June-02-2007 period is shown in Figure 3.3. This plot

shows that the HCP is located near the warm surface front of the LC. The absence of low-

temperatures expected with upwelling supports the suggestion that the HCP is not the

result of local upwelling.
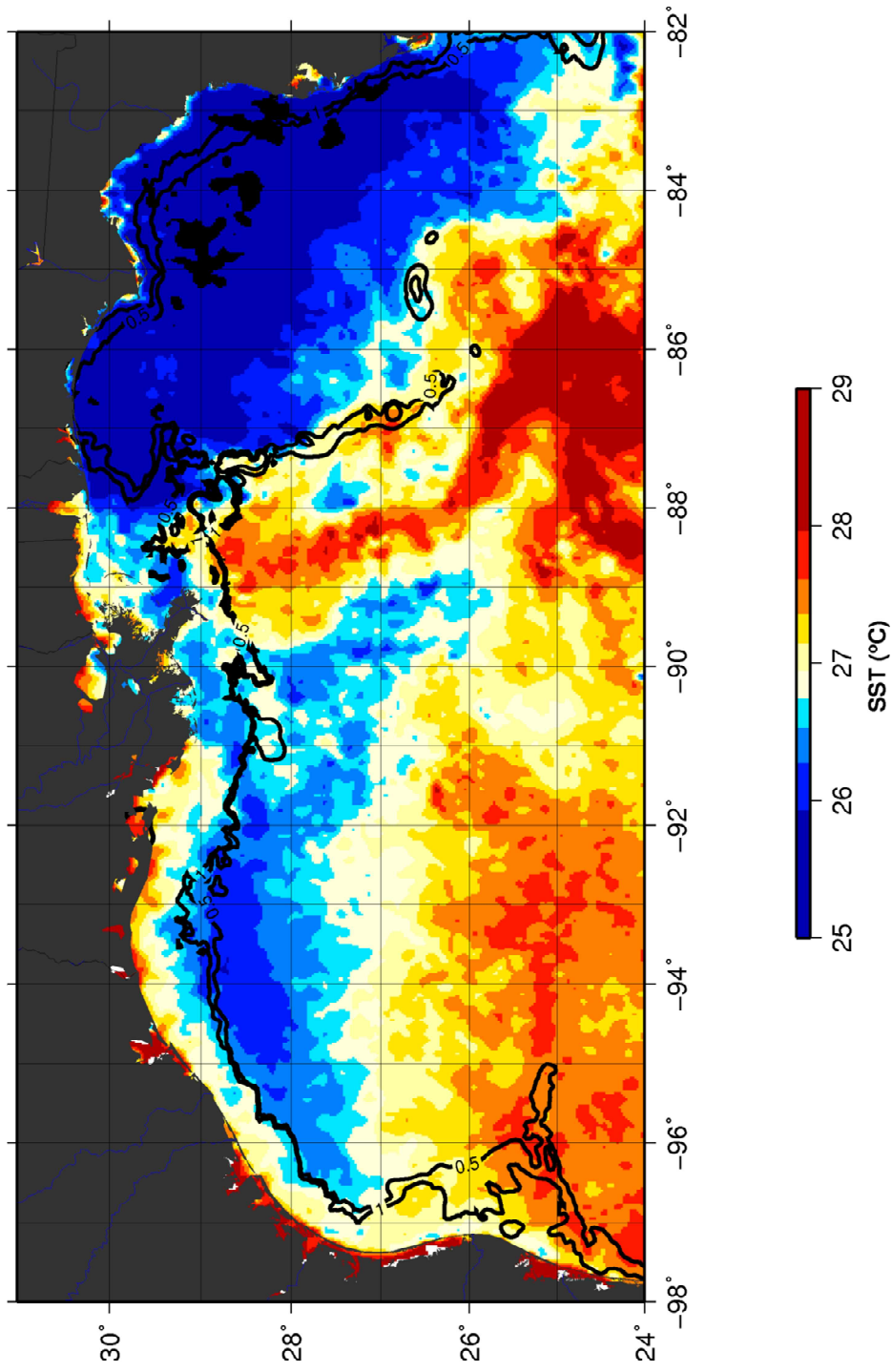
Figure 3.3. A contour line of 0.5 mg/m³ CHL from MODIS-Aqua superimposed on a high contrast MODIS-Terra SST image. Both parameters are 8-day composite measurements for June-2-2007.

Seasonal CHL

To determine the significance of the June 2007 HCP on offshore phytoplankton concentration, the seasonal cycle of CHL was evaluated. When initially considering the NGMx region as a whole, it was found that the CHL cycle was both seasonally and interannually irregular with variability in CHL peak magnitudes and timing. Tracking the pathway of the 2007 HCP extending from the Birdfoot Delta, the affected area was divided into three bathymetrically distinct sub-regions that extend southward of the NGMx shelf (Figure 3.4): 1) the DeSoto Canyon sub-region (SR_{DC}) located near the mouth of DeSoto Canyon; 2) the continental slope sub-region (SR_{CS}) and; 3) the central gulf sub-region (SR_{CG}). All sub-regions were designated in waters deeper than 500 m to target HCP impact off the shelf. Each sub-region is a ~1° x 1° box encompassing 576 MODIS-Aqua 4km CHL pixels with an area of 9216 km^2 or 144 MODIS-Aqua and SeaWiFS 9 km CHL pixels with an area of 11,664 km^2. Differences in estimated domain area are due to pixel exclusion/inclusion imposed by the boundary selection. The domain choice excludes two impacted areas: 1) those areas affected north of 29°N and therefore mainly shelf and shelf break waters and 2) the distal end of the HCP where the HCP visually appeared to curl northeastward. This latter cutoff was chosen due to bio-optical and physical observations, pointing to this being a distinct CHL enhancement.
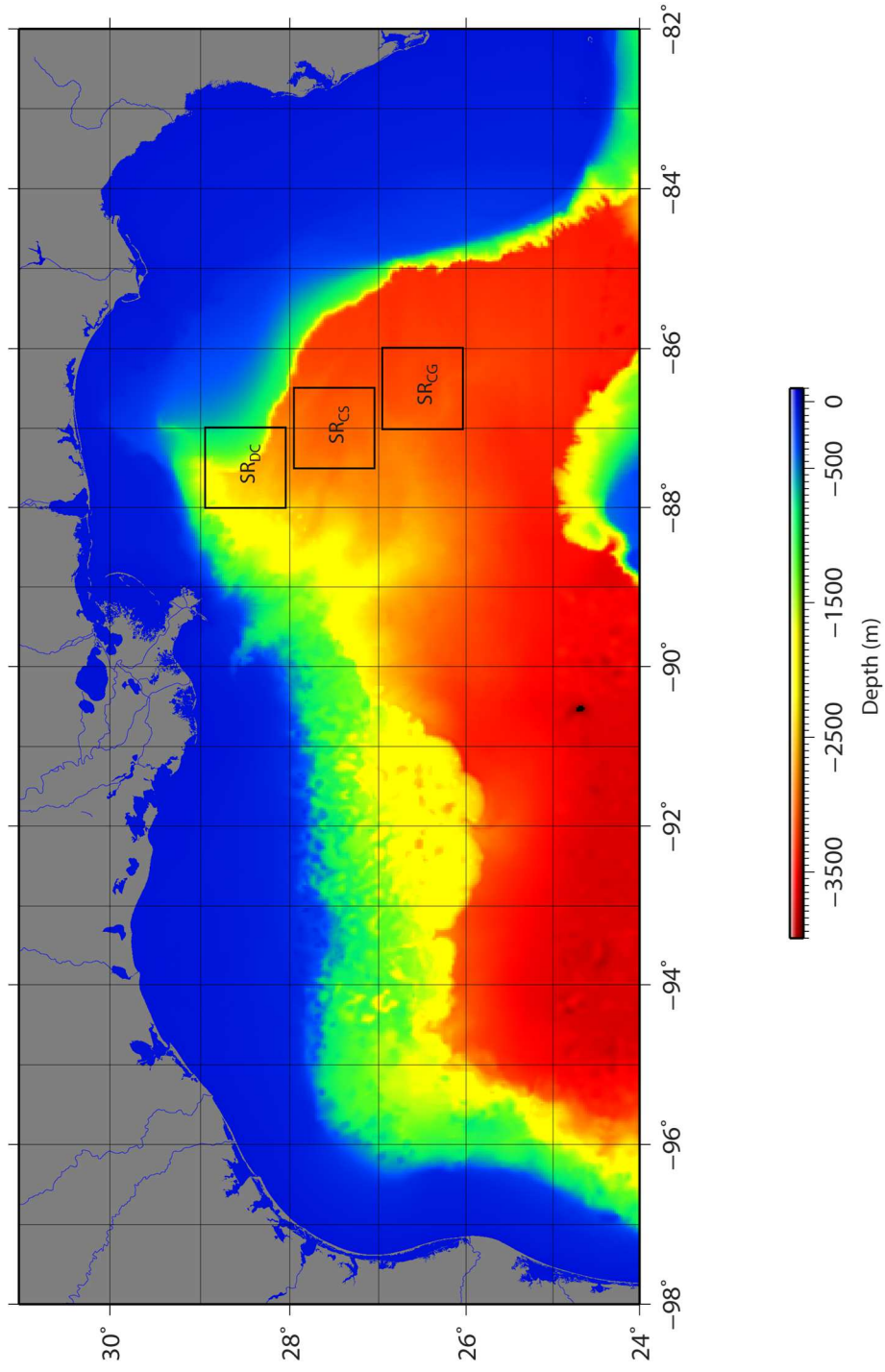
Figure 3.4. Bathymetry (m) for the study area with outlined sub-regions. The three sub-regions shown here are the SR_{DC} (DeSoto Canyon sub-region), SR_{CS} (continental slope sub-region) and SR_{CG} (central gulf sub-region). DeSoto Canyon, a region of steep slopes and cyclonic eddy energy in the NGMx, is located beneath and to the northeast of the SR_{DC}.

SR$_{DC}$ seasonal CHL. In the SR$_{DC}$, a seasonal CHL pattern is detectable and quite distinct from the seasonal cycle observed in the other sub-regions (Figure 3.5a.). Here, CHL reaches an annual maximum during summer months and is minimal during spring and fall months. CHL within this region is the most varied, with 8 of the 10 years in the MODIS-Aqua CHL data range showing a midyear or summer peak in CHL contributing to the seasonal summer maximum. On average, the midyear peaks occur after June 19 in the SR$_{DC}$. The CHL signal associated with the June-02-2007 HCP is observed 18 days earlier than these typical midyear peaks, yet the timing of the HCP falls within the observed temporal range of the summer maximum. The magnitude of the HCP-associated signal is not anomalous for the SR$_{DC}$, falling below the period-20 sub-regional mean CHL concentration (Figure 3.5a.). In 2007 alone, nine CHL peaks are seen with values of more than twice the HCP-associated peak value.
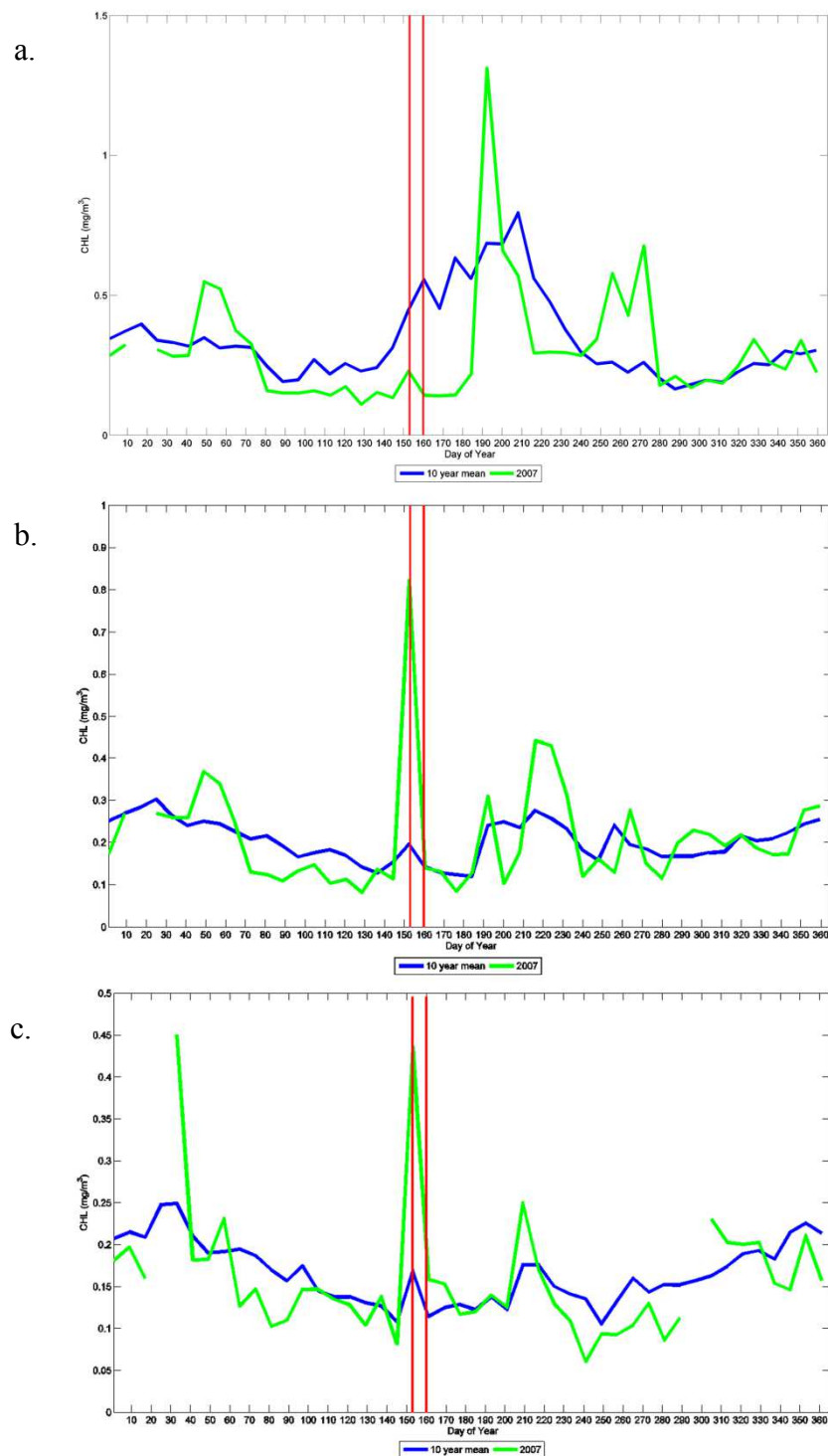
Figure 3.5. Mean MODIS-Aqua `CHL values. Time series of 8-day mean chlorophyll concentrations for 2007 (green line) plotted against the 10-year mean (blue line). The red vertical lines outline the period-20 time-frame associated with the 2007 HCP. These plots are for the three sub-regions: (a) SR_{DC}; (b) SR_{CS}; and (c) SR_{CG}.

SR_{CS} seasonal CHL. A bimodal seasonal pattern of high-winter/summer to low-spring/fall CHL seasonal pattern is detectable for the SR_{CS} (Figure 3.5b.). Unlike the SR_{DC}, the HCP-associated peak falls earlier than the seasonal summer maximum temporal range for the SR_{CS}, as most midyear peaks in this sub-region occur after July 20th (a 48 day offset). The magnitude of the 2007 HCP-associated peak in the SR_{CS} is more anomalous than in the SR_{DC}, with a value ~4 times greater than the climatological value.

SR_{CG} seasonal CHL. A seasonal pattern of higher mean-CHL during colder months and lower mean-CHL during warmer months, similar to that found by Muller-Karger et al. (1991) for the entire Gulf of Mexico, is exhibited in the SR_{CG} (Figure 3.5c.). Although this region does experience midyear peaks in CHL during some years, the intra-annual frequency of the peaks and individual peak magnitudes do not contribute enough to the seasonal CHL cycle to create a summer maximum in the 10-year mean. As in the SR_{CS}, the HCP-associated peak significantly precedes the timing of other midyear peaks within the SR_{CG}. While not visible in the 10-year mean, midyear peaks in this sub-region typically occur after July 28th (a 56 day offset). The magnitude of the 2007 HCP-associated peak is ~2x greater than the climatological value for this time period.

The separation of the NGMx into the three sub-regions allows the identification of distinct seasonal CHL patterns across the HCP affected area. Generally, the magnitude of seasonal CHL variability decreases with increasing distance from shore. Nearest to shore, the seasonal pattern is summer dominated, likely due to the presence of shelf and coastal processes (e.g. wind-driven upwelling and shelf circulation) impacting the nearer-shore region. All examined sub-regions experience summer or midyear peaks of high CHL

during most years observed, with magnitudes and frequencies of CHL high enough to create seasonal maxima in the SR_{DC} and SR_{CS}.

Period-20 Spatial CHL Variability

Satellite CHL statistics for period-20 (i.e., the time frame of the 2007 HCP) are listed for each year of available observations (Table 3.2). The statistics for this 14-year data set are derived from SeaWiFS observations for 1998-2002 and the 9 km MODIS-Aqua observations for 2003-2011. The 9 km MODIS-Aqua data are used (rather than the 4 km data) in order to be consistent with the spatial resolution available for SeaWiFS observations. The 4 km and 9 km resolution values from MODIS-Aqua were consistent for both the SR_{CS} and SR_{CG} sub-regions and within the same order of magnitude for the SR_{DC}. Differences in estimated area, combined with the capacity of the 4 km observations to resolve more shoreward influences in the SR_{DC}, lead to the slight difference in 4 km and 9 km CHL values for the SR_{DC}.

Table 3.2

Period-20 (June 2-9) Annual CHL and NPP

| | SR_{DC} | | | | | |
| | CHL | | | NPP | | |
Year/ sensor	Mean	Std	Max	Mean	Std	Max
1998_SW	0.63	1.59	9.79	0.75	0.71	3.58
1999_SW	0.89	1.02	5.09	1.45	1.07	3.47
2000_SW	0.18	0.11	0.51	0.42	0.10	0.72
2001_SW	0.49	0.53	3.26	1.07	0.76	4.32
2002_SW	0.28	0.13	0.52	0.55	0.18	0.78

Table 3.2 (continued).

Year/ sensor	Mean	Std	Max	Mean	Std	Max
2003_SW	0.22	0.18	0.88	0.68	0.20	1.17
2004_MA	0.10	0.03	0.29	0.48	0.06	0.66
2005_MA	0.15	0.23	1.83	0.50	0.28	1.63
2006_MA	0.40	0.25	1.35	0.86	0.39	1.74
2007_MA	0.46	0.82	4.90	0.77	0.56	2.79
2008_MA	0.29	0.19	1.02	0.47	0.21	1.01
2009_MA	0.25	0.13	0.96	0.22	0.10	0.47
2010_MA	0.27	0.44	2.40	0.46	0.50	2.18
2011_MA	0.10	0.03	0.26	0.30	0.05	0.39
14-year Mean*	0.35	0.66	9.79	0.63	0.56	4.32

	SR_{CS}					
	CHL			NPP		
Year/ sensor	Mean	Std	Max	Mean	Std	Max
1998_SW	0.10	0.03	0.20	0.46	0.04	0.54
1999_SW	0.07	0.02	0.14	0.32	0.05	0.44
2000_SW	0.11	0.01	0.14	0.46	0.03	0.50
2001_SW	0.11	0.04	0.25	0.48	0.10	0.83
2002_SW	0.10	0.03	0.20	0.36	0.05	0.49
2003_SW	0.06	0.01	0.08	0.23	0.07	0.41

Table 3.2 (continued).

Year/ sensor	Mean	Std	Max	Mean	Std	Max
2004_MA	0.09	0.01	0.12	0.44	0.08	0.58
2005_MA	0.19	0.21	1.21	0.55	0.30	1.31
2006_MA	0.08	0.03	0.18	0.33	0.06	0.44
2007_MA	0.25	0.26	1.57	0.66	0.36	1.48
2008_MA	0.17	0.11	0.70	0.42	0.10	0.89
2009_MA	0.12	0.02	0.19	0.37	0.05	0.54
2010_MA	0.09	0.01	0.11	0.31	0.03	0.35
2011_MA	0.10	0.02	0.13	0.29	0.06	0.45
14-year Mean*	0.12	0.11	1.57	0.39	0.14	1.31

	SR_{CG}					
	CHL			NPP		
Year/ sensor	Mean	Std	Max	Mean	Std	Max
1998_SW	0.12	0.02	0.19	0.50	0.05	0.61
1999_SW	0.10	0.05	0.21	0.36	0.05	0.52
2000_SW	0.12	0.02	0.18	0.46	0.11	0.62
2001_SW	0.14	0.02	0.17	0.38	0.05	0.49
2002_SW	0.14	0.03	0.20	0.41	0.06	0.52
2003_SW	NaN	NaN	NaN	0.36	0.12	0.53
2004_MA	0.04	0.01	0.07	0.28	0.04	0.44

Table 3.2 (continued).

Year/ sensor	Mean	Std	Max	Mean	Std	Max
2005_MA	0.19	0.08	0.40	0.57	0.12	0.79
2006_MA	0.07	0.02	0.15	0.25	0.03	0.31
2007_MA	0.20	0.24	1.54	0.70	0.34	1.66
2008_MA	0.07	0.02	0.13	0.31	0.05	0.47
2009_MA	0.06	0.01	0.09	0.22	0.02	0.28
2010_MA	0.07	0.01	0.12	0.28	0.06	0.39
2011_MA	0.10	0.03	0.14	0.29	0.05	0.45
14-year Mean*	0.11	0.08	1.54	0.36	0.12	0.79

Note. Sub-region specific annual means, maxima and standard deviation is presented for both CHL and NPP. All measurements are based on 9 km resolution observations. SeaWiFS measurements are shown for 1998-2003 and MODIS-Aqua for 2004-2011. NaN is not measured by the sensor. *Maximum values represent 14-year high values not averaged values.

In order to characterize the relative spatial impact of the HCP on affected pixels, histograms of the period-20, 14-year climatological condition (CHL_{CL}), and for the 2007 HCP (CHL_{HCP}) event were generated. To develop a common reference, the CHL_{CL} for each pixel within a given sub-region was normalized by the overall 14-year period-20 mean for that sub-region resulting in a distribution of normalized chlorophyll (CHL^*) for the climatological distribution (CHL^*_{CL}). Equation 1 illustrates how CHL^*_{CL} is obtained from CHL (x_i,y_j,t_k) for all period-20 instances for a given sub-region, where nx=12, ny=12 and nt=14 are the nominal values given complete data return (i.e., in practical application the averaging is adjusted for missing values). The normalized chlorophyll

distributions for the HCP events (CHL*$_{HCP}$) are similarly obtained, except that the numerator has no time dependence (i.e., CHL (x_i,y_j) for 2007 is used).

$$CHL^*_{CL}(x_i, y_j) = \frac{\dfrac{1}{nt}\sum_{k=1}^{nt} CHL(x_i, y_j, t_k)}{\dfrac{1}{nx\ ny\ nt}\sum_{i=1}^{nx}\sum_{j=1}^{ny}\sum_{k=1}^{nt} CHL(x_i, y_j, t_k)} \qquad \text{Eq. 1}$$

For the histograms of CHL*$_{CL}$ that follow (Figures 3.6, 3.7, 3.8), the mean of the period-20, 14-year climatology for each sub-region has a dimensionless value of 1 by definition. The bin width for all histograms is 0.1. The right-most bin for each histogram represents all pixels > one standard deviation above the climatological mean (Table 3.2) normalized by the mean or ((mean + standard deviation)/mean). Thus, for the SR$_{DC}$ sub-region, which has a 14-year mean and standard deviation of 0.35 (mg m^{-3}) and 0.66 (mg m^{-3}), respectively, the right-most bin will include all CHL*$_{CL}$ values > 2.9 or ((0.35+0.66)/0.35). The number of occurrences in this right-most bin is ≤ 5 in the CHL*$_{CL}$ histograms for all three sub-regions; for the CHL*$_{HCP}$ distributions the number of occurrences is notably higher (see below). HCP-associated pixels were therefore defined as occurrences of CHL*$_{HCP}$ pixels > one standard deviation above the mean. For the CHL*$_{HCP}$ histograms, the x-axis is identical to that used for the climatological distributions. Thus, the mean for the HCP feature will deviate from 1. Again taking the SR$_{DC}$ sub-region as an example, the mean for the HCP (0.46 mg m^{-3}, Table 3.2) will map to a value of 1.3 on the histogram's CHL* axis.
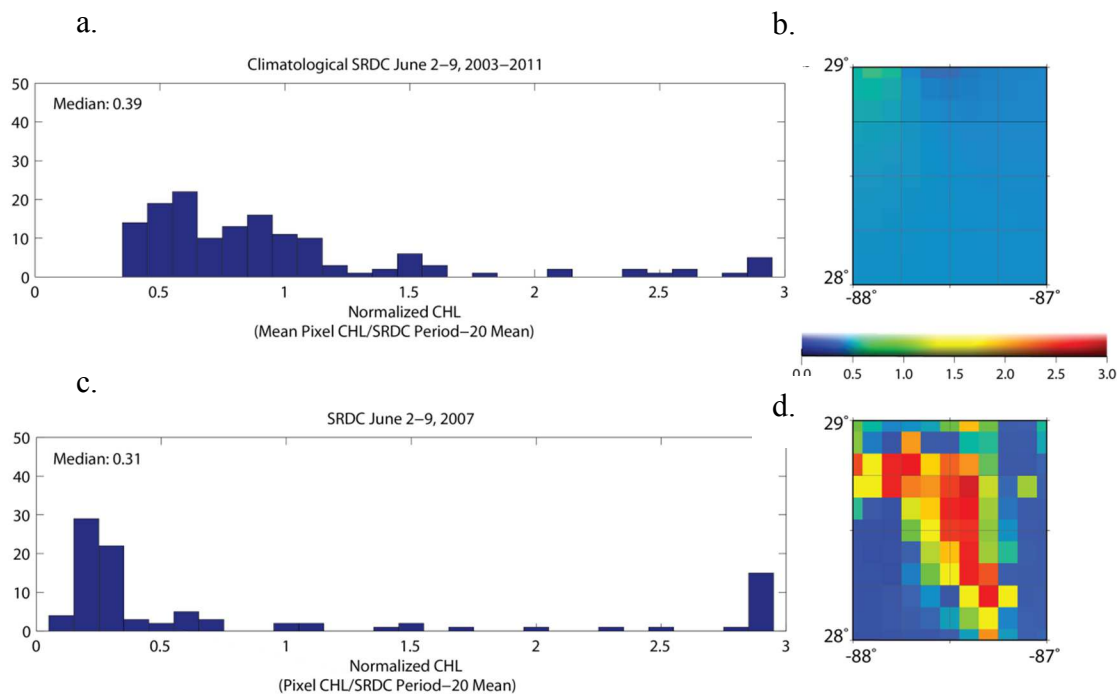
Figure 3.6. Histograms and spatial distribution for the DeSoto Canyon sub-region. The histogram and spatial distribution for the 14-year (climatological) normalized CHL (CHL^*_{CL}) are shown in panels (a) and (b), respectively. The corresponding histogram and spatial distribution for the HCP distribution (CHL^*_{HCP}) are shown in panels (c) and (d), respectively. For both histograms the x-axis is normalized CHL (CHL^*), with the climatological mean for the sub-region having a value of 1.0 by definition. The bin width is 0.1. The right-most bin of each histogram represents all values that are above the climatological mean plus one standard deviation. The CHL climatological mean and standard deviation for this sub-region are 0.35 mg m^{-3} and 0.66 mg m^{-3} (Table 3.2). Thus the right-most bin includes all CHL^* values > 2.9.

Figure 3.7. Histograms and spatial distribution for the Continental Slope sub-region. See description of plots in Figure 6. The climatological mean and standard deviation for the SR_{CS} are 0.12 mg m^{-3} and 0.11 mg m^{-3} (Table 3.2). Thus the right-most bin includes all CHL^* values > 1.9.
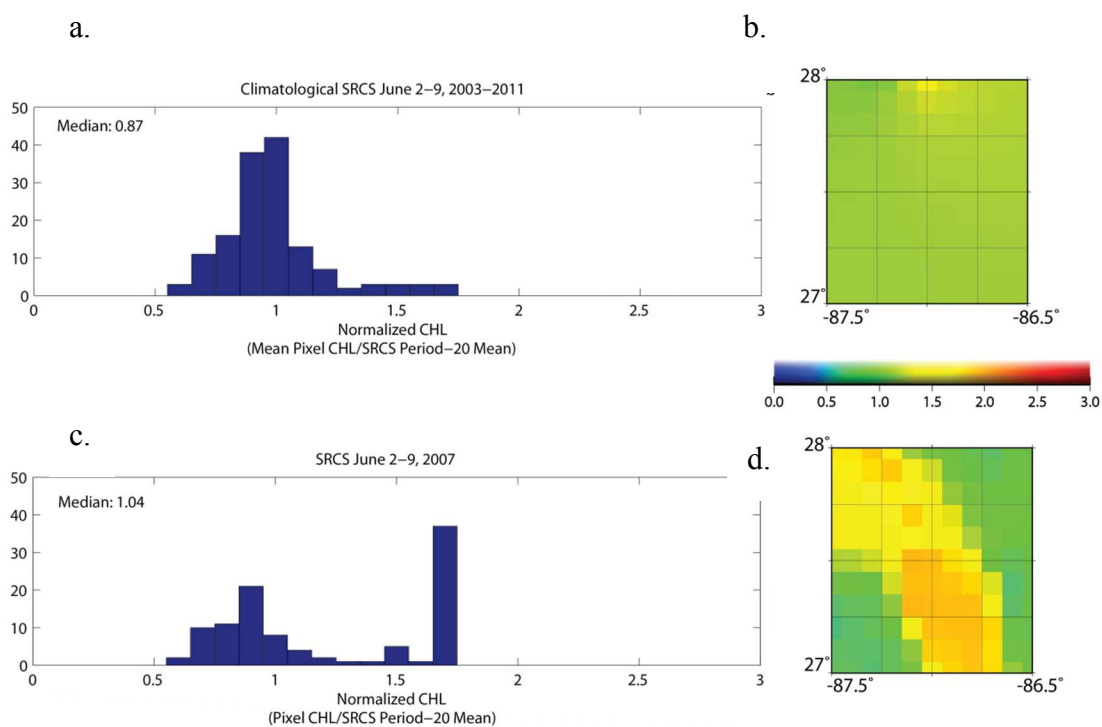
a.

b.

c.

d.
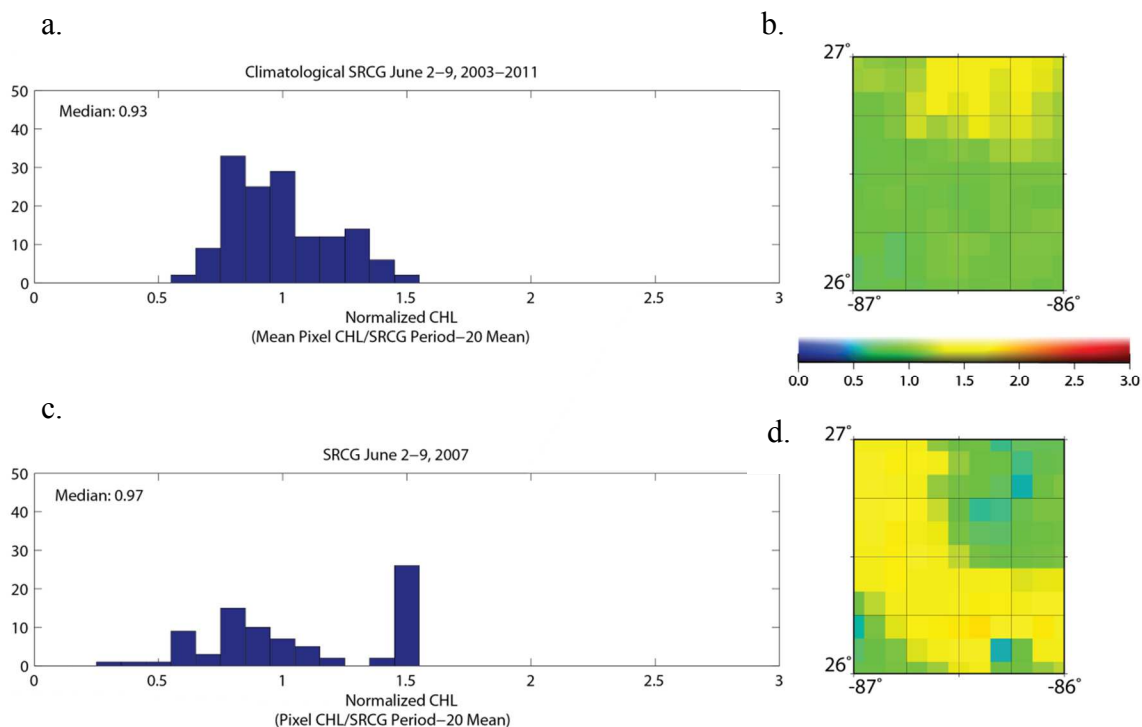
Figure 3.8. Histograms and spatial distribution for the Central Gulf sub-region. See description of plots in Figure 6. The climatological mean and standard deviation for the SR_{CG} are 0.11 mg m^{-3} and 0.08 mg m^{-3} (Table 3.2). Thus the right-most bin includes all CHL^* values > 1.7.

In an effort to visually explore spatial variability within the sub-regions, spatial distributions of CHL^*_{CL} and CHL^*_{HCP} were plotted for each of the three sub-regions. Due to the effect of the 2007 HCP on period-20 climatology for the impacted area, the 2007 data were not included in the CHL^*_{CL} spatial distributions. Therefore, the CHL^*_{CL} spatial distributions are based upon 13 years of SeaWiFS and MODIS-Aqua observations for period 20 CHL conditions differing from the histograms which are based upon 14 years of observations. Geographic-dependent variability decreased with lengthening distance to shore for CHL^*_{CL} spatial distributions. From these distributions, the HCP was estimated to cover an off-shelf area of ~ 5,832 km^2 or 16.7% of the total study domain (combined

area of the three sub-regions). This estimate was based on an assumed consistent

resolution of 9 km (i.e. pixel size of 81 km^2) and did not take into account the inherent

gradient in pixel sizes due to the angles of measurement, or changes in orbit

or terrestrial conditions.

DeSoto Canyon sub-region (SR$_{DC}$) CHL. As noted above, for period-20 in the

SR$_{DC}$ the 14-year mean and standard deviation of CHL are 0.35 mg m^{-3} and 0.66 mg m^{-3}

respectively (Table 3.2). The variability for the SR$_{DC}$ is highest amongst the three sub-

regions and is attributable to proximity to the shelf and river plume. During the June 2007

HCP event, the mean CHL increased to 0.46 mg m^{-3} and standard deviation to 0.82 mg

m^{-3} (Table 3.2). Maximum CHL values (4.90 mg m^{-3}) observed during the HCP event

were the greatest SR$_{DC}$ period-20 values since the launch of MODIS-Aqua and the 3rd

greatest over the full data range.

The CHL$^*_{CL}$ histogram for the SR$_{DC}$ (Figure 3.6a) does not exhibit a dominant

mode, rather the bulk of pixels range from 0.5 – 1.0 along the CHL* axis. This suggests

that, in this sub-region, phytoplankton biomass normally exhibits high spatial variability.

Indeed, the spatial distribution of CHL$^*_{CL}$ clearly reflects this spatial variability;

moreover, there is a clear pattern of heterogeneity that features higher shoreward

concentrations and an offshore gradient (Figure 3.6b). This cross-shelf gradient is a result

of the nearshore processes that are encompassed within the northern portion of

the sub-region.

The CHL$^*_{HCP}$ histogram exhibits significant deviation from its climatological

counterpart; for the HCP event a primary mode is apparent below 0.5 on the CHL* axis,

and the number of occurrences in the right-most bin has increased nearly three-fold

(Figure 3.6c). Further, the spatial distribution of CHL$^*_{HCP}$ shows that the elevated biomass is displaced offshore from the normal location of peak values apparent in the CHL$^*_{CL}$ distribution (Figures 3.6b, 3.6d). For the 14 occurrences in the right-most bin that track this offshore displaced HCP event, this represents 9.7% of the SR$_{DC}$ sub-region (or 1134 km^2), which has biogeochemical implications that will be considered below.

Continental Slope sub-region (SR$_{CS}$) CHL. The 14-year period-20 mean CHL for the SR$_{CS}$ was 0.12 mg m^{-3}, with a standard deviation of 0.11 mg m^{-3} (Table 3.2). While less influenced by shelf and coastal processes, the variability is nearly equivalent with the mean CHL value indicating a geographically influenced distribution of pixel means, where pixel means are greater for both northern and eastern pixels. As with the SR$_{DC}$, the mean for the entire sub-region increased during June 2007 HCP event. Here the sub-region mean doubled to 0.25 mg m^{-3} with a standard deviation of 0.26 mg m^{-3}. The maximum CHL value (1.57 mg m^{-3}) observed during the HCP event were the greatest SR$_{CS}$ period-20 values over the full observation period. The spatial distribution of CHL$^*_{HCP}$ (Figure 3.7d) was altered from the climatology (Figure 3.7b). Overall pixel CHL* concentrations increased, and areas of high CHL* values shifted from the northeast and north central pixels to the northwest and to the south central pixels.

The distribution of the CHL$^*_{CL}$ for the SR$_{CS}$ (Figure 3.7a) is positively skewed with most individual pixel means falling below the sub-regional mean (normalized value < 1). Only two pixels (or 162 km^2) exceeded one standard deviation above the mean (CHL* > 1.9). This is in direct contrast with the CHL$^*_{HCP}$ (Figure 3.7c) showing a bimodal distribution with the major mode, 33 pixels (or 2673 km^2), at or above 1.9. This is an increase from 1.4% to 22.9% of the total sub-region now exceeding more than one

standard deviation above the mean. Pixel CHL^*_{HCP} concentrations measured during the HCP event (Figure 3.7d) were higher in magnitude than the sub-regional CHL^*_{CL} (Figure 3.7b).

Central Gulf sub-region (SR_{CG}) CHL. As expected for central gulf waters, the mean CHL is lower (0.11 mg m^{-3}) and more stable (standard deviation of 0.08 mg m^{-3}) than in the two nearer shore sub-regions (Table 3.2). During the June 2007 HCP event, the mean CHL across the sub-region rose to 0.20 mg m^{-3} and the standard deviation exceeded the mean at 0.24 mg m^{-3}. This diversion points to the sharp divide between HCP impacted waters and nearby oligotrophic waters within the boundary of the SR_{CG}. The maximum CHL values associated with the HCP (1.54 mg m^{-3}) were the greatest values measured for period-20 within the SR_{CG} throughout the full data range (Table 3.2).

The SR_{CG} distribution of CHL^*_{CL} (Figure 3.8a) is markedly similar to the SR_{CS} CHL^*_{CL} distribution. As in the SR_{CS}, the CHL^*_{CL} distribution is positively skewed with most individual pixel means falling below the sub-regional mean (normalized value < 1) and two pixels exceeded one standard deviation above the mean (normalized value > 1.7). The histogram of CHL^*_{HCP} for the SR_{CG} (Figure 3.8c) shows a bimodal distribution, with the major mode more than one standard deviation above the mean comprising 25 pixels (2025 km^2 or 17.4% of the SR_{CG}). Like the SR_{CS}, the spatial distribution of CHL^*_{HCP} (Figure 3.8d) was altered from the climatology (Figure 3.8b). Pixel CHL^* concentrations increased and areas of high CHL^* values shifted from the northeast to the northwest and to the south. This difference from the effect seen in the SR_{CS} is likely due to the infrequency of HCPs extending beyond 26° N in the eastern NGMx. While 34

apparent cross-shelf HCPs were observed east of the Birdfoot Delta throughout the 14-year observational period, only 6 of these HCPs extended below 26°N as a continuous filament.

Bio-Optical Relationships (CHL-FLH-CDOM)

Satellite imagery shows the presence of CDOM, a common component of coastal and shelf waters, extending the length of the HCP (Figure 3.9). CDOM, like all ocean color parameters, is difficult to quantify in nearshore waters. However, increased magnitudes and altered ratios to other parameters add to the evidence of changing conditions and water mass advection. Therefore, to investigate the likelihood that some modified shelf waters were advected to the central Gulf, an HCP corresponding CHL-FLH-CDOM bio-optical signature for each sub-region was calculated and compared with corresponding 24-day rolling climatologies (compilation of three 8-day climatologies spanning the 8-day period before the HCP to the 8-day period following the HCP). To emphasize the HCP's influence within each sub-region, only those CHL values greater than one standard deviation above the mean, as determined by the previously discussed histogram analysis, are shown on the scatter plots (Figure 3.10). A linear regression model was used to determine the r^2 coefficient for each parameter-parameter relationship plotted (Table 3.3). The centroid (i.e. point plotted as mean X, mean Y) for each parameter-parameter relationship was then calculated to establish the Euclidian distance between the climatological and episodic states, emphasizing the distinction between typical conditions and HCP-impacted conditions (Table 3.3).

Table 3.3

Basic statistics for bio-optical parameters

	FLH:CHL		CDOM:CHL		CDOM:FLH	
	Climatology	HCP	Climatology	HCP	Climatology	HCP
$SR_{DC}\ r^2$	0.156	0.545	0.407	0.0899	0.0209	0.0862
centroid	0.0025	0.019	2.7	5.2	2.7	5.2
	0.28	0.18	0.28	1.8	0.0025	0.019
$SR_{CS}\ r^2$	0.15	0.53	0.148	0.207	0.0334	0.022
centroid	0.0017	0.0087	1.9	3.9	1.9	3.9
	0.11	0.48	0.11	0.48	0.0017	0.0087
$SR_{CG}\ r^2$	0.0422	0.712	0.053	0.0224	0.00074	0.0268
centroid	0.0016	0.0055	1.7	3.8	1.7	3.8
	0.083	0.38	0.083	0.38	0.0016	0.0055

Note. For each parameter-parameter comparison within each sub-region, a correlation coefficient (r2) is calculated based on linear regression. The centroid is also given as the coordinates (mean(X), mean(Y)) for each parameter-parameter scatter plot.
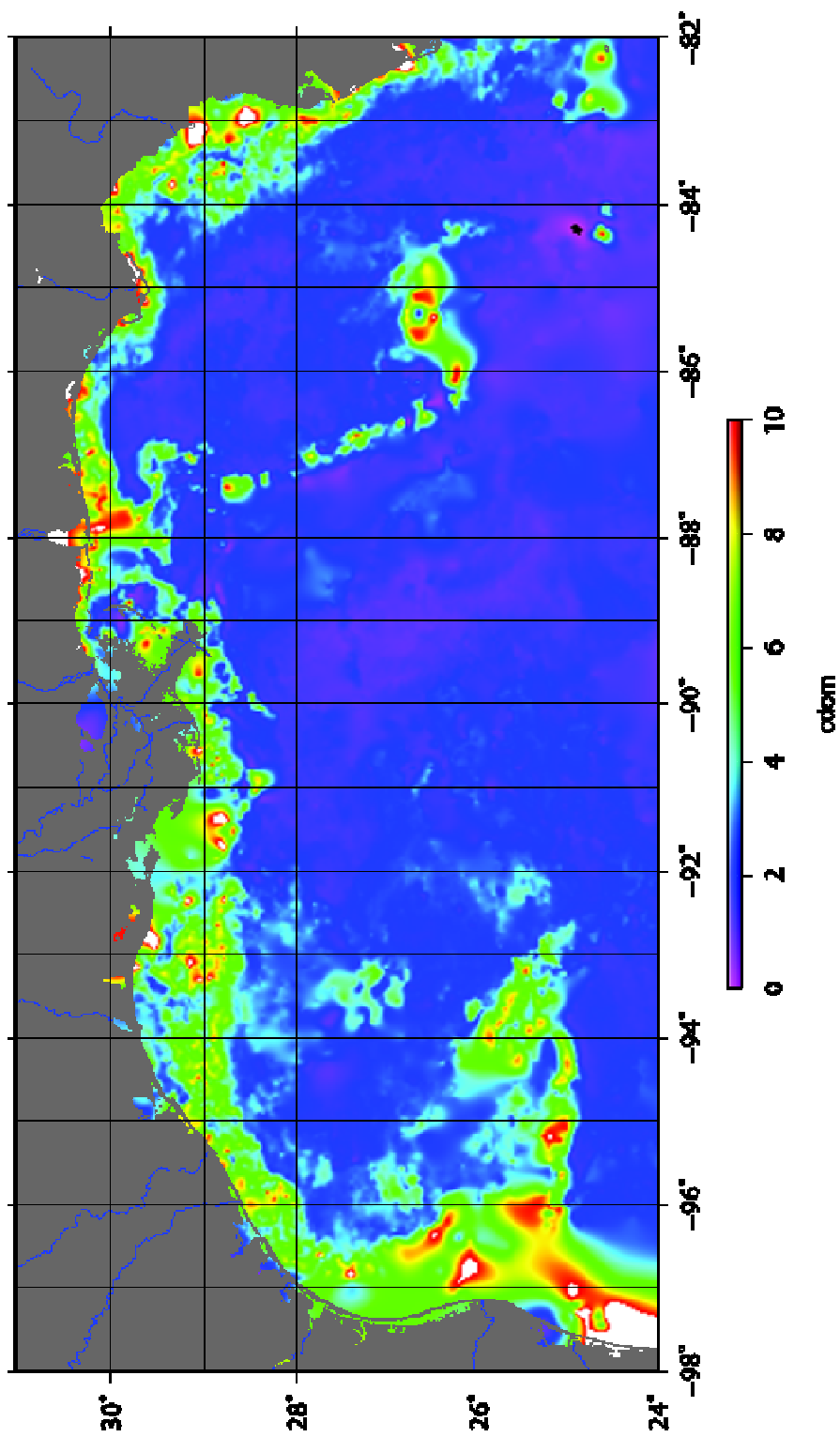
Figure 3.9. 8-day composite MODIS-Aqua CDOM field for 2-9 June 2007 (period-20).
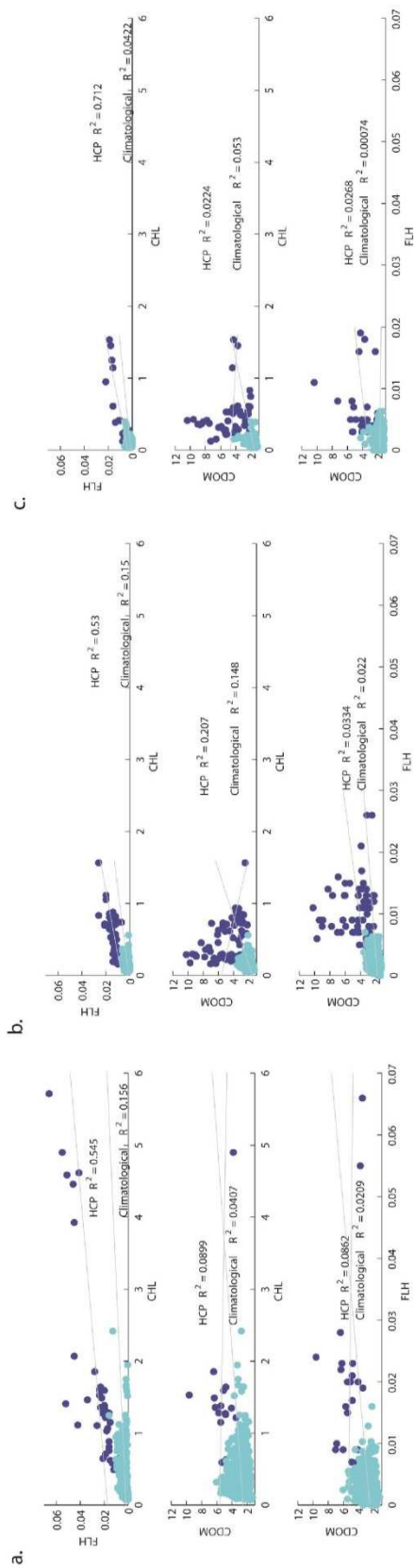
Figure 3.10. CHL-FLH-CDOM parameter plots for (a) SR$_{DC}$, (b) SR$_{CS}$, (c) SR$_{CG}$. The lighter values represent the three 8-day combined climatologies of each parameter for each sub-region. The darker values are the measurements taken during the observed plume. A linear regression line is added to each plot showing that parameter-parameter correlations as well as parameter values were altered during the exchange event.

The relationship between FLH and both CHL and CDOM was limited by a narrowly ranging FLH across the SR_{DC} sub-region (Figure 3.10a). Overall parameter-parameter relationships were not well defined (climatological r^2 ranged from 0.02 – 0.16). Observations made along the HCP were considerably different from the climatological values. Although all parameter-parameter correlations increased above the typical status, only the CHL:FLH correlation notably changed (r^2=0.545 from 0.156).

Within the SR_{CS} the FLH to CHL relationship was not discernible (Figure 3.10b). FLH varied little across the range of CHL. CDOM and CHL revealed a stronger climatological correlation than seen elsewhere in the study area, yet remained poorly correlated in general ($r^2 = 0.148$). As in the SR_{DC}, the HCP period observations were altered from the climatology. The CHL:FLH correlation was the strongest calculated for the sub-region ($r^2 = 0.53$). The HCP-associated deviation from the CDOM climatological condition, wherein SR_{CS} CDOM is ~ 1/2 nearer shore SR_{DC} CDOM, resulted in similar CDOM concentrations for the two sub-regions.

In the SR_{CG} the climatological parameter-parameter correlation coefficients were weak and no statistical correlations could be defined (Figure 3.10c). During the 2007 cross-shelf flow period, correlations between parameters remained weak with the exception of the CHL:FLH correlation strengthening to an r^2 of 0.7.

Bio-optical parameter magnitudes increased along the HCP at all points measured, with CDOM index values approximately doubled within each sub-region, and mean period-20 CHL values raised by an order of magnitude for the SR_{DC} and SR_{CG} sub-regions. For all studied sub-regions, the HCP resulted in an increased correlation between CHL and FLH, consistent with the hypothesis that the HCP is comprised of advected

coastal/riverine phytoplankton and is not entirely the result of nutrient input elevating local phytoplankton growth.

Productivity

A climatology of NPP estimates for each sub-region was compiled (Table 3.2). Seasonal NPP cycles for each sub-region were similar and showed progressively decreasing mean NPP with distance to shore. The NPP contribution of the HCP to each sub-region was also calculated (Table 3.4). SR_{DC} NPP values for period-20 were typically 0.63 ± 0.56 g C m^{-2} d^{-1}, or a period-20 contribution of 2.71% to the annual estimated NPP. During the 2007 cross-shelf flow, the SR_{DC} NPP value was 0.77 g C m^{-2} d^{-1}, or a period contribution of 3.32% to the annual NPP estimate. On average, period-20 in the SR_{CS} contributed 2.03% (0.39 g C m^{-2} d^{-1}) to the annual estimated NPP. The HCP-coincident NPP estimate for the SR_{CS} was 0. m^{-2} d^{-1}, a period contribution of 3.43% to the total annual estimate. The NPP estimate within the SR_{CG} during the HCP event was 0.70 m^{-2} d^{-1} (4.78% of the annual estimate), approximately twice the average contribution of 2.46% or 0.36 m^{-2} d^{-1} for this time period.

Table 3.4

Productivity Estimates

	Annual Carbon Budget	Mean Period-20 C-Flux	2007 Period-20 C-Flux
	$/m^2$	$/m^2/d$	$/m^2/d$
SR_{DC}	185.75	0.53 (2.28%)	0.87 (3.75%)
SR_{CS}	153.80	0.40 (2.08%)	0.68 (3.54%)
SR_{CG}	117.22	0.37 (2.53%)	0.74 (5.05%)

Sub-regions are listed in order relative of distance from shore. The NPP annual budget shows average annual estimate of productivity for each sub-region over a 9-year period. The mean period-20 C-flux is specific to the period corresponding with the HCP. The HCP C-flux is the NPP estimate for the 8-day period corresponding to the HCP. The percent contribution to the average annual budget is shown in parentheses for both the mean period C-flux and the HCP event C-flux.

Normalized NPP (NPP*), calculated similarly to CHL* were used to evaluate the areal coverage of elevated NPP* (NPP* > one standard deviation above the mean). A comparison of typical and HCP associated NPP* areal coverage revealed that the surface domain of elevated NPP* during the 2007 HCP event grew from 342 to 2052 km^2 in the SR_{DC}, from 0 to 7524 km^2 in the SR_{CS} and from 0 to 9918 km^2 in the SR_{CG}. The range of the increase in percent of sub-region exhibiting elevated NPP* was 13.9% to 80.5%, with the lowest increase seen in the SR_{DC}. These percentages of HCP areal impact are notably greater than those identified in the CHL* distributions. The spatial distributions of NPP* across each sub-region are shown in Figure 3.11. These distributions show a similar increase in magnitude as those seen in the CHL* spatial distributions presented earlier, although resolution is coarser for the productivity estimates (1/ 6° for NPP vs. 9 km for CHL). The difference in resolution between the NPP* and CHL* pixel maps is also likely to contribute somewhat to the reported differences in HCP-associated areal coverage by the two parameters. Greater lateral expansion is observed in the SR_{CS} and SR_{DC} NPP*

plots than was observed in the corresponding CHL* spatial plots, an indication of

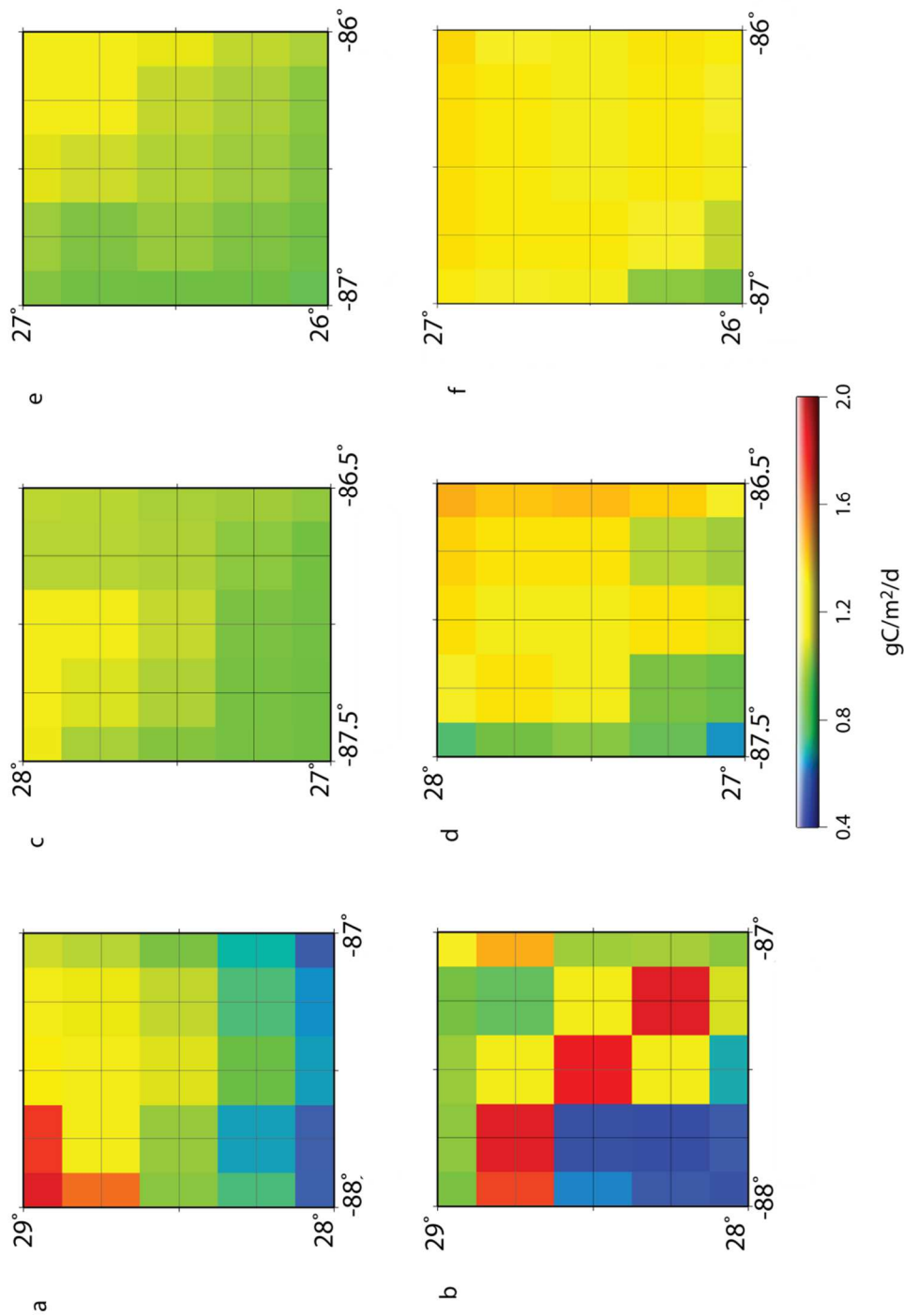increased productivity beyond the phytoplankton biomass coverage of the HCP.

Figure 3.11. Normalized NPP (NPP*) spatial distributions. (a) SR_{DC} climatology, (b) SR_{DC} HCP, (c) SR_{CS} climatology, (d) SR_{CS} HCP, e) SR_{CG} climatology and f) SR_{CG} HCP. The pixel size is set for ease of comparison with the CHL* 9km resolution plots (Figures. 6-8).

To explore the divergence of NPP* increases within each sub-region from the CHL* increases, spatially-averaged NPP was plotted against CHL for the 14-year mean pixel estimates (open symbol with standard deviation bars) and for the 2007 period-20 estimates (open symbols) in Figure 3.12. The 14-year spatial averages show that both the magnitude and relationship between CHL and NPP is similar for the SR_{CS} and SR_{CG}. The SR_{DC} values reveal a greater magnitude and standard deviation, as anticipated. During 2007 period-20, the sub-regional data pair values converge as the SR_{DC} values increase slightly, within one standard deviation of the mean values, while the SR_{CS} and SR_{CG} data pairs exceed one standard deviation above their respective 14-year means. Also presented in Figure 3.12 are averages of the CHL and NPP points strictly associated with the 2007 HCP (pixels > one standard deviation above the mean). The HCP-associated data pairs are more than doubled for each sub-region respective to the 14-year means and are elevated above the period-20 means. While still lower than the SR_{DC} data pairs, the SR_{CS} and SR_{CG} data pairs during the HCP were similar to the mean period-20 conditions within the SR_{DC}.
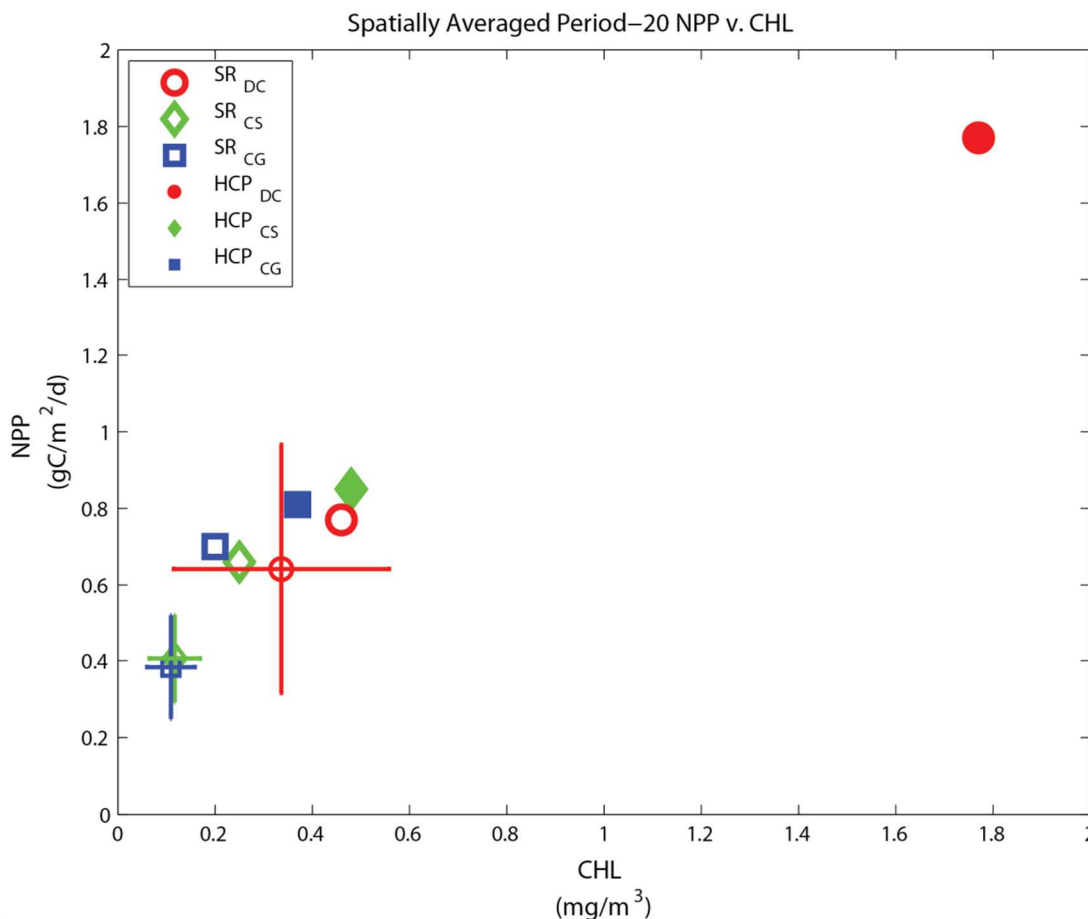
Figure 3.12. Spatially-averaged period-20 NPP-CHL. NPP is averaged across each sub-region and plotted against correspondingly averaged CHL. The 14-year mean spatial averages are shown with error bars and the 2007 sub-regional averages are un-filled markers. Error bars are drawn to one standard deviation (horizontal for CHL and vertical for NPP). Also plotted are HCP-associated values (pixels > one standard deviation above the mean) isolated from the 2007 sub-regional averages (filled markers).

Discussion

Cross-shelf HCPs in the NGMx tend to occur during late summer and are associated with eddy-driven cross-shelf flow during periods of eastward extension of the Mississippi River plume. The seasonality of HCPs was established by Morey et al. (2003a) who showed that the DeSoto Canyon area of the NGMx was a hotspot for cross-shelf flow toward the central basin during July-August when south-westerly winds drive

the Mississippi River plume toward the energetic DeSoto Canyon eddy field. Although the June 2007 HCP presented here is earlier than the mean observed range of regional HCPs (late June - early August under typical seasonal wind patterns), concurrent QuikSCAT winds did confirm favorable conditions for HCP formation, with subsequent propagation into the central Gulf. An examination of SSHa fields revealed a cyclone-anticyclone eddy pair in the vicinity of DeSoto Canyon creating an offshore current flow. The HCP was situated along the advective path of the eddy-driven flow, and eastward of the LC edge. The dependence of cross-shelf HCP formation on both wind and eddy rotation supports the interpretation of Carnes et al. (2008) who determined that while eddy rotation drove cross-shelf flow, it could not account for the total exchange observed. Comparing the data presented here with geostrophic velocity surface currents available through AVISO suggests that the cross-shelf flow was set up prior to June-07. This indicates that while eddy-driven circulation drives the cross-shelf flow, it is the seasonal wind component that triggers the HCP extension across the shelf break. This is consistent with Salisbury et al.'s (2004) findings of the extensive southeastern reach of particulates within the Mississippi River plume during summer wind events.

Entrainment of the freshwater surface layer and subsequent advection across the shelf and into the central Gulf would be expected to deliver nutrients to the oligotrophic deep water and even modified shelf phytoplankton stock. The importance of the advection is evidenced in work by Salmerón-Garcia et al. (2011) who define the central basin waters south and east of the Mississippi River delta as a separate zone within the Gulf due to late summer Mississippi River discharge influence. In the mid-Atlantic Bight region, such a cross-shelf transport of marine materials was indicated by Marra et al.

(1990) to be favorable to the affected phytoplankton populations by the delivery of nutrient rich waters to the euphotic offshore water column. The HCP explored here resulted in both altered phytoplankton concentration and primary productivity rates (i.e., order of magnitude increases in chlorophyll-based biomass and carbon-based estimates of net primary productivity); these findings are consistent with a 1999 HCP in the eastern Gulf (Wawrik et al., 2003), wherein *in situ* productivity rates of surface waters were shown to increase by 9.5% in conjunction with altered phytoplankton community structure. Biomass and production increases of this magnitude are similar to those reported for biogeochemical responses to episodic events elsewhere that are associated with mesoscale dynamics, hurricane impacts, and climate modes (Babin et al., 2004; McGillicuddy et al., 2007, 1998; Wiggert et al., 2009).

The June 2007 HCP has the advantage of being temporally isolated so that the plume's associated bio-optical parameters are easily discernible from surrounding waters. The 2007 HCP is also spatially extensive, allowing for comparative analysis across varied marine environmental conditions. To highlight the seasonal CHL pattern of phytoplankton biomass and minimize conflicting offshore-coastal influences on the CHL signal, the study domain was divided into sub-regions. Nearest to the shelf, where CHL signals are most variable and frequent midyear peaks of greater magnitude to the studied HCP are common (i.e. the HCP-associated values are typical of the surroundings). The frequency of summer peaks and their broad temporal range of occurrence contributes to a summer maximum in the 10-year mean nearshore seasonal pattern. Further offshore, the temporal offset of the HCP from the typical time frame of the midyear CHL peaks is more pronounced with the HCP occurring several weeks earlier. Similarly, the difference

in the magnitude of CHL within the HCP relative to climatological values is more profound for the offshore sub-regions that are less prone to experience multiple elevated CHL events in a given year. Those sub-regions nearer to shore are; however, more likely to experience frequent episodes of high CHL and may be more ecologically dependent upon these episodes. Marine populations within these more dynamic sub-regions would likely be adapted to a frequent influx of coastal and riverine waters. As such, the 2007 HCP would have fit within the typical seasonal pattern, facilitating local phytoplankton growth and production as opposed to fostering anomalous production, as seen in the further offshore sub-regions.

Within the region as a whole, the lateral spatial expansion of the HCP to adjacent waters was minimal at best. The lack of elevated CHL in the waters adjacent to the HCP indicates that the surface biomass increase is almost entirely due to surface advection with lateral spatial expansion of the biomass and nutrient input constrained by the circulation conditions imposed by the eddy pair. Supporting this hypothesis, histograms and mapped distributions of normalized CHL during the HCP show both elevated values (> one standard deviation above the mean) within the HCP and lower than typical normalized CHL values along the eastern and western boundaries of the HCP. This relationship points to the effects of eddy frontal boundaries on constraining the HCP. Deciphering why the CHL values are lower than typical normalized CHL values at the northern, eastern, and western HCP boundaries is less straightforward. Speculatively, the western boundary low values are attributable to the presence of the anticyclonic eddy, for which low CHL would be expected. While a cyclonic eddy on the eastern boundary would be expected to raise CHL values due to eddy pumping, this effect may be less

dominant than the advection southward of the surface waters due to the flow of the eddy pair. Similarly, the low northern boundary CHL values are possibly due to the advection of the typically CHL-rich surface waters being advected southward during the cross-shelf flow.

Although the June 2007 HCP clearly impacted phytoplankton concentration in the regions affected, providing insight to the ecological importance of such events, it cannot be assumed that remotely sensed CHL is only phytoplankton biomass. Coastal waters, particularly those influenced by river inputs, are optically complex in both their dissolved and particulate content; suspended particles often contribute to the observed optical properties and can influence the chlorophyll concentration estimates. Investigation of HCP-associated suspended material, utilizing MODIS-Aqua FLH and CDOM measurements, confirms the divergence of the CHL:FLH:CDOM relationship from the typical status of offshore surface waters along the extent of the plume, raising mean bio-optical signals and generally strengthening the parameter-parameter correlation coefficients.

The consistent bio-optical signatures along the length of the HCP indicate advection of surface shelf waters. Assuming that the HCP was comprised of modified shelf waters, it is reasonable to expect the HCP's distinguishing properties to be retained, similarly, to the buoyant riverine discharge found on the shelf. Although not discussed here, examination of 1-day resolution MODIS-Aqua CHL measurements do show that the surface HCP spreads at a rate consistent with riverine/freshwater residence time. While the coverage is sparse due to satellite cycling, the daily observations suggest that the HCP remains shelf-bound from June-02 thru June-07 when the distal end of the HCP

quickly migrated southward into the Gulf. The full length of the HCP was reached by June-09, two days later. Hitchcock et al. (1997) reported a ~2 day residence time of riverine water masses in the surface waters of the NGMx shelf and stated that these waters would retain their salinity for a period of a few days. The persistence of the HCP was on a similar scale, supporting the hypothesis that the HCP was composed of advected riverine waters.

NPP estimates during the June 2007 HCP event approximately doubled in contribution to the annual NPP budget for each sub-region. This, considered in light of the narrow impact of the HCP, may indicate that for those sub-regions furthest offshore, these types of events can dramatically impact the regional annual carbon budget and biogeochemical cycling. Resolving the significance of this productivity impact is not simple. NGMx productivity estimates, particularly shelf productivity, are highly variable due to riverine influences such as nutrient input and turbidity (Lohrenz et al., 1994). Productivity estimates in the Mississippi River plume vicinity range from 30 m^{-2} y^{-1} (Hitchcock et al., 1997) to 584 m^{-2} y^{-1} (Cai and Lohrenz, 2010), whereas for the central Gulf a range of 30 m^{-2} y^{-1} (Lohrenz and Verity, 2006) to 190 m^{-2} y^{-1} (Walsh et al., 1989) has been reported. The satellite based productivity estimates used in this study for the central Gulf (117.22 m^{-2} y) were within the range set by Walsh et al. (1989). The cross shelf HCP-associated estimates ranged from 215.29 – 357.25 m^{-2} y, on order with estimates found by Cai and Lohrenz (2010) within the Mississippi River plume, supporting the association of the 2007 HCP with advected riverine waters. Further complicating our understanding of productivity in the NGMx are physical conditions induced by the Mississippi River system (Lohrenz et al. 1994), and the LC. Song et al.

(2010) showed that the timing of physical forcing leading to vertical mixing can alter the magnitude of the phytoplankton response, thus the temporal variation associated with LC eddy formation makes studying the consequences of eddies to NGMx biogeochemical conditions less straightforward.

The results presented here indicate that HCPs in the NGMx are both contributory to the local marine system and dependent upon it. The satellite data made possible the co-examination of biological impacts and physical drivers of the event across a large spatial scale. A modeling study and targeted *in situ* work could potentially provide insight to the depth-dependent effects of HCPs and to the specific components of the advected waters. Additional efforts to further understanding of the processes controlling HCP formation, magnitude, and composition are ongoing, including a mechanistic study of the 37 HCPs listed in Table 3.1.

CHAPTER IV

PHYSICAL DRIVERS AND ENVIRONMENTAL CONDITIONS ASSOCIATED

WITH HIGH CHLOROPHYLL PLUMES IN THE NORTHERN GULF OF MEXICO

Introduction

This work contributes to research aimed at understanding the mechanisms by which dipole eddy, or counter-rotating eddy systems induce chlorophyll enhancement in offshore waters of the central Gulf of Mexico (Gulf). A modeled marine system of southerly summer winds driving buoyant and productive Mississippi River waters to the known energetic eddy field south of DeSoto Canyon in the northern Gulf of Mexico (NGMx) (Morey et al. 2003a) is explored via satellite observations of chlorophyll-a (CHL), sea surface height anomaly (SSH) and wind fields. Mississippi River discharge and variations in the El Niño-Southern Oscillation (ENSO) global climate indicator, compiled as the Multivariate ENSO Index (MEI), add to the mechanistic study by providing a sense of environmental conditions potentially impacting Gulf CHL.

Gulf circulation is controlled primarily by fluctuations in the Loop Current (LC). The LC enters the Gulf as the Yucatan Current 'loops' north then south in the central Gulf and finally exits the Gulf as the Florida Current (Schmitz et al., 2005; Muller-Karger et al., 2015). The LC brings warm surface waters from the Caribbean Sea into the cooler Gulf (Muller-Karger et al., 2015). The LC impingement into the Gulf varies irregularly (Alvera-Azcárate et al., 2009; Hyun & Hogan, 2008; Sturges et al. 2005) affecting surface circulation across the Gulf.

The aperiodic extension of the LC north toward the continental shelf of the southern United States leads to the formation of cyclonic eddies along the edges of the

LC (Hyun & Hogan, 2008; Muller-Karger et al., 2015). These cyclonic eddies, and those formed due to bathymetric influences near the shelf break, flank the LC and contribute to the separation of stable and persistent anticyclonic rings (LCEs) from the distal end of the LC (Schmitz et al., 2005). LCEs are mesoscale (200-400 km diameter and depths of up to several hundred meters) warm-core, anticyclonic rings that propagate west-southwest across the Gulf (Hamilton et al., 2007; Jochens & DiMarco, 2008; Morey et al., 2003a).

Adjacent LCEs and cyclonic eddies often continue to interact (Hyun & Hogan, 2008), at times leading to the formation of counter-rotating cyclone-anticyclone systems or dipole eddies (Biggs et al., 1997; Walker et al., 1996). Counter rotation of the dipole eddy can induce a horizontal current of up to 0.8 m s^{-1} (Teague et al., 2006) along the front between the cyclonic and anticyclonic rings. The resultant transport of water volume is on the order of 30 Sv (Biggs & Muller-Karger, 1994; Brooks & Legeckis, 1982), similar to the 24-32 Sv water volume transport reported for the LC (Muller-Karger et al., 2015). Modeled simulations of mesoscale circulation have pointed to the energetic eddy field near DeSoto Canyon (Wang et al., 2003) as an area frequently impacted by cross-shelf transport (Morey et al., 2003a). When proximal to the continental shelf, the induced current can transport water and particulates from the nutrient rich shelf to the oligotrophic central Gulf (Jochens & DiMarco, 2008; Ohlmann et al., 2001; Teague et al., 2006). During seasonally low central Gulf CHL (summer months) the transport of productive shelf waters to the deeper water column is visible in satellite CHL signals as filamentous plumes of CHL (HCPs) (Brooks & Legeckis, 1982; Schiller et al., 2011).

HCPs are seasonal, with formation typically occurring in spring and summer (Morey et al., 2003b; Teague et al., 2006; Jones & Wiggert, 2015). This contrast to the

irregular periodicity of causative dipole eddies is thought to be dependent on seasonal wind patterns (Morey et al. 2003b; Muller-Karger et al., 2015). Walker et al. (1996) describe the wind dependence on low salinity plume formation near the Mississippi River Delta where they find that wind speed and direction control plume magnitude and morphology over short (days) timescales. Wind fields across the NGMx follow a seasonal cycle of strong northerly winds 60% of the year from October to May and shift to southerly winds seen in July and August following a transitional period in spring (Morey et al., 2003a; Walker & Rabalais, 2006). During fall and winter months, the strong northerly winds set up strong westward alongshore currents in the NGMx forming a southern boundary for shelf waters. In spring and summer, winds are southerly and southeasterly. This wind pattern allows Mississippi River waters to spread eastward. This eastward spread allows highly productive riverine waters to enter the active DeSoto Canyon regions, potentially forming an HCP. Summer winds can also lead to an eastward alongshore current that can constrain impinging riverine waters to the Mississippi-Alabama shelf. The wind conditions thus necessarily impact the largest contributor to shelf waters of the NGMx, the Mississippi River plume (Hitchcock et al., 1997; Jochens & DiMarco 2008). River discharge from the Mississippi River equates to ~13000 cubic meters of buoyant, low salinity and nutrient rich water entering the NGMx every second. The fate of these waters and the associated particulates, organic matter and nutrients could impact CHL dynamics and biogeochemical processes throughout the NGMx, including HCPs. The morphology of the Mississippi River delta effectively divides the NGMx shelf into eastern and western shelf regions. This division combined with aforementioned seasonal winds driving the Mississippi River plume eastward (Hitchcock

et al., 1997; Morey et al., 2003a, 2003b; Salisbury et al., 2004; Teague et al., 2004)

during spring/summer months facilitates the spread of the plume toward the energetic

eddy field near DeSoto Canyon during summer months (Jochens & DiMarco, 2008;

Morey et al., 2003a,b).

<div align="center">Data and Methods</div>

Data

      The identification and characterization of dipole eddies in the NGMx was based

on the fact that cyclonic eddies have depressed elevation (progressively negative sea level

toward the center of the ring) and that anticyclonic eddies have a progressively positive

sea level toward the center of the ring. To evaluate the effect of dipole eddy entrainment

of shelf/riverine waters on HCP formation and characteristics, daily sea surface height

(SSH) fields generated by the Colorado Center for Astrodynamics Research Group

(CCAR) were examined from the GOMEX-PPP data products

(http://abcmgr.tamu.edu/gomexppp/). The data consist of merged multi-platform SSH

fields from 2004–2010. CCAR produces these fields using daily sea surface height

anomaly fields (SSHa), which are then added to climatological and modeled mean SSH

values to produce daily sea surface height fields for the study region. The method used to

produce the SSH from SSHa is documented in Leben et al. (2002). Where necessary due

to data limitations, the CCAR SSH fields were supplemented with similar merged multi-

platform SSH fields obtained from AVISO (http://www.aviso.altimetry.fr/). Daily

temporal resolution was maintained for consistent comparison.

      To investigate the wind-driven Mississippi River plume dispersal, QuikSCAT

weekly mean wind fields (½° x ½° resolution) produced by CERSAT were examined

(http://cersat.ifremer.fr/). The wind fields were plotted using GMT scripts designed to generate graphics consisting of color distributions of wind magnitude overlain with wind vector fields to visualize the correlation of HCPs with both wind direction and wind speed.

CHL fields of 8-day composite L3 mapped chlorophyll-a concentrations for the years 1998-2011 were obtained from NASA's Ocean Color Web (http://oceancolor.gsfc.nasa.gov/cms/). The data for the NGMx (bounded by 98° W, 82° W, 24° N and 31° N (Figure 2.1)) were extracted from the global data set geographically using MATLAB programs developed in house. Isobath specific data were extracted using programs written in Fortran. Plotting of the data for visualization was accomplished through GMT processes. For comparison with river and ENSO, data anomalies were determined from both the CHL values and normalized CHL values.

To explore the HCP vertical signal and the potential for sub-surface nutrient upwelling associated with the HCP, modeled salinity and currents were obtained from the Naval Oceanographic Office's American Seas Prediction system (AMSEAS) (http://www.northerngulfinstitute.org/edac/oceanNomads/AmSeas.php). The AMSEAS salinity and current fields for May 2013 were obtained and processed using GMT. Depth levels of 0, 3, 4, 5, 8, 12, 15, 20, 30, 50, 100, and 200 m were examined to detect shelf water migration.

Daily Mississippi River discharge values from the U.S. Army Corps of Engineers site mis00111 were obtained for the period 1949-2010. The temporal range of the discharge for the 14-year ocean color satellite record discussed above was isolated and

normalized using a standard z-score calculation. The daily normalized data were compiled into 8-day periods for comparison with the CHL data set.

ENSO variations were obtained via the MEI website supported through NOAA (http://www.esrl.noaa.gov/psd/enso/mei/).

Methods

To validate the mechanisms of HCP development proposed in model studies of HCPs (Morey et al., 2003; Schiller et al., 2011) against observed HCP events (such as the 2007 HCP examined in Chapter III of this thesis), the CHL fields associated with four observed HCPs are presented here with relevant physical forcing fields. The timing of HCPs established in Chapter III of this thesis (Table 3.2) serves as a guide for selecting the HCPs for this study. In general, it is found that HCPs are coincident with southerly or southeasterly winds. Wind strength and dipole eddy systems contribute to the extension of individual HCPs.

The wind and SSH fields, concurrent with select HCPs from Table 3.2, are compared with CHL plots to investigate the proposed HCP model. HCPs occurring during 8-day periods beginning with the dates August-5-2005 (HCP-1), June-2-2007 (HCP-2) and August-5-2011 (HCP-3) are presented along with the addition of a 2013 HCP (HCP-4). HCP-1 is selected to describe the physical fields associated with a limited HCP (confined north of 27° N). HCP-2 was described in Chapter III and is included here to determine physical parameters concurrent with a well understood HCP event. HCP-3 is explored due its formation during a period of high CHL south of the northeastern Gulf shelf. HCP-4 occurs during the period beginning May-9-2013, not during the 14-year

CHL record used for most of the thesis. HCP-4 is included here as an example of a distally extensive HCP and as a preface to the AMSEAS results section below.

Modeled conditions for the proposed HCP-forming marine system include southerly and/or southwesterly winds near the Mississippi River delta and the presence of a southward current induced by dipole eddy rotation (Morey et al., 2003a, Schiller et al., 2011). A southward current is generated by anticyclonic rotation west of adjacent cyclonic rotation. Anticyclonic eddies are identified as positive SSH features and cyclonic eddies as negative SSH features. A polarized color scale is used in SSH visualization to exclude small variations in SSH and thereby highlight eddies. In all wind plots, wind speed is indicated by color and vector length, while wind direction is represented by vector direction.

To explore the steps involved in the formation of an HCP, fields of CHL and SSH were superimposed for HCP-2. Wind fields are not included due to the consistency of wind direction among HCPs. The images are daily CHL and daily SSH. Images shown are odd days from June-3-2007 to June-9-2007 due to CHL measurement quality. May-31-2007 and June-12-2007 are also included to show the state of CHL and SSH in the area before and after the HCP event.

The remotely sensed data portray the spread and subsequent entrainment of Mississippi River plume waters toward the center of the Gulf. To provide insight to the question of HCP phytoplankton origin, modified shelf communities or nutrient-elevated off-shelf communities, AMSEAS salinity and current output for HCP-4 are provided. The AMSEAS output is able to estimate salinity and current at depth and therefore show the vertical extent of the HCP. It is assumed that dipole-eddy induced currents will extend to

as much as 1000 m based on anticyclonic eddy rotation (Oey et al., 2005). However, low-salinity as a proxy for riverine and inner shelf waters should remain buoyant due to low relative density.

Environmental influences such as freshwater input, nutrient availability, mixing, and episodic circulation features can alter the concentration and patterns (spatially and temporally) of CHL in the region of HCP development. To examine the dynamics of CHL due to environmental conditions, the CHL fields for the Gulf are analyzed in the context of local continuous river output and the global El Niño-Southern Oscillation (ENSO). In the ENSO and Mississippi River discharge analysis, the regions defined in Chapter II (NGMx, Open Water and Study Area) are reassigned for compatibility.

Discharge from the Mississippi River, in terms of nutrient, freshwater and particulate output, is expected to significantly contribute to CHL dynamics. To ascertain the relationship between discharge from the Mississippi River and CHL dynamics across the Gulf, a series of Hovmöller diagrams were generated depicting CHL concentrations at three isobaths. The Hovmöller diagrams were assembled by first writing a Fortran program to read the CRM bathymetric field across a given domain then locate and extract CHL pixels along a specified isobath. A detrended (mean subtracted) CHL signal (CHL_A) for each isobath was then derived to determine anomalous CHL. Finally, to minimize the strong Mississippi River signal, a z-normalized (mean subtracted and then standard deviation divided) was generated. The Hovmöller diagrams are centered at 90° W, the approximate location of the Mississippi River's largest output channel, and focus on isobaths 200m (shelf break), 500m, and 2500m to determine the range of river's influence both laterally and zonally. To reference the Hovmöller diagrams within the

region, a bar indicating the Hovmöller longitudinal domain is shown in Figure 2.1. Shelf waters are excluded from the analysis to reduce influence from coastal processes and allow focus on the waters associated with off-shelf HCP formation. This omission also effectively excludes the complex hypoxic zone west of the Mississippi River delta, a phenomenon typically constrained to the Louisiana-Texas shelf.

To more thoroughly consider the role of the Mississippi River itself in the CHL_Z trends and dynamics discussed above, U.S. Army Corps of Engineers river gauge data were obtained and analyzed. The data were first averaged into 8-day composites to match the satellite measurements of CHL and then normalized for simpler comparison to CHL_Z. The CHL_Z data were also employed for this analysis and were partitioned into the NGMx, Open Water and Study Area regions denoted in Figure 2.1 to facilitate comparison between seasonal and interannual Mississippi River- CHL_Z cycles. Covariance between normalized river data and CHL_Z were computed for each region (NGMx, Open Water and Study Area).

<div align="center">Results</div>

HCP Examples within the System

Figure 4.1a shows the evolution of the HCP-1 CHL field obtained through MODIS-Aqua. HCP-1 extends southward to 28° N and brings high CHL waters east to 88° W. The following 8-day period only a remnant of the HCP remains near the shelf. The associated wind field is shown in Figure 4.1b. Weak southwesterly winds (0.5 - 2 m s^{-1}) near the Mississippi River delta are indicative of the eastward river plume spread expected with HCP formation. The associated SSH field (Figure 4.1c) shows a large (~400 km zonal width) positive SSH feature south of the Mississippi River delta. The

feature is indicative of LC circulation, or possibly an anti-cyclonic eddy, and the northern

edge of the feature forms a southern boundary to the HCP at ~28° N. No cyclonic

circulation features are observed near the HCP.
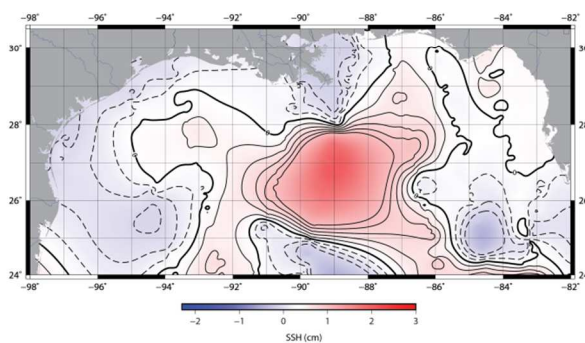
a.
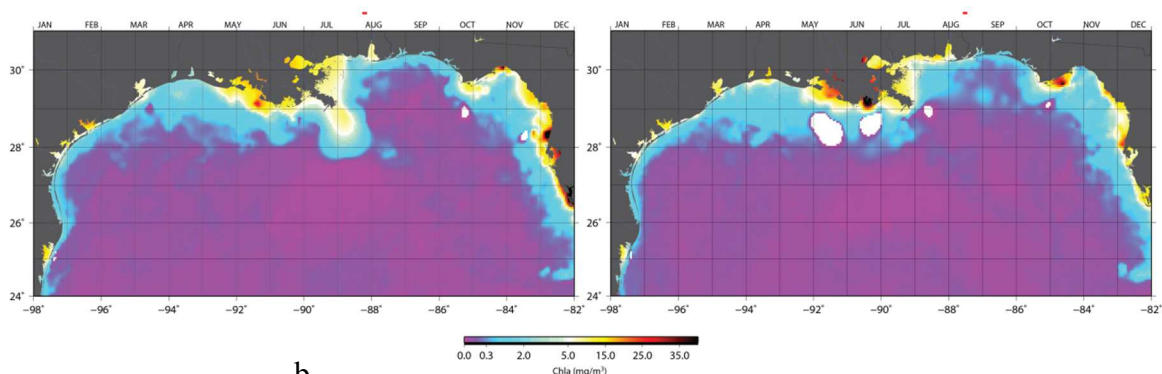
b.
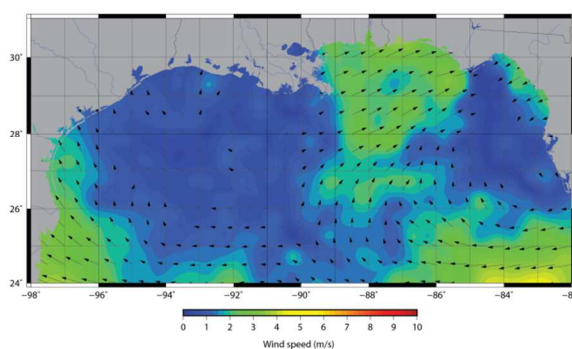
c.

Figure 4.1. HCP-1 Biophysical fields. (a) The 8-day composite CHL field of the period beginning August-5-2005 indicates an HCP south of the Mississippi River delta. (b) QuikSCAT wind fields support HCP development and (c) Merged SSH shows a large anticyclonic feature interacting with the HCP.

Winds associated with HCP-2 (Figure 4.2a) are shown in Figure 4.2b. HCP-2 extends southward to 26° N, one of the longest HCP extensions observed in the 14-year satellite images. A CHL signal for the HCP is not evident in the CHL field for the following 8-day period (Figure 4.2a). The associated wind field (Figure 4.2b) is stronger (3 - 4.5 m s^{-1}) near the Mississippi River than seen in HCP-1. The southerly wind direction is indicative of eastward river plume spread. SSH fields (Figure 3 2c) for HCP-2 show a system of positive and negative SSH features along the length of HCP-2 (Figure 4.2a). The positioning of the SSH features (positive west/negative east) fits the criteria established to identify a southward eddy-induced current in the vicinity of HCP-2. The distal end of the LC is undergoing LCE separation.

The evolution of the CHL signal for HCP-3 is shown in Figure 4.3a. The filamentous HCP-3 is coincident with a second CHL plume immediately east. The eastern HCP does not fit the criteria for inclusion in the study (defined in Chapter III as filamentous, forming near the Mississippi River delta, and CHL > 0.5 mg m^{-3}) due to its distance from the Mississippi River delta and lack of filamentous morphology. The eastern HCP forms prior to HCP-3 formation and may indicate shelf processes involved in the formation of HCP-3 that differ from the expected HCP model, such as coastal upwelling. HCP-3 extends south to 24° N. The following 8-day period shows that remnants of HCP-3 remain in the CHL signal, again differing from other HCPs investigated. The wind field in the vicinity of the Mississippi River delta associated with HCP-3 is southerly at 4.5 – 5.5 m s^{-1} (Figure 4.3b). The HCP-3 concurrent SSH field reveals a dipole eddy south of the HCP (Figure 4.3c). The dipole eddy is the result of one of four cyclonic eddies flanking a separating LCE as discussed in Walker (2011). The

eddy is positioned such that cyclonic rotation is east of anticyclonic rotation indicative of

possible HCP entrainment.
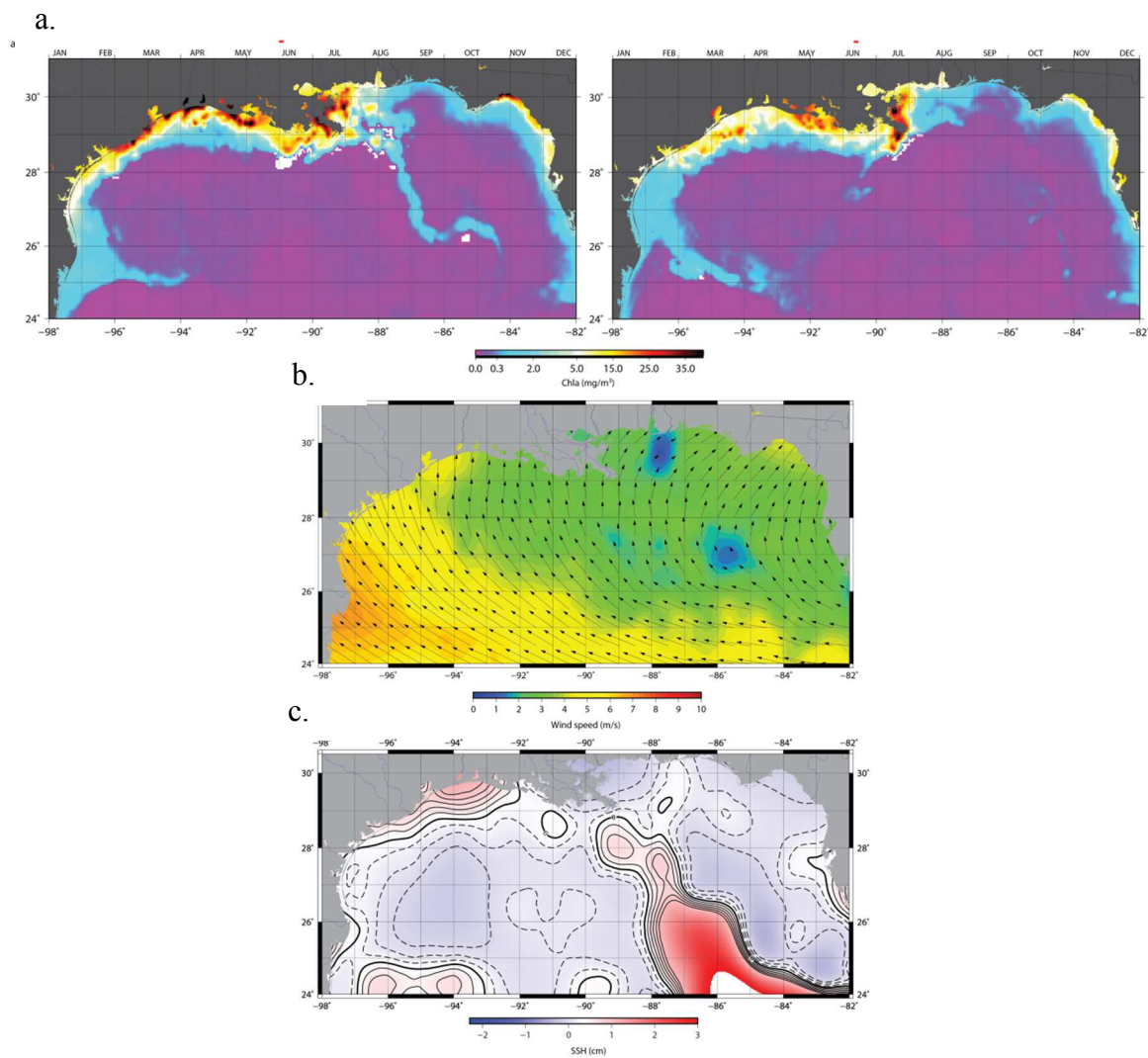
a.

b.

c.

Figure 4.2 HCP-2 Biophysical fields. (a) The 8-day composite CHL field of the period beginning June-2-2007 indicates an HCP southeast of the Mississippi River delta. (b) QuikSCAT wind fields support HCP development and (c) Merged SSH shows a dipole cyclonic-anticyclonic feature interacting with the HCP.

Figure 4.3 HCP-3 Biophysical fields. (a) The 8-day composite CHL field of the period beginning August-5-2011 indicates an HCP southeast of the Mississippi River delta. (b) QuikSCAT wind fields support HCP development and (c) Merged SSH shows a dipole cyclonic-anticyclonic feature interacting with the HCP.
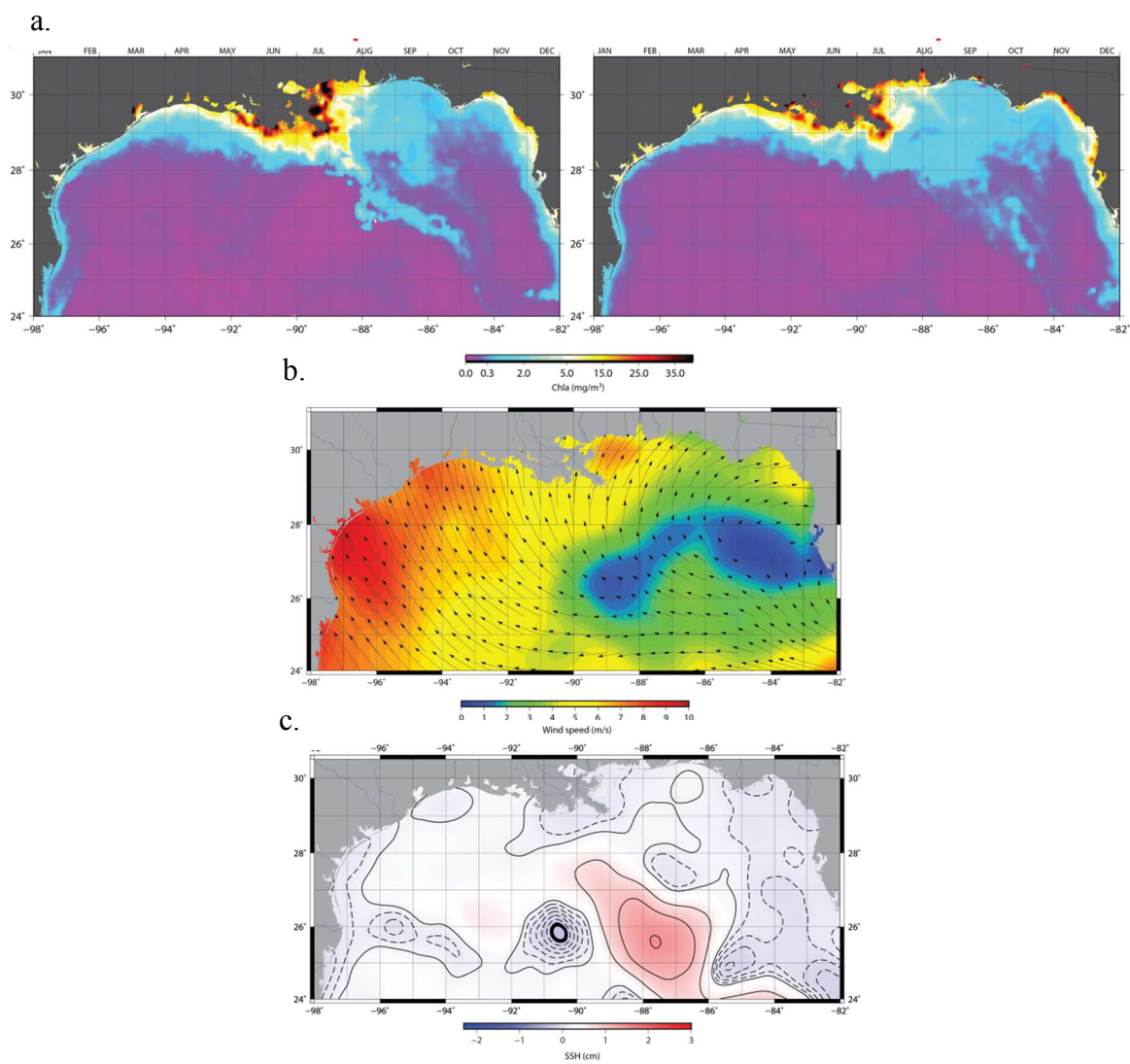
The HCP-4 CHL signal (Figure 4.4a) extends to 26.5° N. Associated SSH shows a distinct dipole eddy along the length of HCP-4 (Figure 4.4b). The eddy poles are aligned so that cyclonic rotation is east of anticyclonic rotation fitting the southward HCP formation criteria. As with HCP-2 and HCP-3, the SSH field reveals an LCE separation.

QuikSCAT winds are not available for HCP-4 and it does not fall within the date range of the work previously presented in this thesis. However, the SSH field, associated with HCP-4 and its availability for analysis through AMSEAS, warrants its inclusion in the marine system section.
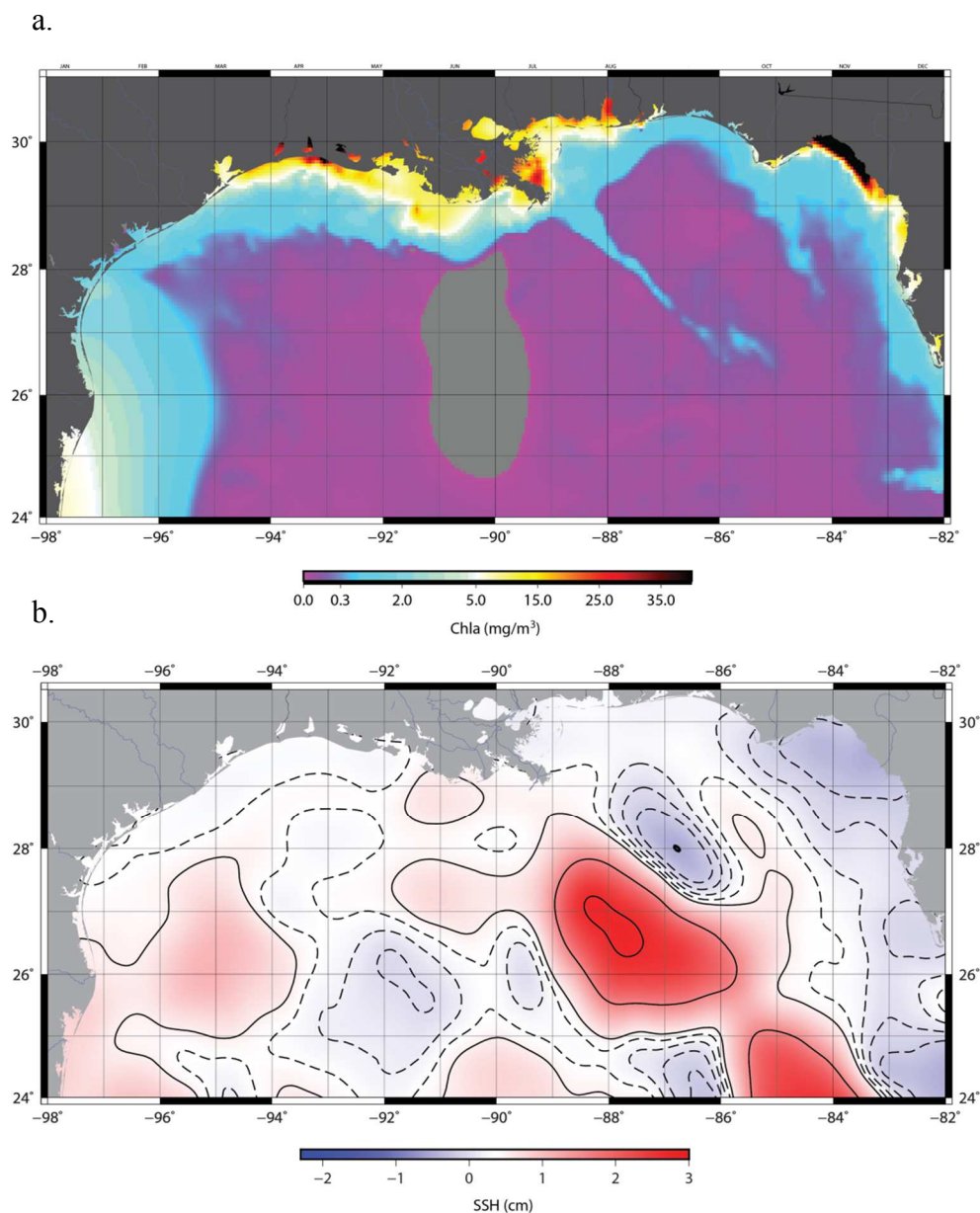
a.

b.

Figure 4.4 HCP-4 Biophysical fields. (a) The 8-day composite CHL field of the period beginning May-9-2013 indicates an HCP southeast of the Mississippi River delta (missing data due to cloud cover is shown as gray). (b) Merged SSH shows a strong dipole cyclonic-anticyclonic feature interacting with the HCP.

HCP Formation

The May-31 daily image (Figure 4.5a) shows low CHL with the LC impinging north beyond 28° N, but without eddy activity near the Mississippi River. On June-3, the LC has travelled to 28.5° N and is approaching the river delta (Figure 4.5b). A small extrusion of productive waters is seen extending from the river delta. By June-5 the CHL extrusion has extended to almost 28° N and a low SSH feature is forming east of the distal end of the LC (Figure 4.5c). On June-7, the CHL extrusion has become an HCP following the apparent advective path of an eddy/current system depicted by the SSH contours (Figure 4.5d). At this point, an LCE forms at the distal end of the LC. The maximum extension observed for HCP-2 is seen on June-9 (Figure 4.5e). Also noted for June-9 is the completed shedding of the LCE. Following the HCP dissolution a residual CHL signal is visible on the June-12 image (Figure 4.5f). The entrainment process determined by the daily SSH/CHL images supports the wind-river-circulation marine system proposed in prior modeling studies.
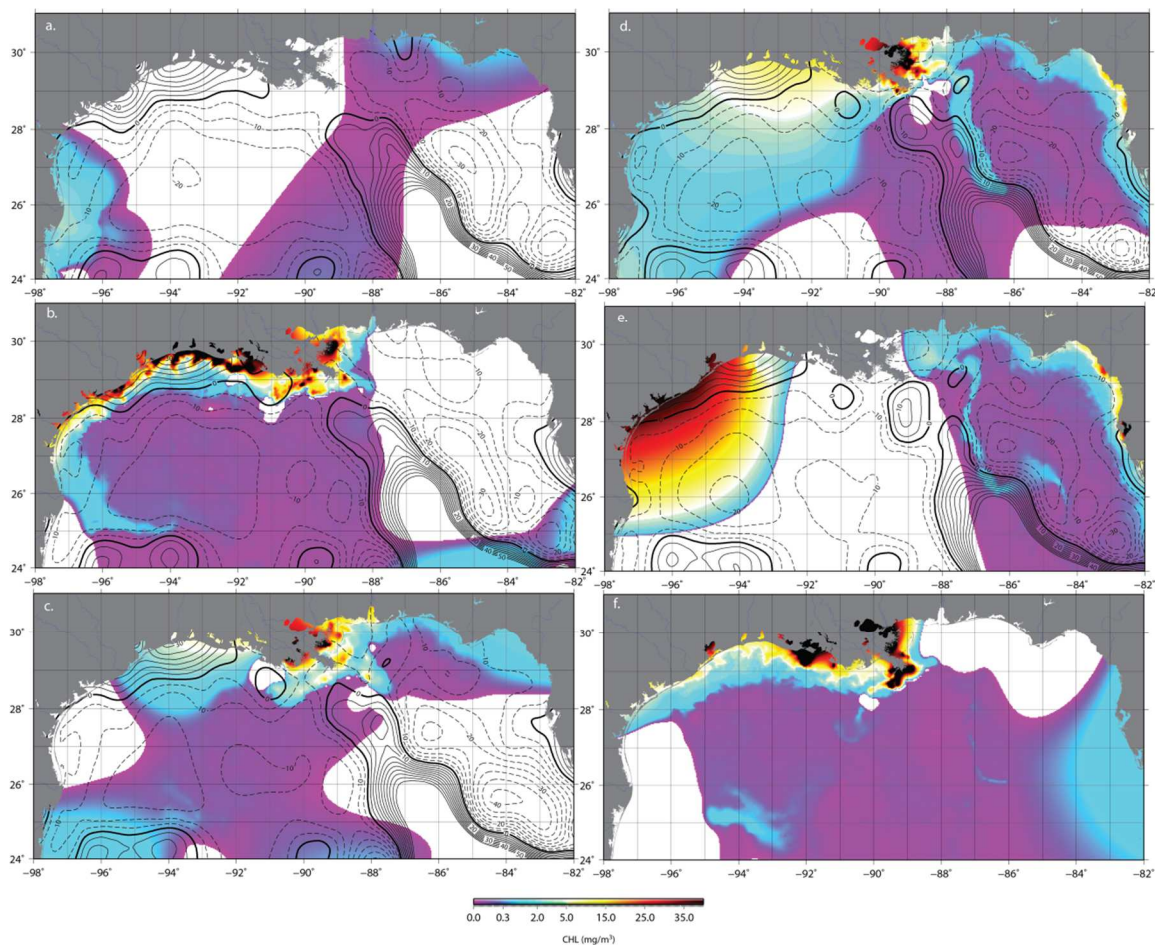
Figure 4.5.HCP-2 Daily CHL-SSH fields. Daily composites of CHL for the June-2-2007 HCP are superimposed with SSH contours to visualize HCP interaction with dipole eddy occurrence. Dates shown include (a) May-3-2007, (b) June-3-2007, (c) June -5-2007, (d) June-7-2007, (e) June-9-2007 and (f) June-12-2007.

Depth of HCP Advection

Figure 4.6a represents surface salinity for May-1-2013 through May-22-2013. A low salinity plume is seen across all of the dates shown and extends to 28° N on May-13, consistent with the MODIS-Aqua signal for HCP-4 which spans May-9-2013 through May-24-2013. Investigation of several depth layers for this time period show that the final low-salinity signal is present at 8m (Figure 4.6b). The shallow low-salinity signal implies that shelf and riverine waters are entrained only along the surface. Currents from

the AMSEAS model also show surface fields consistent with HCP formation (Figure

4.7a). Here currents of up to 1 m s^{-1} (similar to the measured 0.8 m s^{-1} measured in

Chapter III for HCP-2) are seen between two areas of counter rotation. The model output

suggests that the angle of the current shifts at the time of low-salinity plume extension.

The circulation patterns continue at depth (Figure 4.7b) with gradually weakening current

strength (0.4 m s^{-1} at 200 m depth).
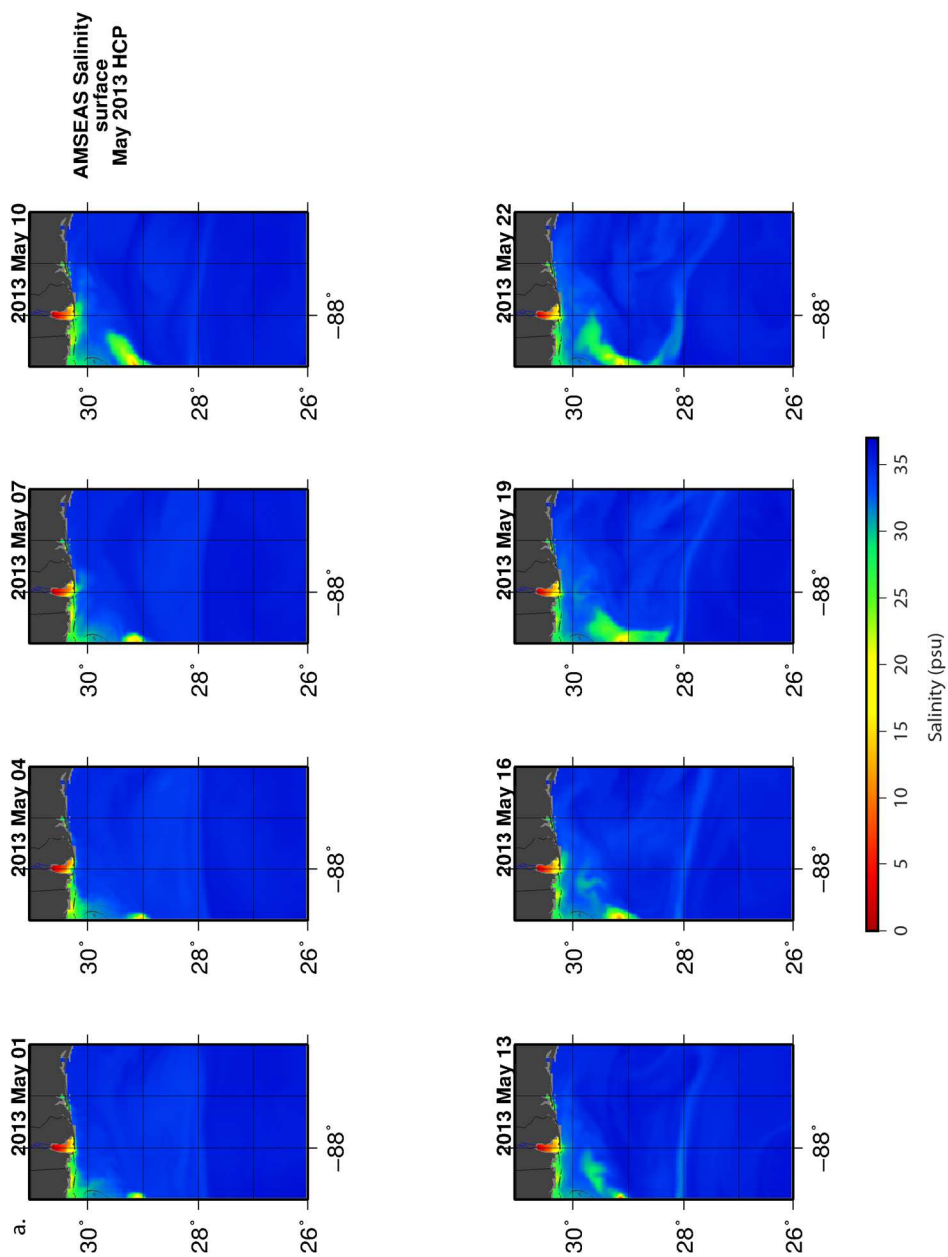
Figure 4.6. AMSEAS salinity output for HCP-4. Modeled salinity fields are shown for the dates before and during HCP-4. Low salinity is observed in (a) surface level fields through (b) 12 m depth fields.
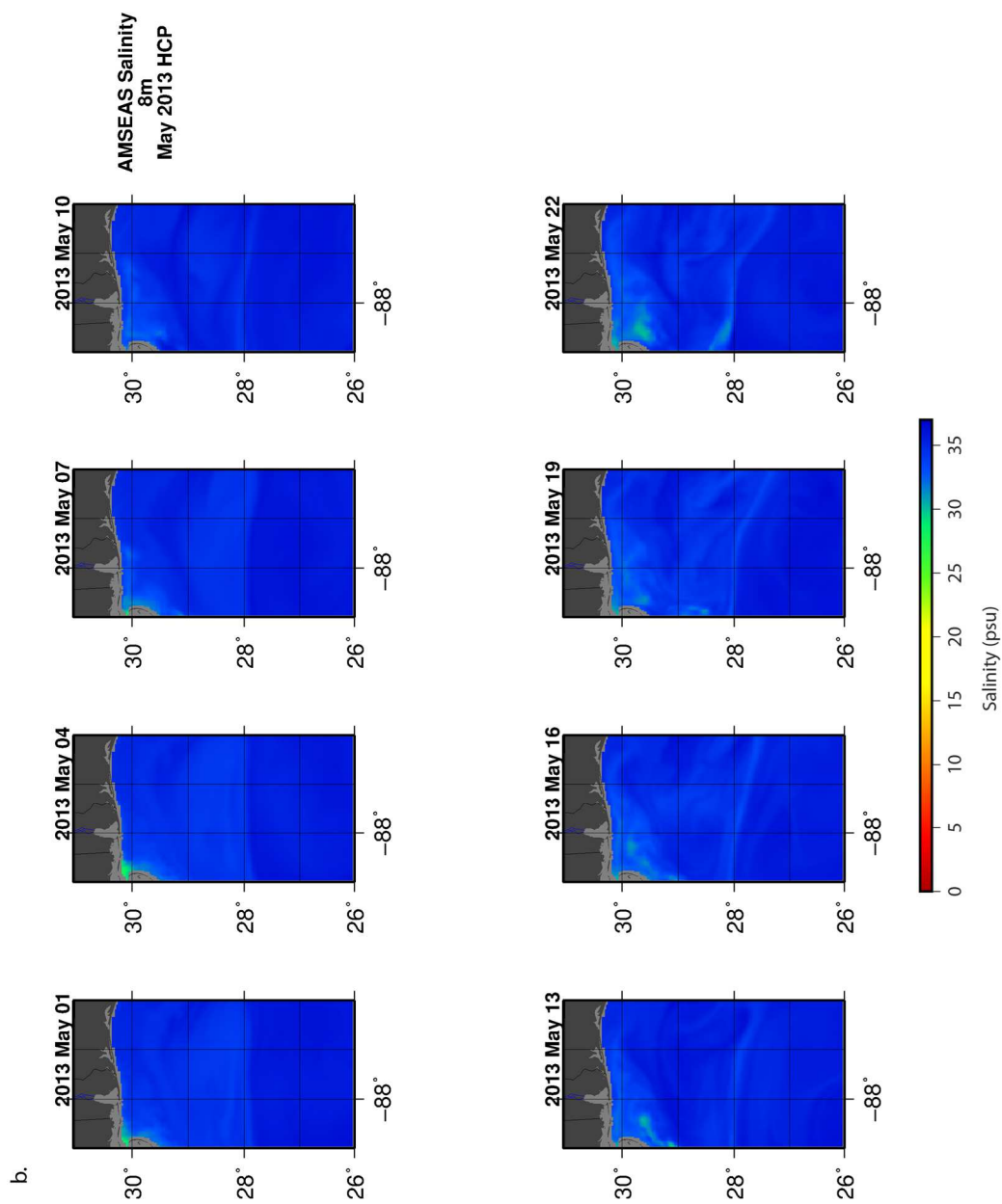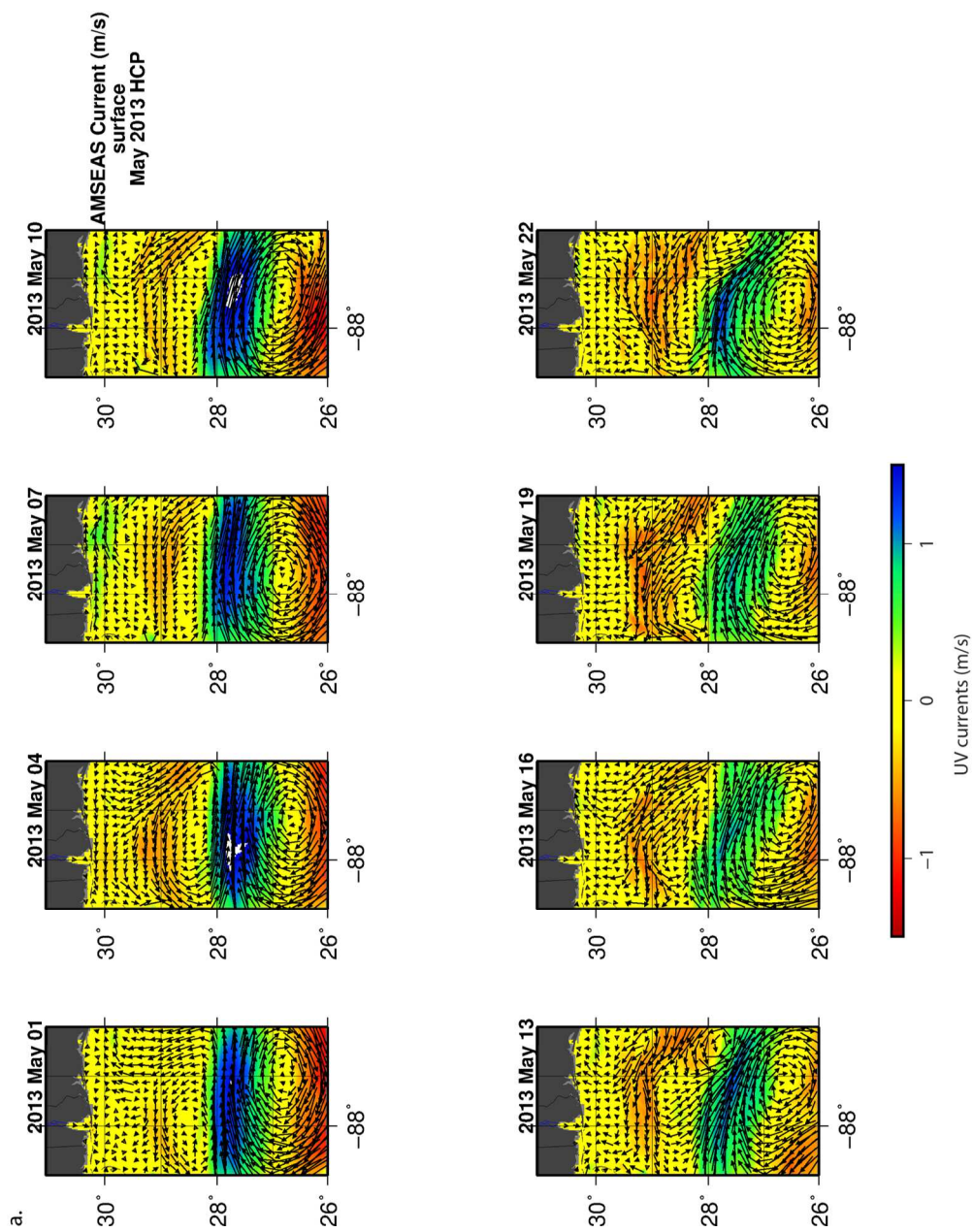
Figure 4.6. (continued).

Figure 4.7. AMSEAS current output for HCP-4. Modeled current fields are shown for the dates before and during HCP-4. HCP-conducive currents are observed in (a) surface level fields through (b) 200 m depth fields.
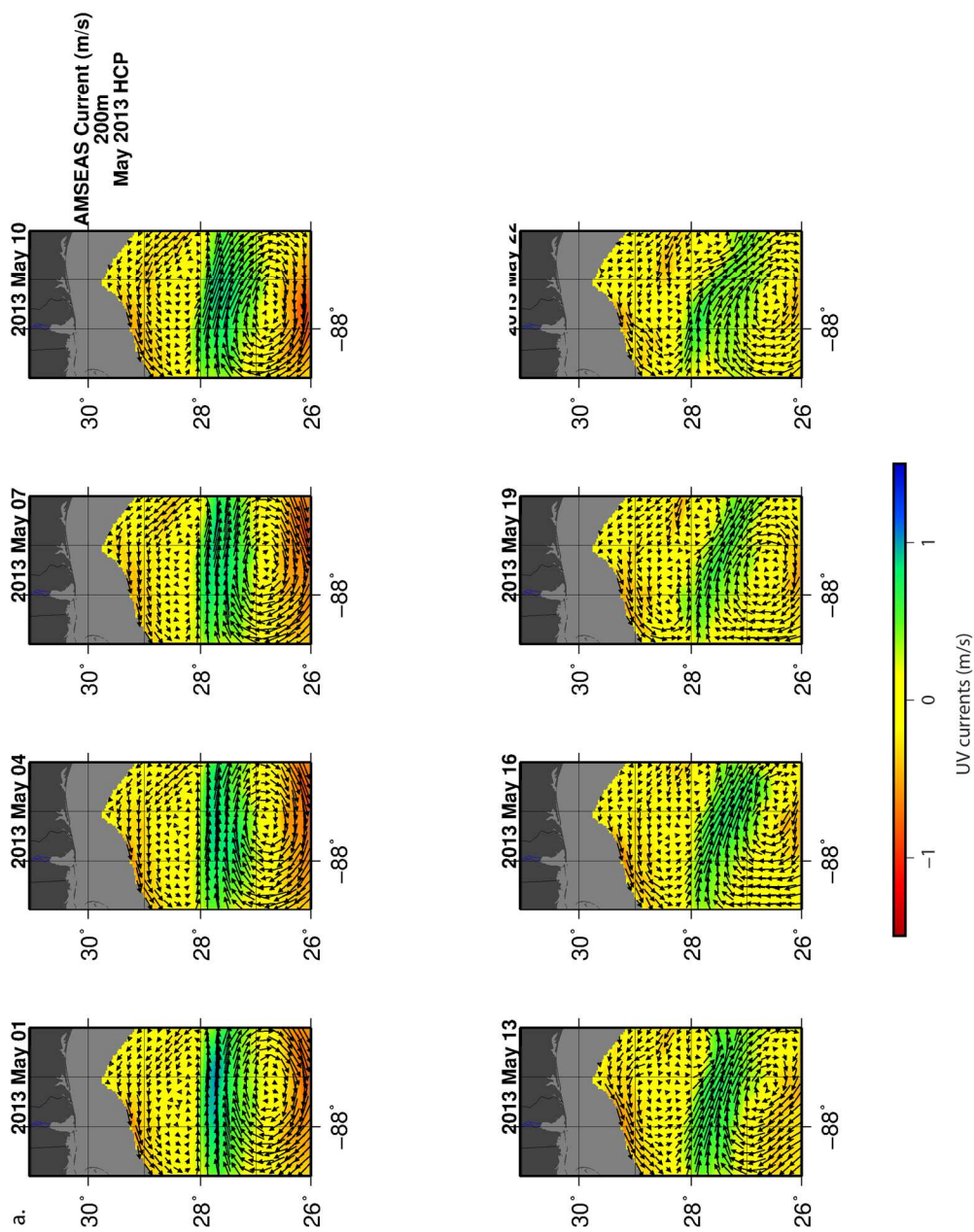
Figure 4.7. (continued).

The model output also provides insight to the role of circulatory features in triggering HCP formation. The surface low-salinity plume extends southward on May 13 (Figure 4.6a). The corresponding surface current panel (Figure 4.7a) shows that although the position of the anticyclonic rotation does not change on May 13, that there is a strengthening of the northeastward cyclonic rotation. The stronger cyclonic rotation also occurs on May 4. Anticyclonic rotation is located further south on May 4, possibly too far removed to entrain low-salinity riverine waters.

Mississippi River Discharge and CHL

At the 200m isobath, the Mississippi River discharge dominates the surface CHL field every year for the 14-year record (Figure 4.8a). A lateral signal in CHL for the Mississippi River is apparent most years between 90° W and 88° W, with occasional excursions west to 92° W and east to 87° W. The strength of the river signal varies interannually with strong signals recorded in 1998, 1999, and 2010. The signal is weakest in 2000, 2006 and 2007. The CHL anomaly (CHL_A) field shows that most years undergo a period of low CHL_A in the first half of the year. Also evident in the CHL_A field is that years 1998, 1999, 2009 and 2010 have unusually positive anomalous CHL_A near the river delta. A normalized diagram (CHL_Z) is included to temper the signal of the river and evaluate anomalous river CHL_A within the context of Gulf CHL_A. The positive anomaly, seen in the years 1998-99 and 2009-10, extends beyond the typical lateral zone of the Mississippi River discharge, as seen in the CHL_Z field, suggesting that the high CHL signal is not entirely based on river discharge. Also notable in the CHL_Z field is a mid-2008 positive anomaly to the west of the river outflow. Negative anomalies are less

common in the CHL$_Z$ diagram and appear somewhat coincident with the years of low
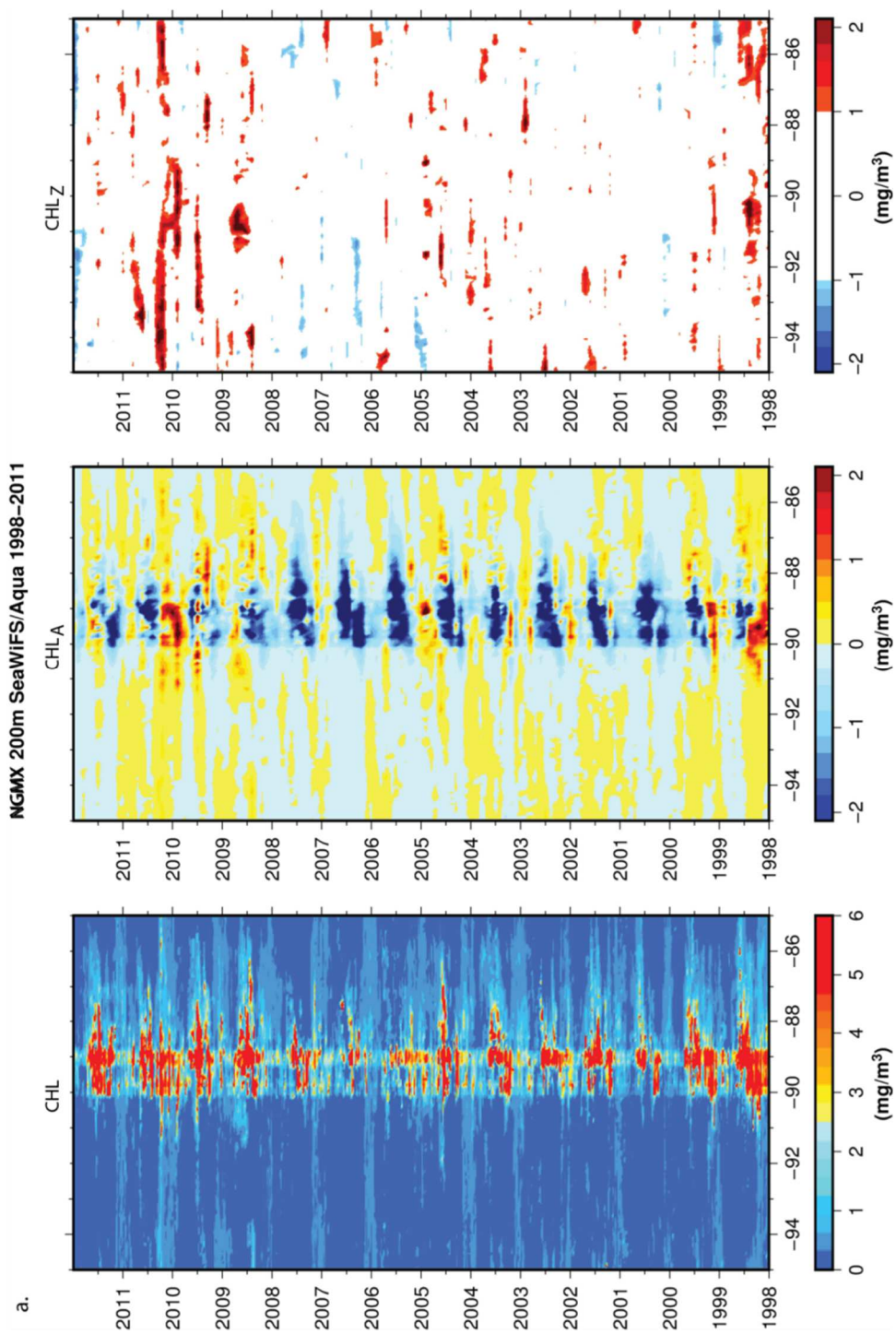
river signal.

Figure 4.8. CHL Hovmoller diagrams. Hovmoller diagrams depicting CHL, anomalous CHL and normalized-anomalous CHL across the Gulf are shown for (a) the 200 m isobath, (b) the 500 m isobath and (c) the 2500 m isobath.
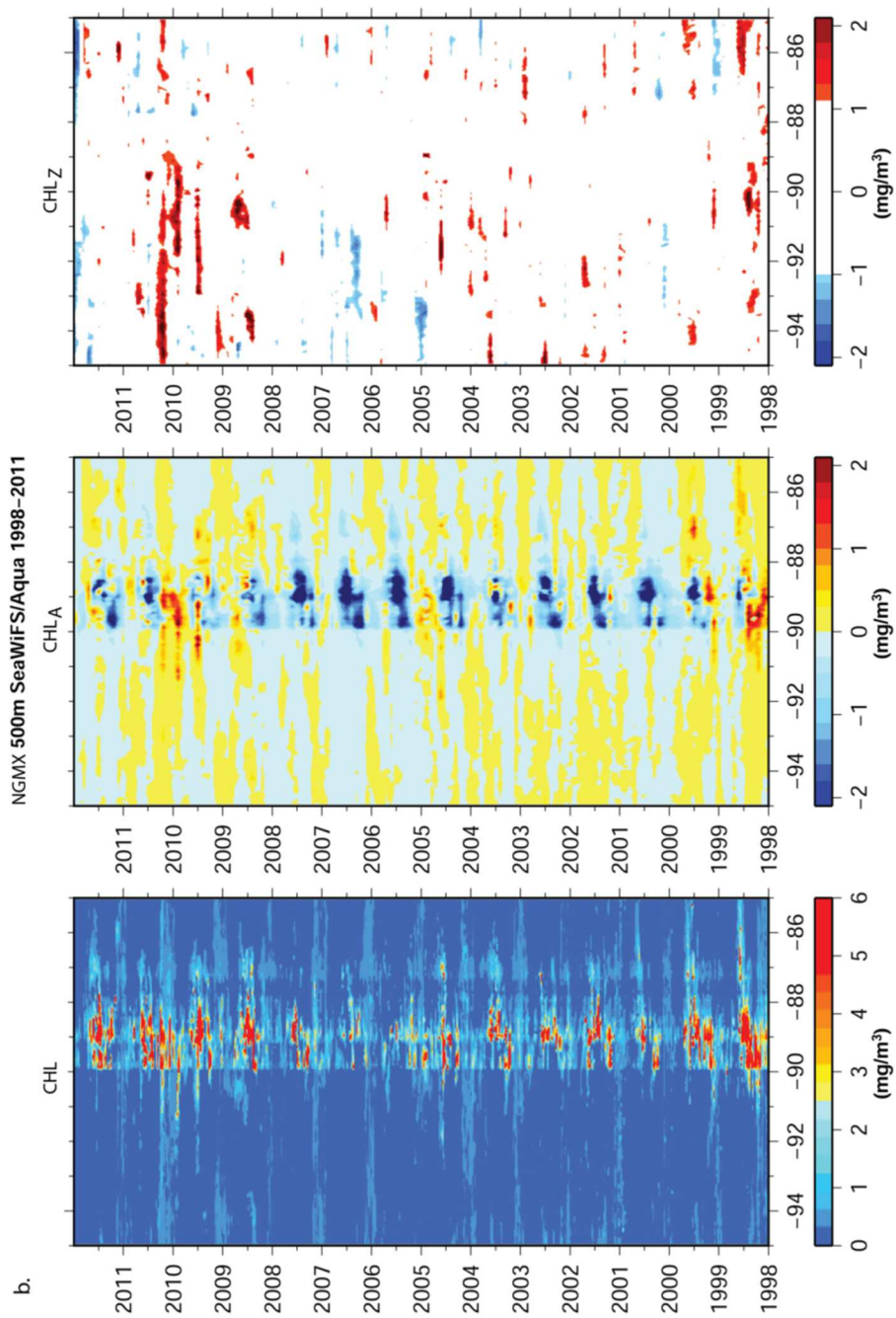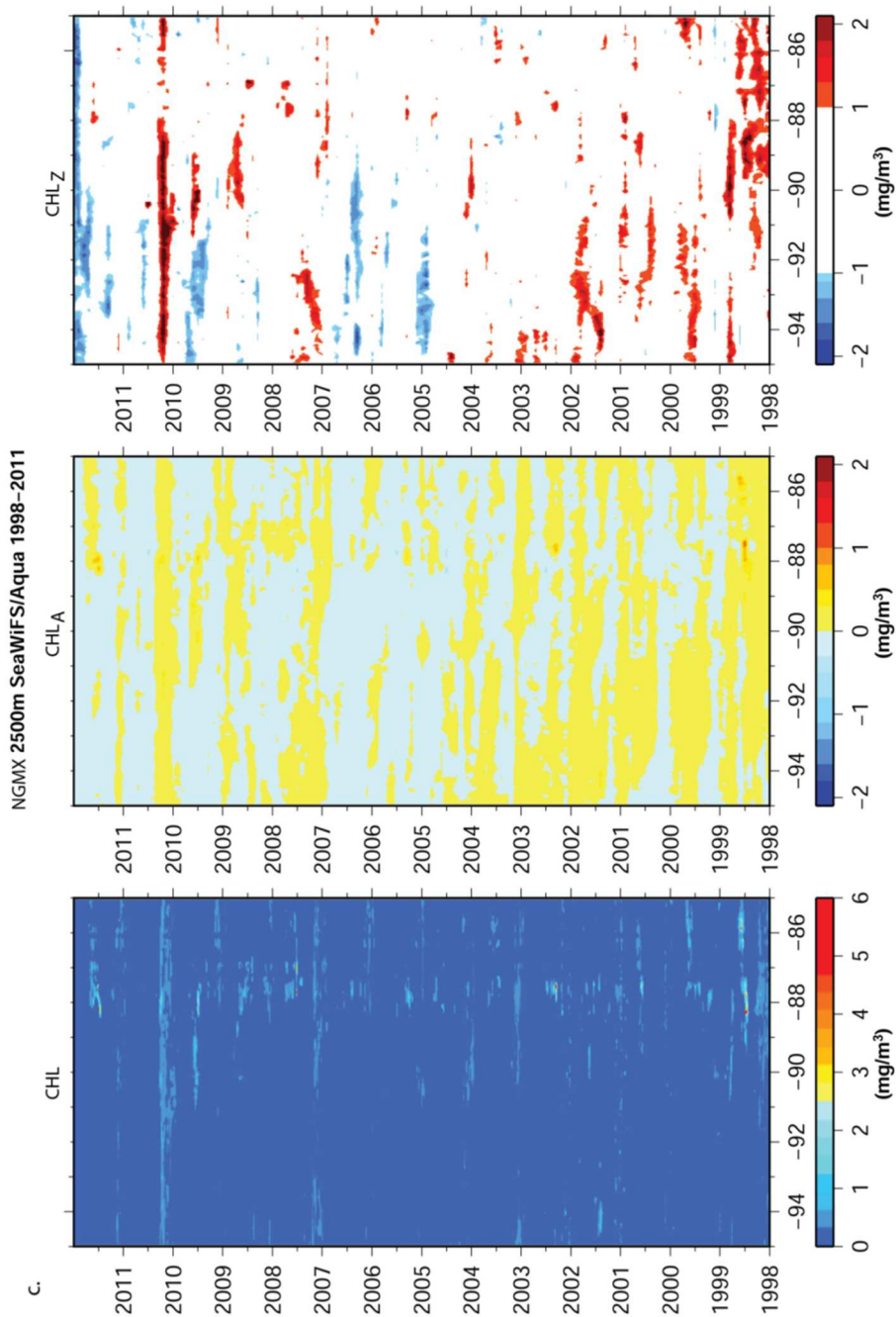
Figure 4.8. (continued).

Figure 4.8. (continued).

The Mississippi River discharge continues to dominate the surface CHL field at the 500m isobath (Figure 4.8b). The strongest positive signal is seen in 1998, while the longest enduring positive signal is seen in 2010. This trend continues in the CHL_A diagram with significant positive anomalies seen only in 1998, 2010 and briefly in 1999. The CHL_Z diagram also highlights positive CHL_Z in 1998 and 2009-10. However, here a lateral difference is noted in that the 1998 signal is strongest from the center eastward while the 2009-10 signal is strongest from the center westward. Low CHL signals near the river are seen in the CHL diagram in years 2000, 2002, 2005, 2006, and 2007. This translates into strong negative CHL_Z in 2000, 2005 and 2006.

Moving to the 2500m isobath, the dominance of the Mississippi River has diminished. Evaluating the surface CHL signal at this isobath gives a sense of non-riverine interannual CHL dynamics as a context for interpreting the river signals. To stay consistent with previous diagrams, the scale used for the CHL field dilutes any notable variability (Figure 4.8c). A trend in the CHL_A field of more positive anomaly during the first 7 years of the satellite record and more negative anomaly during the last 7 years is evident. The trend is more apparent in the CHL_Z field (Figure 4.8c) where little negative anomaly is indicated before the end of 2004. The positive CHL_Z noted during years 1998 and 2010 of the 250 m and 500 m diagrams are also present in the 2500 m diagram. This indicates processes across the Gulf during these years that are not limited to river-dominated regions.

The Mississippi River seasonal pattern detected is higher discharge in spring and summer months with lower discharge during fall and winter months (Figure 4.9 inset). Annual minima are consistent while annual maxima vary both in amplitude and duration

of high flow. The lowest discharge maxima are seen in years 2000, 2006 and 2007. The highest amplitudes are seen in years 2008 and 2009. Years 2001, 2008 and 2009 have short-lived maxima, while years 2002 and 2010 (including late 2009) show relatively longer periods of high discharge. The relationship of the CHL_Z to these river trends differs by region. For the NGMx region, a weak positive correlation is seen between discharge and CHL_Z (covariance 0.24). A peak in CHL_Z following the strong discharge maximum in 2008 and the persistent maximum of 2010 are observed; however, the lack of consistency between these parameters suggests that rather than the river discharge leading to a rise in CHL_Z, the peaks are due to independent forcings or to an external force on each parameter. In the Open Water region, the normalized river discharge and CHL_Z do show a similar seasonal pattern, yet the covariance is only 0.16. The rise in CHL_Z amplitude precedes the rise in river discharge amplitude, indicating that the similar patterns are independent seasonal patterns as it is unlikely that CHL_Z in the basin is affecting discharge rates. The 2008 peak in CHL_Z is not seen for the Open Water, but the 2010 peak is present. This discrepancy is similar to that seen in the earlier seasonal trend analysis above and points to the 2008 CHL_Z peak being due to shelf processes and to the 2010 CHL_Z peak being due to a basin-wide or atmospheric process. CHL_Z in the Study area is less seasonally constant than the Open Water region and peak CHL_Z does not covary with river discharge (covariance 0.11). The 14-year CHL_Z maximum follows the 14-year Mississippi River discharge maximum, indicating a localized process when considered in relation to the Open Water region. The 2010 river discharge maximum is also followed by a peak in CHL_Z within the Study area although the peak is less anomalous than in the NGMx and Open Water regions.
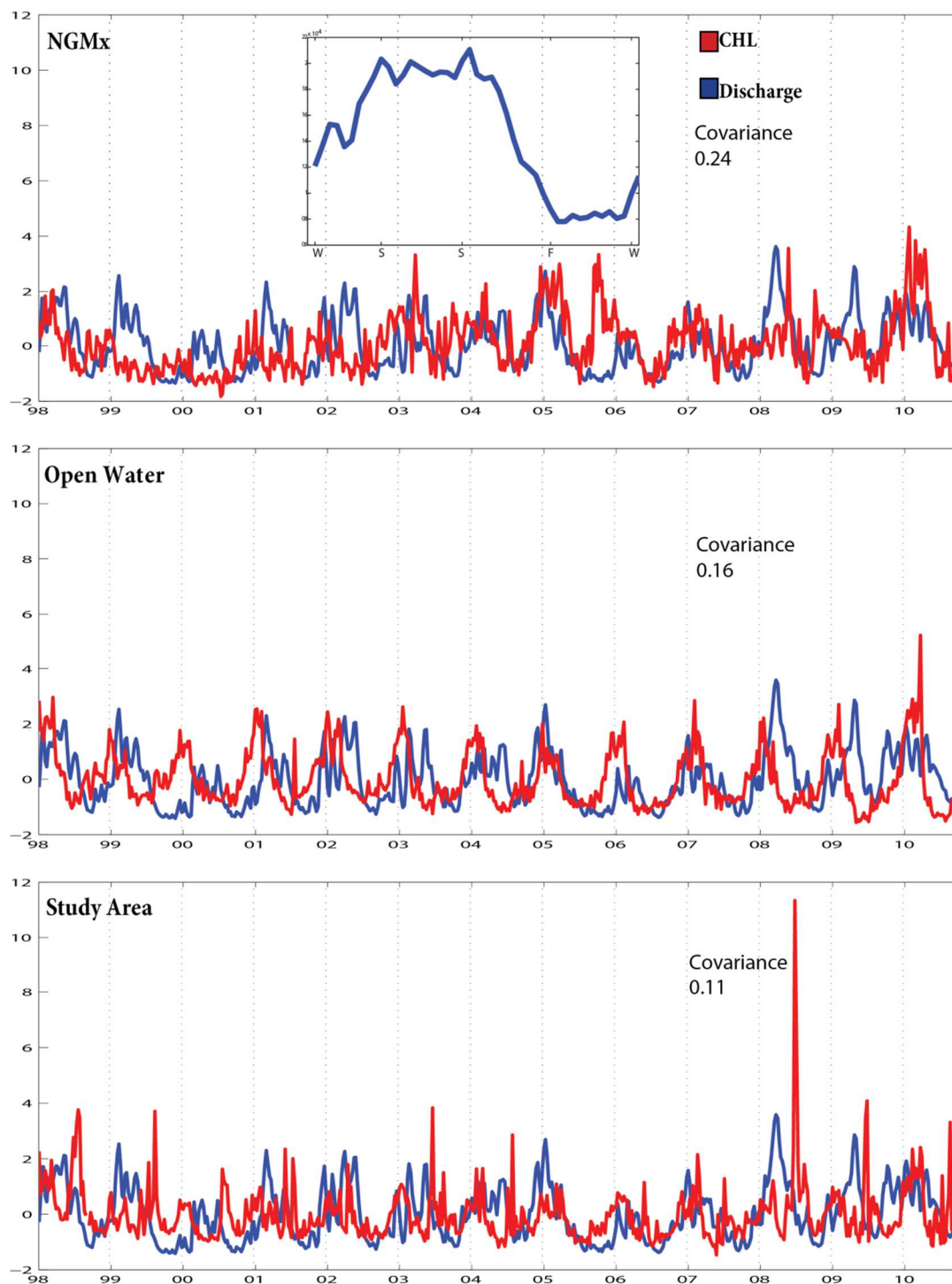
Figure 4.9. River-CHL. The z-normalized Mississippi River discharge (blue) and z-normalized 9-day CHL (red) are shown for the regions defined in Chapter II. Daily river values are binned into 8-day mean flow values to correspond with CHL composites. Seasonal Mississippi River discharge is shown in the inset plot.

El Niño-Southern Oscillation and CHL

A link between Gulf CHL dynamics and changing ENSO conditions was investigated using the MEI monthly dataset and the 8-day SeaWiFS and MODIS-Aqua combined 14-year CHL dataset. MEI monthly assessments of ENSO have recorded 13 MEI values > 1 standard deviation above the mean or El Niño events since December 1949 (Wolter & Timlin, 2011). Of the top eight events throughout the recorded data, considered strong El Niño years, two fall within the ocean color satellite record. These events occur in 1997-1998 and 2009-2010. The strongest negative anomaly (La Niña event) during the satellite data range is seen in 2010-2012 (Wolter & Timlin, 2011). The 2010-2012 La Nina event is the strongest recorded since 1988. Again considering the isobaths prescribed in the Mississippi River-CHL discussion above, interannual normalized-anomaly fields of CHL are evaluated within the context of the MEI.

Along the 200m isobath, the strongest positive normalized-anomalies of CHL are seen in years 1998, 2008, 2009 and 2010 (Figure 4.8a). Of these, only the 2008 anomaly is narrowly confined, the 1998 and 2009-2010 positive anomalies extend across the -95 W to -85 W domain. These years coincide with the MEI El Niño events with the exception of the more localized 2008 anomaly. This trend continues with the 500m isobath with a less significantly positive anomaly seen in 1998 (Figure 4.8b). At the 2500m isobath, positive and negative anomalies are more frequent (Figure 4.8c). The 2009-2010 is the strongest positive anomaly in terms of magnitude and concurrent lateral coverage, while the 1998 positive anomaly is longer lasting yet with a stronger signal east of 90° W. The end of 2011 also shows a strong negative anomaly, the only negative anomaly to cover the entire longitude band. This signal is observable at all isobaths, but

is most apparent at the 2500m isobath. The 2011 negative anomalies are concurrent with the 2010-2012 La Niña event of the MEI.

Within the three regions prescribed above in the river-CHL analysis (NGMx, Open Water and Study Area), a similar significance in enhancement-peaks (CHL > 2 standard deviations above the mean) for years 1998 and 2010 are seen for the Open Water and Study Area regions (Table 2.1 from Chapter II). In the Open Water region, the typical enhancement-peak frequency is 1.3 enhancement-peaks/yr. Years 1998 and 2010 are the only years within the 14-year range with 3 or more enhancement-peaks. This is repeated again in the Study Area which has an enhancement-peak frequency of 1.2 enhancement-peaks/yr yet experiences 4 and 3 enhancement-peaks during year 1998 and 2010 respectively. This pattern is not repeated in the NGMx region, suggesting that ENSO may be less influential across all areas of the water body or may have different effects which are muted from the CHL signals.

Both HCP frequency and timing within the Study Area show a relationship to the MEI. The HCP frequency of ~2.7 HCPs/yr is reduced during years 1998 (1 HCP) and 2010 (0 HCPs). These two years are the only years in the 14-year record without a spring or summer HCP observed. This indicates a change in environmental conditions (wind or circulation) necessary for HCP development. Due to coincident Mississippi River discharge values which are at or above the mean in the winters preceding the spring/summer HCP season for years 1998 and 2010, a lower than normal CHL concentration in HCP headwaters is not indicated.

Discussion

A modeled marine system of seasonal winds driving Mississippi River plume waters east combined with dipole eddy induced cross-shelf transport of the plume has been shown in previous work to contribute to the formation of HCPs in the NGMx (Morey et al., 2003; Schiller et al., 2011). This study utilizes satellite observations of HCP-associated fields to validate the proposed marine system contributing to HCP development.

Dipole-eddy induced currents are typically implicated as physical drivers of cross-shelf transport (Morey et al., 2003, Schiller et al., 2011, 2013) and would therefore be expected to play a role in HCP formation. For the HCPs presented here, dipole eddy involvement (and/or eddy-LC system) was directly linked to HCP extension. The formation of a limited HCP (HCP-1) without dipole eddy or LC/eddy involvement indicates that wind-driven migration of Mississippi River waters is the necessary factor in forcing HCP formation. However, only those HCPs that were coincident with an offshore dipole eddy or LC/eddy system evolved to extensive HCPs (south of 27° N). A similar finding is also noted in Chapter III (Table 3.1). These findings point to the importance of offshore circulation in the delivery of shelf/riverine waters to the central basin.

Daily CHL and SSH observations for HCP-2 (June-2-2007) point to the differentiation of anticyclonic and dipole rotation. HCP-2 is ongoing for several days as a limited HCP, not extending south of 28° N, when only anticyclonic rotation is proximal to the shelf. However, as cyclonic rotation spins up and the HCP gradually migrates toward the resultant current, the HCP quickly extends down the length of the dipole eddy's advective path. This suggests that anticyclonic rotation is generally a factor in

HCP presence, while adjacent cyclonic rotation denotes extensive HCP formation (extension to 27° N). This is perhaps due to a stronger current induced by the counter-rotation, but may also be due to the eddy dynamics themselves such as eddy strength. All HCPs shown in this section were coincident with LCE shedding. The effect of this phenomenon on surface circulation could potentially set up conditions necessary to form extensive HCPs such as current intensification due to increased strength of the anticyclonic LC eddy as it separates.

The suggested trigger for extensive HCP formation is offshore circulation (dipole eddy or LC/eddy system); however, seasonal winds are seen to been the contributory factor for both limited and extensive HCPs (Jones & Wiggert, 2015). The winds in the NGMx tend to follow a pattern of strong northerly winds from October – March and weaker southerly winds from late June – August. Transitional winds are observed in April – June and again in September. The summer southerly winds, and at times the transitional spring winds, can relax the westward along-shore current constraining the Mississippi River plume to the Louisiana-Texas shelf. This allows the eastward spread of riverine waters to the high eddy energy DeSoto Canyon region (Schiller et al., 2011, 2013). All HCPs investigated in this study support this model with southerly and southwesterly wind patterns seen during each event.

The shallow plume of low-salinity water in the AMSEAS model output is indicative of the vertical extent of HCPs. Deeper shelf water, rich with nutrients and particles, would still be expected to have a lower salinity profile than central Gulf waters. Thus the model suggests that the CHL signal is of modified shelf waters and does not reflect only growth of local (central Gulf) phytoplankton spurred by nutrient delivery

from cross-shelf flow. However, even deep shelf waters could shoal to the surface of the deep water column. The depth of the current signal from the model could support either proposal. An *in situ* field study of the vertical profile of an HCP would be valuable to broaden the understanding of HCP mechanisms and determine phytoplankton species composition, but remains impractical for this study.

The magnitude of CHL within a given HCP is potentially linked to the environmental conditions controlling NGMx CHL dynamics at the time of the HCP. Mississippi River discharge, expected to significantly contribute to Gulf CHL concentrations, dominates the Gulf CHL profile to beyond the 500m isobath. River output shows a strong seasonal pattern as does CHL. A comparison of the NGMx CHL/river relationship and the central Gulf CHL/river relationship reveals that NGMx CHL follows river patterns with high CHL following high discharge, but the central CHL precedes river discharge. These findings indicate that CHL, which is seasonally controlled in the central Gulf, and river discharge are both seasonally dependent and that only shelf waters are sensitive to fluctuations in river output. The similarity in anomalous years seen between NGMx CHL and river output also suggests that NGMx CHL is sensitive to anomalies in Mississippi River discharge volume. Only anomalies in years 1998 and 2010 are shared between river output and central Gulf CHL.

The CHL anomalies seen in years 1998 and 2010 are concurrent with lower than normal frequency of HCPs during these years and in the frequency of enhancement-peaks in CHL (higher than normal). These shared anomalies are only present during years 1998 and 2010 throughout the 14-year satellite record. Interestingly, this coincides with strong El Niño years as indicated by the MEI. A low anomalous value in late 2011 is also

coincident with a strong La Nina event. The MEI is constructed of several data points to monitor ENSO variations, therefore a comparison between each contributor to the MEI calculation and the anomalies found here would be necessary to analyze how ENSO is affecting the Gulf CHL dynamic. While not fully resolved, the potential climate relationship to the CHL signals does provide insight to the NGMx versus more localized anomalous CHL values seen in Figure 4.8. Global climate influence is indicated for zonally inclusive 1998, 2010, and 2011 anomalies whereas, river flooding is more likely contributing to the 2008 positive anomaly only present near the river delta. The shift in mode from a condition of CHL normalized-anomaly positive to CHL normalized-anomaly negative seen at the 2500m isobath is not explained by the MEI, but is similar to the Gulf SST/ Atlantic Multidecadal Oscillation positive association which Muller-Karger et al. (2015) found..

The results found in this study support previous investigations of cross-shelf flow and HCP development in the NGMx by providing satellite evidence for the wind-river-circulation model of HCPs. This work would greatly benefit from depth profiles of bio-optics during HCPs (modeled and/or in situ) as well as continued exploration into the variations in CHL of individual HCPs.

CHAPTER V

CONCLUSIONS

Satellite measurements from MODIS and SeaWiFS instruments were used, in conjunction with other remote and *in situ* measurements, to observe and analyze physical and biological phenomena across the full temporal range of data available from these sensors. The regional analyses of ocean color and environmental conditions reveal the phytoplankton response to marine environmental drivers, with a focus on HCPs or cross-shelf transport induced offshore phytoplankton blooms following the advection of surface shelf waters to the oligotrophic offshore waters of the Gulf of Mexico. The ocean color and physical fields associated with the development and characteristics of the HCPs presented here provide insight to the complex relationship of HCPs with the NGMx water column.

Across the NGMx and the central basin waters, a seasonal pattern of CHL was detected with higher CHL in winter months and low CHL in summer months. This winter bloom seasonal pattern has been reported to imply sufficient light penetration during winter mixing (deepening of the mixed layer depth) to allow continued phytoplankton growth (Muller-Karger, 2015). Another explanation for the winter bloom is that the deepening of the mixed layer depth during winter months dilutes the euphotic zone thereby decoupling phytoplankton growth and loss due to grazing (Behrenfeld, 2010). This decoupling effectively increases phytoplankton biomass. For either scenario, the seasonal cycle of CHL, particularly near the shelf, is subject to summer or midyear peaks in CHL.

The frequency of midyear enhancement-peaks of CHL, often coinciding with the formation of HCPs, was shown to contribute to a CHL summer maximum along the NGMx shelf break, south and east of the Mississippi River delta. Seasonality and interannual variability of CHL and other bio-optical parameters across the Gulf were shown to depend on largely on proximity to the continental shelf. Near the shelf river discharge from the Mississippi River is the primary source of variability in ocean color while in central Gulf waters seasonal cycles consistent with SST variability dominate the ocean color cycles. Interannual variability was higher near the shelf where CHL concentrations are prone to shelf/coastal processes. The interannual variability of all regions considered exhibited a weak link to ENSO variations with increased enhancement–peak occurrence and decreased HCP occurrence. Further exploration of this link would be useful to understand how the Gulf will respond to expected climate change. Also, exploring HCP occurrence in connection with other climate indicators known to affect this region (AMO) or similar systems could provide tools for predicting Gulf response. For instance, Wang et al. (2014) show that although ENSO and the Missouri River are linked, as is this study region, that it is actually the more spatially distant Pacific Quasi-decadal Oscillation that has a stronger impact on river flooding events. This is a particularly important find as it reveals a lead-lag effect on the Missouri River that may be missed in some estimations, possibly relevant to Mississippi river studies as well.

Although HCPs are not distinct in averaged spatial regions, due to muting of the narrow ocean color effect of HCPs during averaging, the data show that impacts are significant in terms of phytoplankton dispersion and primary productivity. The results

from the investigation of a 2007 HCP contributes to the understanding of the biological impact seen at various locations in the NGMx during an HCP event. The increased values and ratio consistency of bio-optical properties along the 2007 HCP provide evidence to the advection of shelf surface waters and materials to the central gulf. Additionally, the 2007 HCP investigation provides evidence suggesting shifting wind direction and dipole eddy induced flow to the formation of HCPs. The increased NPP values during the 2007 HCP led to carbon budget contributions above the typical condition, but also pointed to the interesting and unresolved divergence of the NPP and CHL measurements.

Assessment of the modeled marine system indicated in HCP formation showed a strong agreement between previous model studies and actual HCP events. Wind fields near the Mississippi River plume were shown to trigger eastward spread of the typically westward constrained plume. HCPs of extensive length were also associated with dipole eddy, or Loop Current/eddy, advection. These observations and inferences are in line with previous analysis of HCP formation on the nearby West Florida shelf (Gilbes et al., 1996; Jolliff et al., 2003), where HCPs were suggested to be driven eastward by LC circulation and southward by shelf circulation. Daily CHL images of the 2007 HCP show the slow meander of productive waters prior to eddy involvement rapidly progress southward following dipole eddy entrainment. The vertical profile of a 2013 HCP revealed that HCPs manifest in only the upper few meters of the water column.

The hypotheses were met with differing results. Hypothesis 1 was not supported as mesoscale circulation features were not shown to contribute directly to midyear peak (NGMx CHL enhancement-peaks). Instead, the timing (late spring/summer) is suggestive of changing wind fields relaxing alongshore currents and the resultant eastward spread of

the Mississippi River plume. Also, rather than reveal a differentiation of midyear peak mesoscale drivers within subdivided regions of the NGMx, the subdivided regions pointed to a lessening of the midyear peak significance to CHL cycles proportional to distance from the shelf.

Hypothesis 2 was not supported as HCPs were not seen to contribute to the seasonal cycles of any of the three sub-regions selected. However, the CHL enhancement-peaks did show a gradient of impact relative to distance to the shelf. The peaks are suggested here to be the result of riverine enhancement of growth east of the Mississippi River during wind-driven summer migration of the plume. Future research into the cause of enhancement-peaks would help to clarify this process.

Hypothesis 3 was supported by a comparison of daily CHL fields and SSH fields. The SSH-CHL fields indicate that once entrained by the dipole eddy, the 2007 HCP was extended toward the central Gulf within the residence time of buoyant riverine waters. This rapid extension indicates the maintenance of water body properties near the HCP headwaters, in this case the continental shelf east of the Mississippi River delta.

Hypothesis 4 was supported by the analyses of bio-optical relationships along the 2007 HCP. The typical bio-optical parameter ratios were altered during the HCP. The effect was that ratios and magnitudes of the parameters were more consistent within the HCP (opposing the general distance to shore gradient of parameter ratios).

Considering the relationship between HCPs and enhancement-peaks of CHL in the context of the physical analysis presented here, it is likely that both are signals of Mississippi River plume migrations. The regularity of the enhancement-peaks and the strong shelf to offshore gradient of peak frequency suggests that the peaks are the result

of seasonal riverine eastward spread. HCPs are also dependent on this spread, but occur with circulation dependent entrainment. This circulation dependence leads to the irregular patterns in HCP formation throughout spring and summer months. Gilbes et al. (1996) found a similar seasonal range of irregular plume, or HCP, presence on the West Florida shelf. Using CZCS observations to detect high-CHL plumes, they found annual HCP occurrence between February and May for years 1979 through 1986. The HCPs were of similar CHL magnitude to those extending from the Mississippi River delta and persisted for one to four weeks on average. The authors proposed that the HCPs were "seeded" by a combination of LC-driven Mississippi and Mobile river waters to the West Florida shelf and local upwelling and discharge.

The analysis of Mississippi River discharge presented here shows that CHL concentrations in the Study Area are not primarily controlled by the volume of the discharge; however, the river waters clearly cause perturbations to the seasonal cycle. This lack of correlation to Mississippi River discharge was also found by Gilbes et al. (1996), despite their suggestion that the river was a contributor to HCPs on the West Florida shelf.

The results presented in this thesis show the significance of HCPs to the NGMx and also further the understanding of the NGMx complex marine system. Future endeavors to quantify ENSO-CHL links in the region and the application of the results in this work as a baseline would provide insight to responses of the NGMx to predicted changes in global climate.

APPENDIX A

SCRIPTING AND PROGRAMMING EXAMPLES

Example of Perl to cycle through multiple files and use source file information in output

file information

```perl
#!/usr/bin/perl


$filestring=@filename[$#filename];

print "$filestring\n";

$year=substr($filestring,1,4);

$doy1=substr($filestring,5,3);

$doy2=substr($filestring,12,3);

($year1,$month1,$day1) = Add_Delta_Days($year,1,1, $doy1 - 1);

($year2,$month2,$day2) = Add_Delta_Days($year,1,1, $doy2 - 1);

$month1=sprintf("%02d",$month1);

$month2=sprintf("%02d",$month2);

$tmonth1=Month_to_Text($month1);

$tmonth2=Month_to_Text($month2);

$day1=sprintf("%02d",$day1);

$day2=sprintf("%02d",$day2);

$increment=(($doy1 + $doy2)/2);

#$increment=$doy1;

$xcord=($increment * 0.04294);

$mapcord=($xcord+262.33);
```

```
$titleover="Northern Gulf of Mexico SeaWiFS 8Day CHLO";

$datestring="$tmonth1-$day1 $year";



        system("mv gomFile.asc @filename[$#filename].asc");

        system("gom_chl_gmt2.gmt \'$datestring\' \'$titleover\' \'$mapcord\'");

        system("mv gomfile.ps gomPS/@filename[$#filename].ps");

        system("mv @filename[$#filename].asc

gomASCII/@filename[$#filename].asc");
```

Example of MATLAB satellite data analysis using user input to easily adapt for differing

files

```
regionname=input('What is the region name?','s');

%the order must be flh,chl,cdom file for a particular region

pat=[regionname '.asc'];


t=46;%

x=1:8:365; %interval based on 8 day weeks

lx=1:7.934:3285; %9 year decadal timeseries (10 yr = 1:7.934:3650)

stp=t*9; %8day/year * years, used for decadal timeseries


work=chl;

work(:,5)=work(:,4)-floor(work(:,4));


%define variables for flclcd

flclcd(:,i)=work(:,1);

end


flclcd(:,4)=work(:,2); %lat=work(:,2);

flclcd(:,5)=work(:,3); %lon=work(:,3);


flag=999.900;

flagloc=find(flclcd(:,1:3)==flag);
```

```
flclcd(flagloc)=NaN;


fl=flclcd(:,1);

cl=flclcd(:,2);

cd=flclcd(:,3);


yer=work(:,5);

%min and max based on 8Dwk20 focus

flagminj=2007.427;

flagmaxj=2007.43;

flagmin8=0.427;

flagmax8=0.43;

flagmin3=0.405;

flagmax3=0.452;

flaglocj=find(work(:,4)>=flagminj & work(:,4)<=flagmaxj);

flagloc3=find(yer>=flagmin3 & yer<=flagmax3);

flagloc8=find(yer>=flagmin8 & yer<flagmax8);


fl3=fl(flagloc3);

cl3=cl(flagloc3);

cd3=cd(flagloc3);

fl8=fl(flagloc8);

cl8=cl(flagloc8);
```

```
cd8=cd(flagloc8);

flj=fl(flaglocj);

clj=cl(flaglocj);

cdj=cd(flaglocj);


%create climatology

div3=(length(fl3))/9;

div8=(length(fl8))/9;

fl3=reshape(fl3,div3,9);

cl3=reshape(cl3,div3,9);

cd3=reshape(cd3,div3,9);

fl8=reshape(fl8,div8,9);

cl8=reshape(cl8,div8,9);

cd8=reshape(cd8,div8,9);

flh3=nanmean(fl3,2);

chl3=nanmean(cl3,2);

cdom3=nanmean(cd3,2);

flh8=nanmean(fl8,2);

chl8=nanmean(cl8,2);

cdom8=nanmean(cd8,2);


%find centroid and std

flcent=nanmean(flh3);
```

```
clcent=nanmean(chl3);

cdcent=nanmean(cdom3);

flstd2=(nanstd(flh3)); %multiply by 2 or more for increased std

clstd2=(nanstd(chl3));

cdstd2=(nanstd(cdom3));


%find plume values within jet week

flaglocp=find(flj<(flcent+flstd2));

flj(flaglocp)=NaN;

flaglocp=find(clj<(clcent+clstd2));

clj(flaglocp)=NaN;

flaglocp=find(cdj<(cdcent+cdstd2));

cdj(flaglocp)=NaN;


flcentj=nanmean(flj);

clcentj=nanmean(clj);

cdcentj=nanmean(cdj);


p1j = polyfit(clj,flj,1);

f1j = polyval(p1j,clj);

[r21j rmse] = rsquare(flj,f1j);

p1c = polyfit(chl3,flh3,1);

f1c = polyval(p1c,chl3);
```

```
[r21c rmse] = rsquare(flh3,f1c);


p2j = polyfit(clj,cdj,1);

f2j = polyval(p2j,clj);

[r22j rmse] = rsquare(cdj,f2j);

p2c = polyfit(chl3,cdom3,1);

f2c = polyval(p2c,chl3);

[r22c rmse] = rsquare(cdom3,f2c);


p3j = polyfit(flj,cdj,1);

f3j = polyval(p3j,flj);

[r23j rmse] = rsquare(cdj,f3j);

p3c = polyfit(flh3,cdom3,1);

f3c = polyval(p3c,flh3);

[r23c rmse] = rsquare(cdom3,f3c);
```

Example of Fortran

```fortran
! Write out arrays from grids


implicit none

real :: chl(20485,3), latu, latl, lonu, lonl, loc(5000,4)

integer :: i, j, q, stpt, enpt, try, f, c, d

integer, parameter :: chla = 7

character :: title

character(33) :: ffile, ifile, ofile, mfile, lfile, list(460,1), counter

real :: year, yrfrac, doya, date

integer :: doy1, doy2




!print*,

!print*, "enter the focal coordinates as upper left and bottom right"

!print*, "(e.g. 31,-79,24,-99)"

ffile="fortran250sea_aqua.asc"

open( unit=5, file=ffile, status="old", action="read" )

do c=1,5000

read( 5,*, end=15) (loc(c,q), q=1,4)

end do

15 continue

 c=c-1
```

```
 close (5)

!input list of files

 lfile="timefiles_s_a.txt"

!read list into 1-d array

 open( unit=4, file=lfile, status="old", action ="read" )

 do i=1,460

 read( 4,*) list(i,1)

 end do

 close (4)


do d=1,c

        latu=loc(d,1)

        lonu=loc(d,2)

        latl=loc(d,3)

        lonl=loc(d,4)

!read (counter,*) latu

!read*, latu,lonu,latl,lonl

        !stpt=((372-((latu+1)*12))*241)

        !enpt=((372-(latl*12))*241)



 ofile="XX"

 mfile="XX"
```

```fortran
!operate on each file

 do f=1,460


!define i/o files

 ifile=list(f,1)



        !optional i/o schemes

        !print*, "enter the name of the inputfile"

        !read*, ifile

        !ifile="S20011532001160.L3m_8D_CHLO_9.asc"

        !print*, "enter the name of the outputfile"

        !read*, ofile



!open i/o files

 open ( unit=7, file=ifile, status="old", action="read" )


!open ( unit=13, file=mfile, status="old", position="append", action="write" )


!calculate decimal year

 read(ifile(2:5),*)  year

 read(ifile(6:8),*)  doy1
```

```fortran
read(ifile(13:15),*) doy2

doya=(doy1+doy2)/2

if (year == 2000 .or. year == 2004 .or. year == 2008) then

 yrfrac=doya/366

else

 yrfrac=doya/365.

end if

date=year+yrfrac


!read title from input file

 read ( unit=chla, fmt='(a60)') title


!read input file values into 3element array

 do i=1,20485

 read ( 7,*, end=21 ) (chl(i,j), j=1,3)

 end do

         !check how file is read into array

         !write (*,*) (chl(i,1), i=1,10)

         !write (unit=10,fmt='(3(f9.3,1x))') chl

         !write(10,*)

     !define lat/lon box for focal area


         do j=1,20485
```

```
            if (chl(j,2)>latl .and. chl(j,2)<latu ) then

     if (chl(j,3)<lonu .and. chl(j,3)>lonl ) then

                  write (10,fmt='(6(f9.3,1x))') (chl(j,q), q=1,3), date
```

Example of NetCDF extraction

```
% Read discharge data from gom_river_discharge.nc


dateOffset=datenum('-4712-01-01 12:00:00', 'yyyy-mm-dd HH:MM:SS');


inStrAll='gom_river_discharge.nc';


%inStrAll='http://10.14.4.99:8080/thredds/dodsC/myData/gom_river_discha
rge.nc?Julian_Day[0:1:38807],Discharge[0:1:38807][0:1:54],End_Date[0:1:
54],Start_Date[0:1:54],Gage_Latitude[0:1:54],Gage_Longitude[0:1:54],Mou
th_Latitude[0:1:54],Mouth_Longitude[0:1:54],Station_ID[0:1:54],River_Na
me[0:1:54]';


%try loaddap(inStrAll);


    Julian_Day=ncread(inStrAll,'Julian_Day',[1], [Inf]);

    Start_Date=ncread(inStrAll,'Start_Date',[1],[Inf]);

    End_Date=ncread(inStrAll,'End_Date',[1],[Inf]);

    Discharge=ncread(inStrAll,'Discharge',[1 1],[Inf Inf]);

    River_Name=ncread(inStrAll,'River_Name',[1 1],[Inf Inf]);
%end
Julian_Day=double(Julian_Day);

Start_Date=double(Start_Date);

End_Date=double(End_Date);


 jday=datevec(Julian_Day+dateOffset);

 [dDay dYr]=date2doy(datenum(jday));
```

```
yr=jday(:,1)+dYr;


tStrt=datevec(Start_Date+dateOffset);

[dDay dStrt]=date2doy(datenum(tStrt));

tmin=tStrt(2,1)+dStrt(2);


tEnd=datevec(End_Date+dateOffset);

[dDay dEnd]=date2doy(datenum(tEnd));

tmax=tEnd(2,1)+dEnd(2);
```

REFERENCES

Adams, C.M., Hernandez, E., & Cato, J.C. (2004). The economic significance of the Gulf of Mexico related to population, income, employment, minerals, fisheries and shipping. *Ocean & Coastal Management 47*, 565–580.

Alvera-Azcárate, A., Barth, A., & Weisberg, R. (2009). The surface circulation of the Caribbean Sea and the Gulf of Mexico as inferred from satellite altimetry. *Journal of Physical Oceanography, 39*, 640-655, doi:10.1175/2008JPO3765.1.

Babin, S.M., Carton, J.A., Dickey, T.D., & Wiggert, J.D. (2004). Satellite evidence of hurricane-induced phytoplankton blooms in an oceanic desert. *Journal of Geophysical Research, 109*, doi:10.1029/2003JC001938.

Behrenfeld, M.J. (2010). Abandoning Sverdrup's Critical Depth Hypothesis on phytoplankton blooms. *Ecology, 91*(4), 977-989.

Behrenfeld, M.J., Westberry, T.K., Boss, E.S., O'Malley, R.T., Siegel, D. A., Wiggert, J.D., Franz, B.A., McClain, C.R., Feldman, G.C., Doney, S.C., Moore, J.K. Dall'Olmo, G., Milligan, A.J., Lima, I., & Mahowald, N. (2009). Satellite-detected fluorescence reveals global physiology of ocean phytoplankton. *Biogeosciences, 6*, 779-794.

Biggs, D.C., & Muller-Karger, F.E. (1994). Ship and satellite observations of chlorophyll stocks in interacting cyclone-anticyclone eddy pairs in the western Gulf of Mexico. *Journal of Geophysical Research, 99*(C4), 7371-7384, doi:10.1029/93JC02153.

Brooks, D.A., & Legeckis, R.V. (1982). A ship and satellite view of hydrographic

    features in the western Gulf of Mexico. *Journal of Geophysical Research, 87,*

    4195-4206.

Buesseler, K.O. (1998). The decoupling of production and particulate export in the

    surface ocean. *Global Biogeochemical Cycles, 12*(2), 297-310.

Cai, W.J., & Lohrenz, S.E. (2010). The Mississippi River plume and adjacent margin in

    the Gulf of Mexico. In K.K. Liu, L. Atkinson, R. Quiñones & L. Talaue-

    McManus (Eds.), *Carbon and Nutrient Fluxes in Continental Margins: A Global*

    Synthesis (pp. 406-421). New York, NY: Springer.

Carder, K.L., Chen, F.R., Lee, Z., Hawes, S.K., & Cannizzaro, J.P. (2003). *Case 2*

    Chlorophyll a. (MODIS Ocean Science Team Algorithm Theoretical Basis

    Document, Version 7).

Carnes, M.R., Teague, W.J., & Jarosz, E. (2008). Low-frequency current variability

    observed at the shelfbreak in the northeastern Gulf of Mexico: November 2004-

    May 2005. *Continental Shelf Research, 28*, 399-423.

Chassignet, E.P., Hurlburt, H.E., Smedstad, O.E., Barron, C.N., Ko, D.S., Rhodes, R.C.,

    Shriver, J.S., Wallcraft, A.J., & Arnone, R.A. (2005). Assessment of data

    assimilative ocean models in the Gulf of Mexico using ocean color. In W. Sturges

    & A. Lugo-Fernandez (Eds.), *Circulation in the Gulf of Mexico Observations and*

    Models, Geophysical Monograph Series (pp. 87-100). Washington DC: AGU.

de Ruijter, W.P.M., van Aken, H.M., Beier, E.J., Lutjeharms, J.R.E., Matano, R.P., &

    Schouten, M.W. (2004). Eddies and dipoles around South Madagascar: formation,

pathways and large-scale impact. *Deep Sea Research I, 51*, 10.1016/j.dsr.2003.10.011, 383-400.

Denman, K.L., & Abbott, M.R. (1994). Time scales of pattern evolution from cross-spectrum analysis of advanced very high resolution radiometer and coastal zone color scanner imagery. *Journal of Geophysical Research, 99*, 7433-7442.

Esaias, W.E. (1996). *Algorithm theoretical basis document for MODIS product MOD-27 ocean primary productivity.* (ATBD-MOD-24). Goddard Space Flight Center.

Ferrari, G.M., & Dowell, M.D. (1998). CDOM absorption characteristics with relation to fluorescence and salinity in coastal areas of the southern Baltic Sea. *Estuarine Coastal and Shelf Science, 47*, 91–105.

Falkowski, P.G., Ziemann, D., Kolber, Z., & Bienfang, P.K. (1991). Role of eddy pumping in enhancing primary production. *Nature, 352*, 55-58, doi:10.1038/352055a0.

Feng, M., Majewski, L.J., Fandry, C.B., & Waite, A.M. (2007). Characteristics of two counter-rotating eddies in the Leeuwin Current system off the Western Australian coast, *Deep Sea Research II, 54*, 10.1016/j.dsr2.2006.11.022, 961-980.

Gilbes, F., Tomas, C., Walsh, J.J., & Muller-Karger, F.E. (1996). An episodic chlorophyll plume on the West Florida Shelf. *Continental Shelf Research, 16(9),* 1201-1224.

Gould, R.W., Jr., Stavn, R.H., Twardowski, M.S., &. Lamela, G.M. (2002). *Partitioning optical properties into organic and inorganic components from ocean color imager*. Proceedings from Ocean Optics XVI, Santa Fe, New Mexico.

Gregg, W. W., & Rousseaux, C.S. (2014). Decadal trends in global pelagic ocean chlorophyll: A new assessment integrating multiple satellites, in situ data, and

models. *Journal of Geophysical Research Oceans, 119*, 5921-5933,doi:10.1002/2014JC010158.

Hamilton, P. (2007). Eddy statistics from Lagrangian drifters and hydrography for the northern Gulf of Mexico slope. *Journal of Geophysical Research, 112*, C09002, doi:10.1029/2006JC003988.

Hamilton, P., & Lee, T.N. (2005). Eddies and jets over the slope of the northeast Gulf of Mexico. In W. Sturges & A. Lugo-Fernandez (Eds.), *Circulation in the Gulf of Mexico Observations and Models, Geophysical Monograph Series* (pp. 123-142). Washington DC: AGU.

Hamilton, P., Berger, T.J., & Johnson, W. (2002). On the structure and motions of cyclones in the northern Gulf of Mexico, *Journal of Geophysical Research, 107*(C12), doi:10.1029/1999JC000270.

Hitchcock, G.L., Wiseman Jr., W.J., Boicourt, W.C., Mariano, A.J., Walker, N., Nelsen, T.A., & Ryan, E. (1997). Property fields in an effluent plume of the Mississippi river. *Journal of Marine Systems, 12*, 109-126.

Hu, C., Muller-Karger, F.E., Biggs, D.C., Carder, K.L., Nababan, B., Nadeau, D., & Vanderbloemen, J. (2003). Comparison of ship and satellite bio-optical measurements on the continental margin of the NE Gulf of Mexico. *International Journal of Remote Sensing, 24*(13), 2597-2612.

Hyun, K.H., & Hogan, P.J. (2008). Topographic effects on the path and evolution of Loop Current Eddies. *Journal of Geophysical Research, 113*, C12026, doi:10.1029/2007JC004155.

Jochens, A.E., & DiMarco, S.F. (2008). Physical oceanographic conditions in the deepwater Gulf of Mexico in summer 2000-2002. *Deep-Sea Research II, 55*, 2541-2554.

Johnson, E.S., Bonjean, F., Lagerloef, G.S.E., Gunn, J.T., & Mitchum, G.T. (2007). Validation and error analysis of OSCAR sea surface currents. *Journal of Atmospheric and Oceanic Technology, 24*, 10.1175/jtech1971.1, 688-701.

Jolliff, J.K., Walsh, J.J., He, R., Stovall-Leonard, A., Coble, P.G., Conmy, R., Heil, C., Nababan, B., Zhang, H., Hu, C., & Muller-Karger, F.E. (2003). Dispersal of the Suwannee River plume over the West Florida shelf: simulation and observation of the optical and biochemical consequences of a flushing event. *Geophysical Research Letters, 30*(13), doi:1-.1029/2003GL016964.

Jones, E.B., & Wiggert, J.D. (2015). Characterization of a high chlorophyll plume in the northeastern Gulf of Mexico. *Remote Sensing of Environment, 159*, 152-166.

Leben, R.R., Born, G.H., & Engebreth, B.R. (2002). Operational altimeter data processing for mesoscale monitoring. *Marine Geodesy, 25*(1-2), 3-18.

Lohrenz, S.E., Fahnenstiel, G.L., & Redalje, D.G. (1994). Spatial and temporal variations of photosynthetic parameters in relation to environmental conditions in coastal waters of the Northern Gulf of Mexico. *Estuaries, 17*(4), 779-795.

Lohrenz, S.E., Redalje, D.G., Cai, W.J., Acker, J., & Dagg, M. (2008). A retrospective analysis of nutrients and phytoplankton productivity in the Mississippi River plume. *Continental Shelf Research, 28*, 1466-1475.

Lohrenz, S.E., & Verity, P.G. (2006). Regional oceanography: Southeastern United States and Gulf of Mexico (2,W). In A. R. Robinson & K. H. Brink (Eds.) *The*

Sea (vol. 14), The Global Coastal Ocean: Interdisciplinary Regional Studies and Syntheses. Campbridge, MA: Harvard University Press.

Kennedy, A.J., Griffin, M.L., Morey, S.L., Smith, S.R., & O'Brien, J.J. (2007). Effects of El Niño- Southern Oscillation on sea level anomalies along the Gulf of Mexico coast. *Journal of Geophysical Research, 112*, doi:10.1029/2006JC003904.

Marra, J., Houghton, R.W., & Garside, C. (1990). Phytoplankton growth at the shelf-break front in the Middle Atlantic Bight. *Journal of Marine Research, 48(4)*, 851-868.

Martínez-López, B., & Zavala-Hidalgo, J. (2009). Seasonal and interannual variability of cross-shelf transports of chlorophyll in the Gulf of Mexico. *Journal of Marine Systems, 77*, 1-20.

McGillicuddy, D.J., Anderson, L.A., Bates, N.R., Bibby, T., Buesseler, K.O., Carlson, C.A., Davis, C.S., Ewart, C., Falkowski, P.G., Goldthwait, S.A., Hansell, D.A., Jenkins, W.J., Johnson, R., Kosnyrev, V.K., Ledwell, J.R., Li, Q.P., Siegel, D.A. & Steinberg, D.K. (2007). Eddy/Wind interactions stimulate extraordinary Mid-Ocean plankton blooms. *Science, 316*(5827),1021–1026.

McGillicuddy, D.J., Jr., Johnson, R.J., Siegel, D.A., Michaels, A.F., Bates, N., & Knap, A.H. (1998). Mesoscale variability of ocean biogeochemistry in the Sargasso Sea. *Journal of Geophysical research, 104*(C6), 381-394.

Morel, A., & Gentili, B. (2009). A simple band ration technique to quantify the colored dissolved and detrital organic material from ocean color remotely sensed data. *Remote sensing of the Environment, 113*, 998-1011. doi : 10.1016/j.rse.2009.01.008

Morel, A., & Prieur, L. (1977). Analysis of variations in ocean color. *Limnology and Oceanography*, *22*(4), 709-722.

Morey, S.L., Martin, P.J., O'Brien, J.J., Wallcraft, A.A., & Zavala-Hidalgo, J. (2003). Export pathways for river discharged fresh water in the northern Gulf of Mexico. *Journal of Geophysical Research, 108*(10), doi:1029/2002JC001674.

Morey, S.L., Schroeder, W.W, O'Brien, J.J., & Zavala-Hidalgo, J. (2003). The annual cycle of riverine influence in the eastern Gulf of Mexico basin. *Geophysical Research Letters, 30*(16), doi:10.1029/2003GL017348

Muller-Karger, F.E., Smith, J.P., Werner, S., Chen, R., Roffer, M., Liu, Y., Muhling, B., Lindo-Atichti, D., Lamkin, J., Cerdeira-Estrada, S., & Enfield, D.B. (2015). Natural variability of surface oceanographic conditions in the offshore Gulf of Mexico. *Progress in Oceanography*, in press.

Muller-Karger, F. E., Walsh, J.J., Evans, R.H., &Meyers, M.B. (1991). On the seasonal phytoplankton concentration and sea surface temperature cycles of the Gulf of Mexico as determined by satellites, *Journal of Geophysical Research, 96*(C7), 12645–12665, doi:10.1029/91JC00787.

Oey, L.Y., Ezer, T., & Lee, H.C. (2005). Loop Current, rings and related circulation in the Gulf of Mexico: a review of numerical models and future challenges. In W. Sturges & A. Lugo-Fernandez (Eds.), *Circulation in the Gulf of Mexico Observations and Models, Geophysical Monograph Series* (pp. 31-56). Washington DC: AGU.

Ohlmann, J.C., Niiler, P.P., Fox, C.A., & Leben, R.R. (2001). Eddy energy and shelf interactions in the Gulf of Mexico. *Journal of Geophysical Research, 106*, 2605-2620.

Pegau, W.S.,Boss, E., & Martinez, A. (2002). Ocean color observations of eddies during the summer in the Gulf of California, *Geophysical Research Letters, 29*, 10.1029/2001gl014076

Risien, C.M., & Chelton, D.B. (2008). A global climatology of surface wind and wind stress fields from eight years of QuikSCAT scatterometer data. *Journal of Physical Oceanography, 38*, 2379-2413.

Risien, C.M., & Chelton, D.B. (2006). A satellite-derived climatology of global ocean winds. *Remote Sensing of the Environment, 105*(3), 221-236.

Robinson, K.L., & Graham, W.M. (2013). Long-term change in the abundances of northern Gulf of Mexico scyphomedusae *Chrysaora* sp. and *Aurelia* spp. with links to climate variability. *Limnology and Oceanography, 58*(1), 235-253.

Salas-de-León, D.A., Monreal-Gómez, M.A., Signoret, M., & Aldeco, J. (2004). Anticyclonic-cyclonic eddies and their impact on near-surface chlorophyll stocks and oxygen supersaturation over the Campeche Canyon, Gulf of Mexico. *Journal of Geophysical Research, 109*, 10.1029/2002jc001614.

Salisbury, J.E., Campbell, J.W., Linder, E., Meeker, L.D., Muller-Karger, F.E., & Vörösmartye, C.J. (2004). On the seasonal correlation of surface particle fields with wind stress and Mississippi discharge in the northern Gulf of Mexico. *Deep Sea Research II, 51*, 1187-1203.

Salmerón-Garcia, O., Zavala-Hidalgo, J., Mateos-Jasso, A., & Romero-Centeno, R.
(2011). Regionalization of the Gulf of Mexico from space-time chlorophyll-a
concentration variability. *Ocean Dynamics, 61*, 10.1007/s10236-010-0368-1, 439-
448.

Schiller, R.V., Kourafalou, V.H., Hogan, P., & Walker, N.D. (2011). The dynamics of the
Mississippi River plume: Impact of topography, wind and offshore forcing on the
fate of plume waters. *Journal of Geophysical Research, 116*,
10.1029/2010jc006883.

Schmitz, W.J., Biggs, D.C., Lugo-Fernandez, A., Oey, L.Y., & Sturges, W. (2005). A
synopsis of the circulation in the Gulf of Mexico and on its continental margins.
In W. Sturges & A. Lugo-Fernandez (Eds.), *Circulation in the Gulf of Mexico
Observations and Models, Geophysical Monograph Series* (pp. 11-30).
Washington DC: AGU.

Siegel, D.A., Behrenfeld, M.J., Maritorena, S., McClain, C.R., Antoine D., Bailey, S.W.,
Bontempi, P.S., Boss, E.S., Dierssen, E., Doney, S., Eplee Jr., R.E., Evans, R.H.,
Feldman, G.C., Fields, E., Franz, B.A., Kuring, N.A., Mengelt, C., Nelson, N.B.,
Patt, F.S., Robinson, W.D., Sarmiento, J.L., Swan, C.M., Werdell, P.J.,
Westberry, T.K., Wilding, J.G., & Yoder, J.A. (2013). Regional to global
assessments of phytoplankton dynamics from the SeaWiFS mission. *Remote
Sensing of Environment, 135*, 77-91.

Siegel, D.A., Peterson, P., McGillicuddy, D.J., Jr., Maritorena, S., & Nelson, N.B.
(2011). Bio-optical footprints created by mesoscale eddies in the Sargasso Sea.
Geophysical Research Letters, 38(L13608), doi:10.1029/2011GL047660.

Song, H., Ji, R., Stock, C., & Wang, Z. (2010). Phenology of phytoplankton blooms in the Nova Scotian Shelf–Gulf of Maine region: remote sensing and modeling analysis. *Journal of Plankton Research, 32*, 1485-1499.

Sturges, W., Lugo-Fernandez, A., &. Shargel, M.D. (2005). Introduction to circulation in the Gulf of Mexico. In W. Sturges & A. Lugo-Fernandez (Eds.), *Circulation in the Gulf of Mexico Observations and Models, Geophysical Monograph Series* (pp. 1-10). Washington DC: AGU.

Sturges, W., Hoffmann, N.G., & Leben, R.R. (2009). A trigger mechanism for Loop Current ring separations. *Journal of Physical Oceanography, 40*(5), 900-913.

Tang, D.L., Kawamura, H., Van Dien, T., & Lee, M.A. (2004). Offshore phytoplankton biomass increase and its oceanographic causes in the South China Sea. *Marine Ecology Progress Series, 268*, 31-41.

Teague, W.J., Jarosz, E., Carnes, M.R., Mitchell, D.A., & Hogan, P.J. (2006). Low-frequency current variability observed at the shelfbreak in the northeastern Gulf of Mexico: May-October, 2004. *Continental Shelf Research, 26*, 2559-2582.

Toner, M., Kirwan, A.D., Jr., Poje, A.C., Kantha, L.H., Muller-Karger, F.E., & Jones, C.K.R.T. (2003). Chlorophyll dispersal by eddy-eddy interactions in the Gulf of Mexico. *Journal of Geophysical Research, 108*(C4), 3105, doi: 10.1029/2002JC001499.

Walker, N.D., & Rabalais, N.N. (2006). Relationships among satellite chlorophylla, river inputs, and hypoxia on the Louisiana Continental shelf, Gulf of Mexico. *Estuaries and Coasts, 29*(6), 1081-1093.

Walker, N.D., Huh, O.K., Rouse, L.J., & Murray, S.P. (1996). Evolution and structure of a coastal squirt off the Mississippi River delta: Northern Gulf of Mexico. *Journal of Geophysical Research, 101*, 20643-20655.

Walsh, J.J., Dieterle, D.A., Meyers, M.B., & Muller-Karger, F.E. (1989). Nitrogen exchange at the continental margin: A numerical study of the Gulf of Mexico. *Progress in Oceanography, 23*(4). http://dx.doi.org/10.1016/0079-6611(89)90002-5.

Wang, F., & Xu, Y.J. (2008). Development and application of a remote sensing-based salinity prediction model for a large estuarine lake in the US Gulf of Mexico coast. *Journal of Hydrology, 360*(1-4), 184-184, http://dx.doi.org/10.1016/j.jhydrol.2008.07.036

Wang, D. P., Oey, L.Y., Ezer, T., & Hamilton, P. (2003). Near-surface currents in DeSoto Canyon (1997-99): Comparison of current meters, satellite observation, and model simulation. *Journal of Physical Oceanography, 33*(1), 321-326, doi:10.1175/1520-0485(2003)033<0313:nscidc>2.0.co;2.

Wang, S.Y., Hakala, K., Gillies, R.R., & Capehart, W.J. (2014). The Pacific quasidecadal oscillation (QDO): An important precursor toward anticipating major flood events in the Missouri River Basin? *Geophysical Research Letters, 41*, 991–997, doi:10.1002/2013GL059042.

Wawrik, B., Paul, J.H., Campbell, L., Griffin, D., Houchin, L., Fuentes-Ortega, A., & Muller-Karger, F.E. (2003). Vertical structure of the phytoplankton community associated with a coastal plume in the Gulf of Mexico. *Marine Ecology Progress Series, 251*, 87-101.

Wessel, P., & Smith, W.H.F. (1998). New, improved version of Generic Mapping Tools released. *EOS, Transactions American Geophysical Union, 79*, GMT, 579.

Wiggert, J.D., Vialard, J., & Behrenfeld, M. (2009). Basinwide modification of dynamical and biogeochemical processes by the positive phase of the Indian Ocean Dipole during the SeaWiFS era. in J.D. Wiggert et al. (Eds.), *Indian Ocean Biogeochemical Processes and Ecological Variability* (p. 350). Washington, D. C: AGU.

Yuan, J., Miller, R.L., Powell, R.T., & Dagg, M.J. (2004). Storm-induced injection of the Mississippi River plume into the open Gulf of Mexico. *Geophysical Research Letters, 31,* doi:10.1029/2003GL019335.